



UPPSALA  
UNIVERSITET

UPTEC K 18010

Examensarbete 30 hp  
Maj 2018

# Silicon-based graphite electrodes for Li-ion batteries

---

Rassmus Andersson



UPPSALA  
UNIVERSITET

**Teknisk- naturvetenskaplig fakultet  
UTH-enheten**

Besöksadress:  
Ångströmlaboratoriet  
Lägerhyddsvägen 1  
Hus 4, Plan 0

Postadress:  
Box 536  
751 21 Uppsala

Telefon:  
018 – 471 30 03

Telefax:  
018 – 471 30 00

Hemsida:  
<http://www.teknat.uu.se/student>

## Abstract

### Silicon-based graphite electrodes for Li-ion batteries

---

*Rassmus Andersson*

The cycling performance of silicon containing graphite electrodes as the anode in lithium-ion batteries has been investigated. Different electrode compositions of silicon, graphite, carbon black, sodium carboxymethylcellulose (CMC-Na), styrene-butadiene rubber (SBR) and using water as the solvent have been prepared and evaluated electrochemically by constant-current-constant-voltage (CCCV) cycling. To understand the impact on the cycling performance of the electrodes, the process parameters in the coating process have been evaluated by rheological measurements of the electrode slurries.

The highest and most stable capacity was found for the electrode containing 5 wt% silicon (vs. graphite), 3 wt% binder, equal amount of the binders CMC-Na and SBR and 70 wt% solvent in the initial electrode slurry. It showed a stable capacity retention of 360 mAh/g after 315 cycles, before it faded. It was found that the CMC-Na and the solvent have a strong impact on the properties of the electrode slurry and the processing parameters. CMC-Na, the solvent and SBR were also found to be important for the adhesion of the electrode coating on the current collector. The worst cycling performance was obtained for electrodes containing 15 wt% silicon, a solvent amount below 65 wt% and a binder ratio of CMC-Na:SBR below 1:1. Different rheological behaviour for different silicon particles was found to depend on the surface area of the particles.

Handledare: Jonas Mindemark  
Ämnesgranskare: Daniel Brandell  
Examinator: Peter Broqvist  
ISSN: 1650-8297, UPTec K 18010

# Sammanfattning

Alla batterier kan bli uppdelade i två huvudkategorier, nämligen primära och sekundära batterier. Skillnaden mellan dessa är att primära batterier endast kan användas en gång för att sedan vara förbrukade, medan sekundära batterier kan laddas upp efter användning och återanvändas. Det dominerande sekundära batteriet för små portabla elektriska apparater, såsom mobiltelefonen och datorn, är idag litiumjonbatteriet. Anledningen till detta är att litium-jon batterier har en hög energitäthet, låg vikt och kort uppladdningstid jämfört med övriga sekundära batterier. Utvecklingen av bilmarknaden med hybrid- och elektriska bilar har dock öppnat upp dörren för litiumjonbatterier även för mer storskaliga användningsområden, då dess egenskaper uppfyller de krav som bilmarknaden kräver.

Ett batteri består av två elektroder, en negativ och en positiv, en elektrolyt samt en yttre strömledande krets. Energi utvinns ur batteriet genom att det är en potentialskillnad mellan elektroderna, vilket driver kemiska reaktioner vid respektive elektrod. Vid urladdning av batteriet frisätts litiumjoner och elektroner från den negativa elektroden och transporteras till den positiva elektroden via elektrolyten (litiumjonerna) och den yttre strömledande kretsen (elektronerna). När elektronerna transporteras i den yttre kretsen skapas en elektrisk ström som kan användas för att driva elektriska apparater. Sekundära batterier kan laddas upp igen genom att lägga på en spänning i motsatt riktning.

Energien som kan utvinnas ur ett batteri bestäms av dess energitäthet. Energitätheten bestäms i sin tur av två faktorer: potentialskillnaden mellan elektroderna samt kapaciteten av respektive elektrod. För att möta efterfrågan av bättre batterier behövs batterier med högre energitäthet, vilket kräver elektroder med högre kapacitet. Kapacitet betyder hur mycket laddning man kan utvinna ur ett material per vikt- eller volymenhet och mäts vanligen i mAh/g. I dagens batterier används endast grafit som den negativa elektroden, vilket har en teoretisk kapacitet på 372 mAh/g. Ett lovande material som antingen helt eller delvis kan ersätta grafit är kisel, som har en maximal teoretisk kapacitet på 4200 mAh/g.

Det finns dock ett flertal problem med att använda kisel som elektrodmaterial. Det största problemet är att det expanderar (och kontraherar) upp till 400% vid laddning och urladdning (cykling) av batteriet. Det medför bl.a. kraftiga mekaniska spänningar i materialet, vilket kan leda till sprickbildning och att elektroden går sönder.

I detta projekt ersattes en liten del av grafiten med kisel för att öka kapaciteten i den negativa elektroden. I och med att endast en liten del av grafiten ersattes med kisel så var förhoppningarna att expansionsproblemen av kisel vid cykling kan undvikas, samtidigt som kapaciteten förbättras med bibehållen stabilitet. Detta lyckades, då en elektrodkomposition med 5 vikt-% kisel i grafit med upprepade försök cyklades stabilt över 200 cykler med en uppmätt kapacitet mellan 371–378 mAh/g (uppmätt kapacitet är alltid lägre än teoretisk kapacitet). Vidare påvisar resultaten vilken betydelse olika mängder av bindemedel och lösningsmedel har, samt processparametrarna vid tillverkning, för prestationen av elektroden.

# Table of contents

Abbreviations .....	6
1. Introduction.....	7
1.1 Background.....	7
1.2 Scope of the project .....	9
2. Theory.....	10
2.1 Batteries.....	10
2.2 Lithium-ion batteries (LIBs) .....	11
2.2.1 LIB chemistry.....	11
2.2.2 Half-cells .....	12
2.3 LIB components .....	12
2.3.1 Anode materials.....	12
2.3.2 Cathode materials .....	13
2.3.3 Electrolyte .....	13
2.3.4 Separator.....	14
2.3.5 Current collectors .....	14
2.4 Silicon and graphite anodes.....	14
2.4.1 Graphite.....	14
2.4.2 Silicon.....	15
2.4.3 Binders .....	16
2.4.4 Carbon Black.....	18
2.4.5 Electrolyte .....	18
2.5 Rheology .....	18
2.6 Electrochemical testing .....	19
3. Experimental .....	21
3.1 Materials.....	21
3.2 Lab-scale electrode preparations .....	21
3.3 Pilot scale electrode preparations .....	21
3.4 Mass loading .....	21
3.5 Thickness.....	22
3.6 Adhesion testing .....	22
3.7 Rheology .....	23
3.8 Dynamic Light Scattering (DLS) .....	23
3.9 N <sub>2</sub> -physisorption.....	24

3.10 Scanning electron microscopy (SEM) and Energy-dispersive spectroscopy (EDS)....	24
3.11 Half-cell assembly .....	24
3.12 Electrochemical testing .....	25
4. Results and discussion.....	26
4.1 Experimental setup .....	26
4.2 Electrode preparation and processing .....	27
4.3 $\mu\text{m-Si}$ vs. $\text{nm-Si}$ .....	33
4.4 Morphology .....	37
4.5 Electrochemical testing .....	41
5. Conclusion.....	50
Acknowledgements .....	51
References .....	52
Appendix A: Calculations .....	58
Appendix B: Cycling data .....	60
C/10: .....	60
C/2: .....	65
RA017 C/2: .....	69

# Abbreviations

BET	Brunauer–Emmett–Teller
CB	Carbon black
CCCV	Constant-current-constant-voltage
OCV	Open circuit voltage
CMC-Na	Sodium-carboxymethylcellulose
C.E.	Coulombic efficiency
DLS	Dynamic light scattering
DMC	Dimethyl carbonate
EC	Ethylene carbonate
EDS	Energy-dispersive spectroscopy
FEC	Fluoroethylene carbonate
LIB	Lithium-ion battery
PAA	Poly(acrylic acid)
PVDF	Poly(vinylidene fluoride)
SBR	Styrene–butadiene rubber
SEI	Solid electrolyte interphase
SEM	Scanning electron microscopy
SEP	Standard electrode potential
SHE	Standard hydrogen electrode
VC	Vinylene carbonate

# 1. Introduction

## 1.1 Background

Batteries can be classified in two different category types: primary and secondary batteries. The difference is that primary batteries are non-rechargeable and only used once before they are disposed, while secondary batteries are rechargeable and can be used multiple times before disposal. Today the most widely used secondary batteries for small electrical appliances and portable IT devices is the Li-ion battery (LIB). This is because LIBs have a high energy density, which is important, as it is the amount of energy that can be delivered per unit mass. For larger electrical appliances, other secondary batteries are more common, owing to their high stability. Recently, the development of the automobile market with plug-in hybrid and electrical vehicles has given LIBs greater attention as they fulfil new demands like being lightweight and fast-charging, and having high performance. These properties together with the high energy density of LIBs have made LIBs promising secondary batteries also for large-scale energy storage. LIBs are therefore a promising choice also for future energy storage applications together with next generation's renewable energy sources and LIB have been associated with green energy production and applications. [1]

The new demand for LIBs is pushing their development to increase the energy density in the batteries. The energy density ( $U$ ) is affected by two properties, the open circuit voltage ( $V_{OCV}$ ) and the total specific capacity ( $Q$ ) in a battery cell.

$$U = V_{OCV} \cdot Q \quad (1)$$

The OCV is the driving force in the battery cell and is decided by the standard electrode potential (SEP) of the electrode materials. The bigger SEP difference it is between the negative ( $E^-$ ) and positive electrode ( $E^+$ ), the higher OCV the battery cell has.

$$V_{OCV} = E^- - E^+$$

The other parameter affecting the energy density is the total specific capacity for a battery cell and it can be calculated theoretically from Faraday's law.

$$Q = \frac{nF}{M_w}$$

where  $M_w$  is the molar mass of the limiting electrode material and  $n$  is the number of electronic charges involved in the chemical reaction of the battery cell. [2]

Two common materials for the positive electrode (cathode) in today's commercial LIBs are  $\text{LiCoO}_2$  and  $\text{LiMnO}_2$ . They have specific capacities of approximately 140 mAh/g. [3] In commercial LIBs, the negative electrode (anode) material is graphite, which has a theoretical capacity of 372 mAh/g. In Figure 1, it is shown how the total specific capacity in the full cell is affected by the specific capacity for the two cathodes mentioned above. [4]

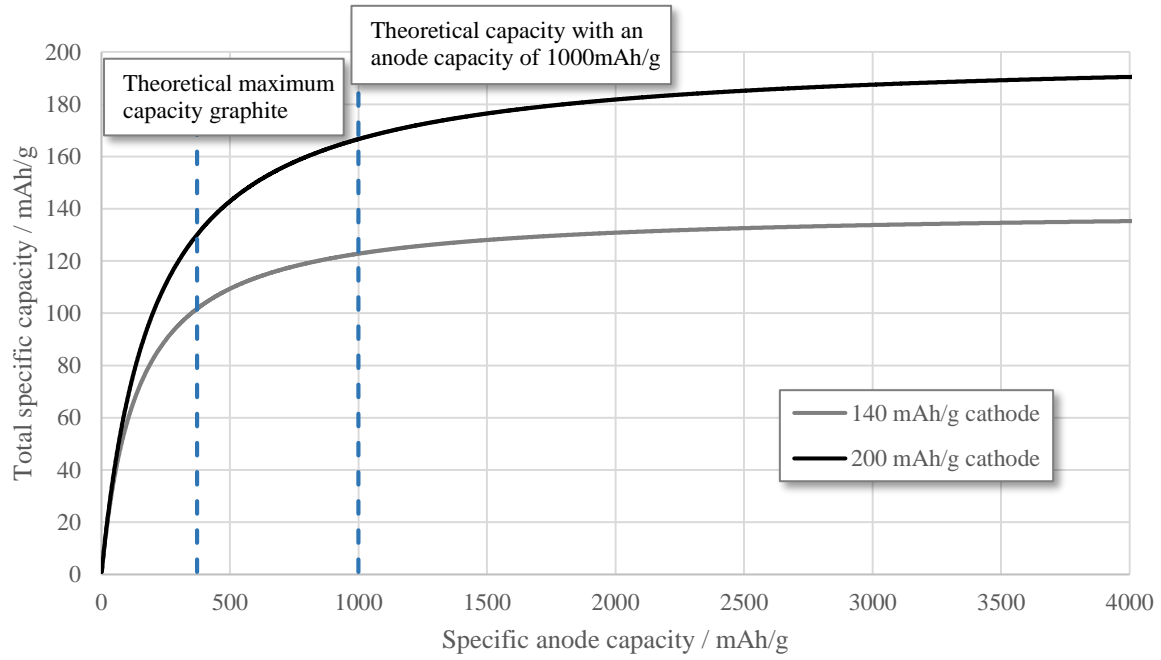


Figure 1: Theoretical specific capacities for batteries consisting of cathode materials with a specific capacity of 200 mAh/g and 140 mAh/g.

As shown in Figure 1, the total specific capacity can be increased with about 20–30% if the specific anode capacity is increased from 372 mAh/g to 1000 mAh/g. This leads to a similar energy density gain, as the energy density is directly affected by the capacity according to Equation (1).

A promising material to increase the specific anode capacity is silicon. Silicon is one of the most common elements on earth and is therefore relatively cheap. Theoretically, it is possible to achieve a specific anode capacity of 800–1200 mAh/g by replacing some of the graphite in the anode with a small amount of silicon, which has a theoretical capacity of about 4200 mAh/g when fully lithiated at elevated temperatures and very low potentials. [2, 5–7]

## 1.2 Scope of the project

The scope of this project was to improve the specific capacity of the anode in Li-ion batteries for commercial use. In today's commercial LIBs, the active material in the anode is graphite which has a comparatively low specific capacity. By replacing some of the graphite with a small amount of silicon, which has a ten times higher specific capacity, the total specific capacity will increase.

In most of the research performed with silicon as the active material in LIBs, it is nanometre silicon particles that have been used, which are too expensive to use as an active material in commercial batteries. It is therefore interesting to evaluate the performance of larger silicon particles, and whether these are realistic to use in commercial batteries.

In this project, also the rheological properties of the electrode slurries (which are cast on current collectors, containing the active material) are studied. It is important to evaluate and control these properties, as they affect the performance of the electrode in a battery cell.

The rheological properties of nanometre silicon particles and micrometre silicon particles are also studied, as it is important to know the difference between the two materials.

Finally, the cycling performance of the electrodes are studied, to evaluate if the capacity can be increased by adding silicon to the anode and what parameters affect its performance.

## 2. Theory

### 2.1 Batteries

Batteries are devices consisting of one or many electrochemical cells that store chemical energy. When batteries are connected to an external circuit, the chemical energy is converted into electrical energy (electricity), which may power electrical appliances. The main components in a battery cell are the two electrodes, which store the chemical energy. The electrodes are commonly referred to as anode and cathode, where in a battery cell the anode is the negative electrode and the cathode is the positive. In between the electrodes, there is an electrolyte and a separator. Their main functions are to facilitate an ion flow between the electrodes and to keep them apart to prevent short circuits.

When an external circuit is connected between the electrodes a redox reaction will occur, which is a reduction and oxidation reaction happening at the same time. In a battery cell, the oxidation reaction (electron loss from a material) occurs at the anode during discharge and the reduction reaction (electron gain in a material) at the cathode. This means that a current of electrons will flow through the external circuit from the anode to the cathode (through the current collectors) during discharge and by connecting an electrical device to the circuit, the electrons will power it. At the same time as the electrons flow between the electrodes, an ion flow will occur in the electrolyte through the separator. Figure 2 shows a schematic picture of the set-up.

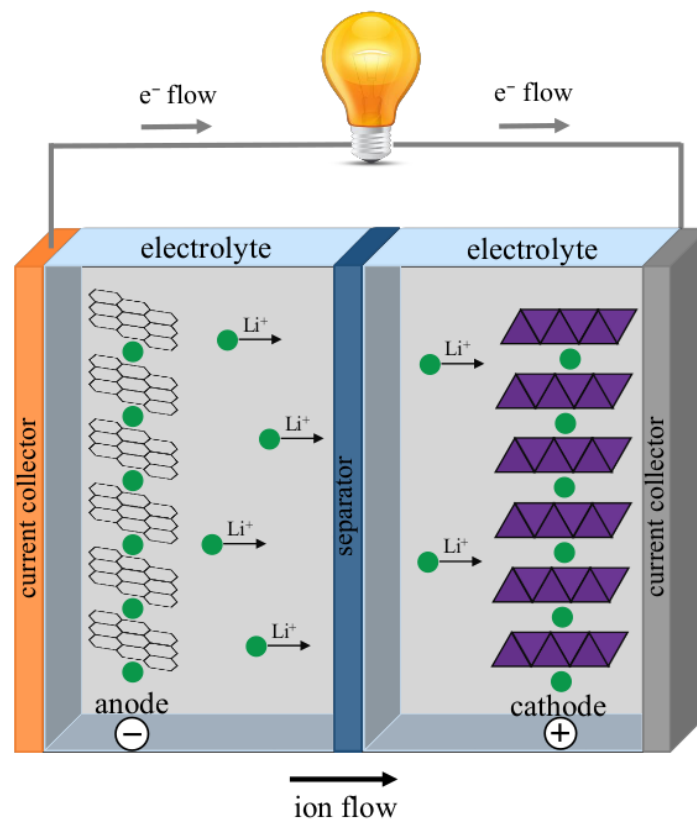


Figure 2: Ion and electron flow in a LIB during discharge.

For secondary batteries, it is possible to reverse the discharge reaction in the battery cell, in other words charge the cell. By applying an external voltage to the battery cell in the opposite

direction, the equilibrium will change in the electrode materials and the ions and electrons will flow in the opposite direction. Hence, the oxidation and reduction will swap sides in the battery cell. A schematic picture of the battery cell during charge is shown in Figure 3.

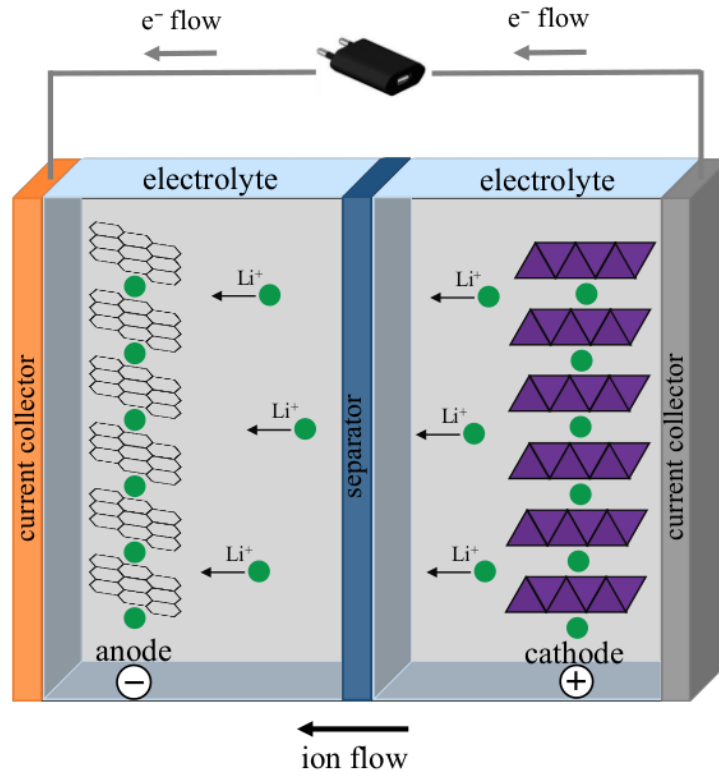


Figure 3: Ion and electron flow in a LIB during charge.

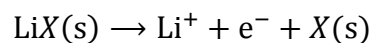
## 2.2 Lithium-ion batteries (LIBs)

Lithium is a desired element in batteries due to its low standard electrode potential (SEP), the lowest of all elements in the periodic table. Lithium's SEP is  $-3.04$  V vs. the standard hydrogen electrode (SHE). Together with the low atomic weight of lithium ( $6.941$  g/mol) and its low density ( $0.53$  g/cm<sup>3</sup>), it gives a higher energy density compared to other battery chemistries. [8] This makes it possible to have a high working potential of around  $3$ – $4$  V, depending on the materials used in the battery cell. [1]

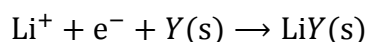
### 2.2.1 LIB chemistry

During the discharge in LIBs, the reactions occur spontaneously in the battery cell due to the electrode materials not being in equilibrium (described in the previous section). The reactions can be divided into two separate half-cell reactions for the anode and the cathode.

The general half-cell reaction for the anode side of the battery cell, where lithium is oxidised, follows the following formula.



In the formula,  $X$  is any given anode material. The lithium ions will flow through the electrolyte and separator to the cathode where they react with the electrons (that flow through the external circuit from the anode to the cathode) and the cathode material ( $Y$ ) by a reduction reaction. The general half-cell reaction for the cathode follows:



If the LIB is a secondary battery, it is possible to reverse the half-cell reactions by applying a voltage in the opposite direction. The LIB will “charge” and the mentioned half-cell reactions will go in the opposite direction.

The discharge process followed by the charge process (or de-lithiation and lithiation) is commonly referred to as cycling in battery terms. The number of cycles performed with a battery is therefore the number of times a battery is discharged and charged.

### 2.2.2 Half-cells

To study the half-cell reactions separately, it is possible to use pure lithium metal as the counter electrode in a battery cell. Lithium metal can be used as the counter electrode for both anode and cathode materials. Important to know is that lithium has the lowest SEP and will therefore always work as the anode in a battery cell, and a proposed anode material studied will act like the cathode. This type of battery cells is called a “half-cell”, because lithium metal is supposed to have a small limiting effect on the battery cell, due to the excess of lithium in the metal. The potential of lithium metal is also relatively constant, which lowers its influence in the system. A drawback is that lithium metal has a poor stability, which may interfere with the results on the studied counter electrode. In early stages of battery development, it is common to use half-cells, as it is easier to find the limiting factors in the studied electrode.

## 2.3 LIB components

In the introduction, the components in the battery were mentioned briefly. This section presents a deeper description of the materials for the LIB components.

### 2.3.1 Anode materials

Desired properties for anode materials in LIBs are low SEP vs. SHE, that the material can accommodate as many lithium ions as possible per weight and volume, and that the material can be lithiated and delithiated reversibly. A possible material for this is pure lithium metal, which has the lowest SEP vs. SHE of all elements and a theoretical specific capacity of 3860 mAh/g. A huge problem with the usage of lithium metal is the safety issue as it reacts violently with water and air. Another problem is the dendrite growth on the surface of the electrode during cycling. If the dendrites reach the counter electrode through the electrolyte and separator, the battery will short-circuit and possibly catch on fire. [2] Generally, the stability of lithium metal as an electrode material is poor, as it is thermodynamically unstable with any kind of organic solvent. Lithium metal reacts easily with the electrolyte components in side reactions, which decrease the battery performance. [9]

Another option as a material for the anode are carbonaceous materials. The dominant material in today's commercial LIBs is graphite. It has a low SEP, only about 0.15–0.25 V higher than lithium metal, it can be lithiated and delithiated reversibly and has good safety properties. Lithiated graphite accommodates one lithium ions per six carbons in the structure ( $\text{LiC}_6$ ) and has a theoretical specific capacity of 372 mAh/g. [2] The lithiation and delithiation mechanism in graphite is called intercalation, meaning that lithium ions enter the structure in between the graphite sheets, see Figure 3.

Silicon is a promising material option for the anode as it fulfils many of the required criteria. It has a low SEP, about 0.3–0.4 V higher than lithium metal. It can be lithiated and delithiated reversibly and has good safety properties. However, the most desired property of silicon is that it theoretically can accommodate 4.4 lithium atoms per silicon atom in its structure ( $\text{Li}_{4.4}\text{Si}$ ) and has a theoretical specific capacity of 4200 mAh/g. [2, 5] Silicon reacts with lithium by an alloying reaction mechanism. [3, 10]

### 2.3.2 Cathode materials

Properties desired for cathode materials are the same as for anodes, except for the point of SEP. Cathode materials should have a high SEP vs. SHE, to achieve a large potential difference between the cathode and the anode, to give a high working potential, *i.e.*, a high energy density in the battery cell.

One of the first cathodes used commercially was  $\text{LiCoO}_2$ , which has a capacity of 140 mAh/g. [2]  $\text{LiCoO}_2$  is still used in today's commercial batteries although there exist cathodes which are both more stable and more environmentally friendly. The perhaps most stable cathode of today's commercial batteries is  $\text{LiFePO}_4$ , which has a capacity of 160 mAh/g. [2]  $\text{LiMnO}_2$  is also used commercially and is environmentally benign, has a low production cost and a good thermal stability. [11]

### 2.3.3 Electrolyte

In all batteries, the main function for electrolytes is to have a high ionic conductivity, to not limit the transport of ions between the electrodes, *i.e.* limit the power density in the battery. Depending on the electrode materials, the battery will have different working potential windows. The LIB working potential window is in the range 0–4.5 V vs.  $\text{Li/Li}^+$  and in this range, there should be no oxidation nor reduction of the electrodes. For the LIB to work without degradation the electrolyte also needs to be stable in the same working potential window. In today's commercial LIBs, the electrolytes are based on aprotic organic liquids like ethylene carbonate (EC) and dimethyl carbonate (DMC) that have high dielectric constants and therefore are good solvents for salt (dissolve large amounts of ions) and have large electrochemical stability windows, although smaller than 0–4.5 V. A problem with EC and DMC is their high vapour pressures, which provokes fire in the case of short circuits. A way of dealing with this problem is to use a solid electrolyte, which also mechanically prevents dendrite growth through the electrolyte. [2]

### 2.3.4 Separator

Separators are necessary in batteries, as they are the barrier that keeps the electrodes apart. Their function is to prevent contact between the electrodes and to have a good permeability to allow ion transport between the electrodes. In the choice of separator, it is dependent on the choice of electrolyte, as it has to have a good wettability with the electrolyte to conduct ions.

### 2.3.5 Current collectors

The current collectors' only function is to deliver electrons from the electrodes to the external circuit reversibly. Therefore, it is preferred to choose a collector with low resistance. It is important to have a good adhesion between the collector and the electrode to not limit the electron transfer between them. Aluminium is a material with these properties, it is lightweight and it is relatively cheap compared with other similar materials. Aluminium is therefore a good choice as the current collector for the cathode. However, aluminium does not work well as the current collector for the anode, due to (alloying) reactions between lithium and aluminium at low potentials. Therefore, copper is used as the current collector for the anode, as it does not alloy with lithium, although it is heavier and more expensive. [12–14]

## 2.4 Silicon and graphite anodes

An interesting material for the anode in LIB is silicon due to its high theoretical specific capacity of 4200 mAh/g at elevated temperatures and very low potentials. [2, 5–7] There are some complications with silicon as an anode material (described below) and therefore a promising material choice for the anode is a mixture of both silicon and graphite. Hypothetically, this solution will give the anode an increased capacity compared with pure graphite and keep the stable reversible cycling properties of graphite. [15–17]

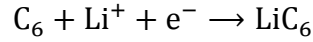
### 2.4.1 Graphite

In today's commercial LIBs, graphite is the main choice as anode material. Graphite has a layered structure where atoms are strongly bonded to each other by covalent bonds within the layers and weakly bonded to each other between the layers by van der Waals bonds. In graphite, the layered structure consists of six carbon atoms bonded covalently to each other hexagonally. Layered structures are good for electrode materials, as it is easy to insert and extract, *i.e.*, intercalate ions in between the layers. Graphite is a good anode material because it accepts charge transfers, does not undergo any major changes in its structure during intercalation and basically retains its original structure when deintercalated. [2] The major drawback with graphite is that it can only accommodate one lithium atom per six carbon atoms in the structure during lithiation. Therefore, it only has a theoretical specific capacity of 372 mAh/g.

During the first lithiation cycle of graphite a protective insulating layer will form on the surface. This layer is called the solid electrolyte interphase (SEI) and it is an irreversibly formed surface layer consisting of organic and inorganic compounds from salts, solvent and impurities in the electrolyte. This SEI is *e.g.* formed at the expense of lithium redox reactions and will therefore cause a capacity loss of the anode. Although the SEI will cause a capacity loss, it is important for the anode. The SEI affects the safety, power capability and the cycle life of the anode, as it

prevents further decomposition reactions of the electrolyte on the anode, improves the thermal and mechanical stability of the anode and hinders further irreversible reactions from occurring. The SEI products formed on the electrode surface depend on the materials used in the system. [18–20] The SEI formation on graphite commonly occurs in the potential range of 0.8–0.3 V. [21]

When the potential is decreased further, graphite will undergo reduction reactions and the overall reduction reaction occurring when graphite is lithiated during cycling is the following:



In Figure 4, it is possible to see at what potentials the reduction reactions take place for graphite. The reduction reactions are seen as plateaus and they take place at 0.196 V, 0.11 V and 0.065 V vs.  $\text{Li}^+/\text{Li}$ .

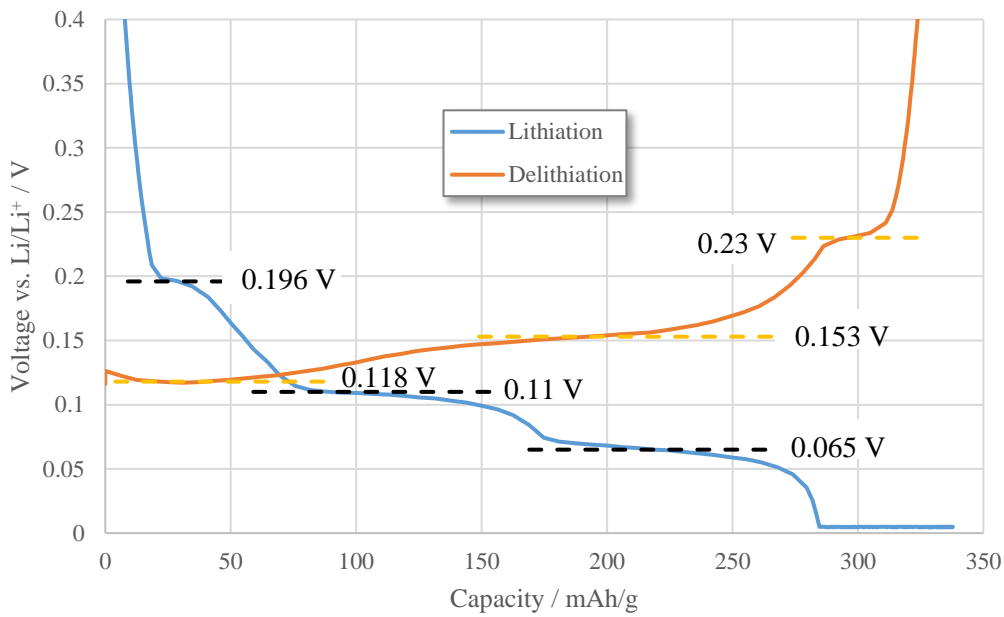


Figure 4: Capacity and voltage profile of a graphite electrode during the second cycle with marked reduction and oxidation potentials during lithiation and delithiation.

When graphite is delithiated during cycling the oxidation reaction will occur at the potentials 0.118 V, 0.153 V and 0.23 V as seen in Figure 4. This is in accordance with the reduction and oxidation potentials in the literature. [3, 16]

## 2.4.2 Silicon

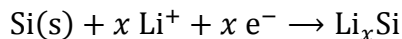
Silicon is as mentioned earlier one of the most promising anode materials for future LIBs due to its high theoretical specific capacity of 4200 mAh/g. [2, 5–7] Although silicon has a smaller working potential window than graphite (onset potential 0.3–0.4 V vs.  $\text{Li}/\text{Li}^+$ ), a specific capacity of 10 times higher magnitude compensates for it.

The main problem with silicon (and other high-capacity materials like tin and antimony [22]) as an anode material is its huge volume expansions and contractions up to 420% during cycling when fully lithiated to  $\text{Li}_{22}\text{Si}_5$ . [2, 5–7, 23] Just like for graphite, SEI formation on the surface area of the anode will cause capacity losses due to decomposition reactions of lithium and the

electrolyte. This is a bigger issue for silicon as it expands during lithiation [5–7] and new surface area is exposed where SEI formation can occur. This causes a large capacity loss, especially during the first cycle, as the SEI formation reactions are irreversible. As silicon will proceed to expand and contract during subsequent cycles, there will always be a capacity loss until the SEI has become thick enough to withstand the volume changes. Another problem caused by the volume changes in the anode is the mechanical strain and stress it is exposed to upon cycling. The mechanical strain/stress will cause cracks and pulverisation of the silicon particles, which leads to disconnection of some particles from the conductive agent attached to silicon. This creates void spaces and poor contact between the particles, which decreases the electronic conductivity; hence, the capacity will fade, as the active material (silicon) cannot be lithiated any longer. The mechanical strain/stress may also impair the adhesion of the anode to the current collector, which limits the conduction of electrons and therefore decreases the performance of the anode. [2, 23–25] Another capacity-limiting defect of silicon anodes is the lithium diffusion trapping effect, an effect occurring due to slow diffusion of lithium ions during delithiation of the active silicon material, *i.e.*, lithium ions will be trapped inside the active material and never contribute to further redox reactions. [14]

One way to overcome the pulverisation of the silicon particles is to use small silicon nanoparticles, as they tend to withstand mechanical stress better compared to larger particles. A problem with smaller particles is that they commonly have low tap bulk density, which leads to lower volumetric density and they are expensive. [26]

During the first cycles, silicon will convert in a phase transition from crystalline silicon to amorphous silicon [7, 15, 16, 27] according to the following reaction mechanism:



This reduction reaction has an onset potential between 0.3–0.4 V vs Li/Li<sup>+</sup>. [5, 17, 22, 28, 29] During further cycling of silicon, it will stay amorphous and not convert back to the pure silicon crystalline phase. It is during this reduction reaction the first SEI formation occurs, which has a huge capacity-decreasing impact on the battery cell.

Depending on what cut-off potential silicon is cycled to, it will form different phases during cycling. Nevertheless, to achieve its full capacity, it is necessary to cycle it to very low potentials, below 50 mV vs. Li/Li<sup>+</sup>. [7, 16, 22, 23, 29] When silicon is cycled to such low potentials, it will undergo another phase transition to one of the crystalline phases Li<sub>22</sub>Si<sub>5</sub> or Li<sub>15</sub>Si<sub>4</sub>, depending on if the cycling is performed at room temperature or elevated temperature. This phase transition has a large impact on the cycle life of the anode due to the volume changes it involves. [7, 16, 27] Due to the decreased cycle life caused by this phase transition, it is suggested to have a lower cut-off voltage above 50 mV to achieve a greater cycle life, even though the full capacity of silicon will not be attained. During delithiation an oxidation reaction occurs around 0.4 V. This contribution arises from the dissipation of one of the crystalline phases Li<sub>22</sub>Si<sub>5</sub> or Li<sub>15</sub>Si<sub>4</sub> back to the amorphous phase Li<sub>x</sub>Si. [16] During further cycling, this oxidation reaction disappears (no plateau), which indicates that the silicon stays amorphous.

### 2.4.3 Binders

Depending on the active material used in the electrodes, different binders are used to enhance the performance of the battery. The main function of the binder is to maintain the structure of

the electrode and help endure mechanical stresses to prolong the cycle life (lifetime) and capacity retention. Today the most conventional binder used in batteries is poly-(vinylidene fluoride) (PVDF), due to its high capacity to withstand strain upcoming during cycling. When silicon is used as anode material, PVDF will attach to the silicon particles via weak van der Waals forces. However, due to the extreme volume expansions arising during cycling of silicon, these weak van der Waals forces will fail to keep the particles together. In addition, PVDF has a permeability to let in solvents between the binder and silicon, for SEI-formation, which further decreases the binder–silicon interface. [22] Better binder options for silicon are materials that have a higher binding strength (to silicon) and elastic moduli (to withstand extremes volume changes) than PVDF. Three options with these properties are sodium carboxymethylcellulose (CMC-Na), poly (acrylic acid) (PAA) and alginate. [22, 24, 26] Particular interest has been shown for CMC-Na and PAA as they both interact with silicon via strong hydrogen bonds between their carboxyl functional groups and the oxygen in silicon dioxide (present at the surface of silicon). CMC-Na and PAA (and alginate) are also favourable because water can be used as the solvent in the slurry as they dissolve in it, while PVDF only dissolves in N-methyl-2-pyrrolidone, which is less environmentally friendly and more expensive. [6] When conductive additives with a high surface area are used in the electrode, CMC-Na tends to have a better performance than PAA, which shows a large number of cracks. This is presumably due to stronger adhesion to the particles from a higher density of functional groups. It is suggested that the stiffer polymer backbone of CMC-Na with a lower density of functional groups is more suitable for dispersing conductive additives with a high surface area. [30]

#### **2.4.3.1 CMC-Na**

CMC-Na (sodium carboxymethylcellulose) is a linear polymeric derivative of cellulose with 0.6 to 1.2 carboxymethyl ( $-\text{CH}_2\text{COO}^-$ ) side groups per monomer. Attached to the CMC-Na chain there is room for three hydroxyl groups per monomer. During derivation, these hydroxyl groups are replaced with carboxyl groups. [31] CMC-Na has shown promising results as a binder in silicon electrodes (and graphite electrodes [32]) as it vastly improves its electrochemical performance. [17, 25, 26, 33] This is somewhat surprising, as CMC-Na has a rigid polymer backbone structure. [31] Ideally, it was thought that an elastic binder would be favourable, as it would adjust for the extreme volume expansions of silicon during cycling. The reason why CMC-Na works well seems to be due to the strong hydrogen bonds between CMC-Na and the particles, which are formed during the preparation of the electrode. In the slurry, CMC-Na binds to the particles in an entangled three-dimensional network by its carboxyl groups in the polymer chains, which tightens up when the solvent evaporates during the drying process. [33] CMC-Na also has an important role of dispersing the conductive additive (which is necessary to improve the conductivity of silicon) homogenously in the electrode. [24, 26, 30]

#### **2.4.3.2 SBR**

SBR (styrene–butadiene rubber) is an elastomeric binder supplied as a latex (dispersed in water), which improves the mechanical stability properties of the electrode due to its flexibility. When added in small amounts, its flexibility suppresses the risk of crack formation in the electrode. It also improves the adhesion of the electrode coating to the current collector, which enhances the cycle life of the electrode. [24, 34]

## 2.4.4 Carbon Black

Carbon Black (CB) is a common conductive additive that is used to improve the otherwise poor electronic conductivity of silicon. When CB is added, the contact resistance between particles and the inner resistance in the particles is decreased, which improves the electronic conductivity, as well as it can construct an effective conductive network between the particles for electron transport. [35] CB will also accommodate for some of the extreme volume expansion of silicon during cycling, which improves the battery performance. [28]

## 2.4.5 Electrolyte

LP57 is a commonly used electrolyte for LIBs and it is composed of 1 M LiPF<sub>6</sub> in a mixture of ethylene carbonate (EC) and ethyl methyl carbonate (EMC) with a mixing volume ratio = 3:7 wt/wt (EC:EMC). [36, 37] LiPF<sub>6</sub> is important for the thermal stability of silicon based electrodes in contact with the electrolyte. [38] Other important electrolyte additives for silicon-based electrodes are fluoroethylene carbonate (FEC) and vinylene carbonate (VC), which have improved the cycle performance of silicon. [39–41] FEC protects the electrolyte from decomposition at the same time as it hinders the oxidation of the silicon electrode. FEC affects the SEI formation on the surface of the silicon electrode, which improves the cycling performance. [39] VC has shown impressive results even at a such low concentration as 2% on the capacity retention and the coulombic efficiency of silicon electrodes. [40]

## 2.5 Rheology

By definition, rheology is the study of deformation and flow of matter and describes the interrelation between an applied force on a material and the upcoming deformation over time. [42, 43]

The rheology of an electrode slurry is important to know, because the knowledge provides helpful information about how the slurry will act during and after the coating process of the current collector. With the knowledge about the slurry behaviour at different shear rates, the coating speed can be set to match desired properties. The viscosity of the slurry will decide how much the slurry will spread on the current collector and the sedimentation speed of the particles during the drying process, *i.e.* the particle gradient in the coating.

The quantitative parameters measured in rheology are stress and strain. The ratio of stress to strain is defined as the modulus. The stress is the amount of forces applied to a given area of a sample and it is measured in N/m<sup>2</sup> (Pa). If the stress is parallel to the surface, which it is during a rheological measurement, it is called shear stress. The strain is the degree of deformation the material experiences during an applied stress. The strain has no unit as it is purely geometrical. It can be described as how far a point moves in space during an exerted stress. The elastic modulus is the quantity how much a material can deform elastically by an applied stress. The strain will be higher the more stress is applied. Important to note is the time contribution to the system, as the magnitude of the strain is affected also by how long the stress is applied. The time contribution arises due to that most materials are not simple solids or liquids, which means that their elastic moduli and viscosity are not constants but functions varying over time, direction and speed of the applied force (flow in material) and surface area. [43]

In general, there are two types of materials, viscous and elastic materials. If the material is viscous, it is ideally Newtonian, which implies that its stress to strain rate response is linear (the stress is proportional to the strain rate with the viscosity being the proportionally constant) and its shear modulus ( $G^*$ ) will only consist of the loss modulus part ( $G''$ ). These materials flow freely during an applied stress, which is dissipated as heat. In contrary, elastic materials will deform instantly in response to an applied stress. For elastic materials, the ratio between the stress and strain is constant during applied stress, because the applied work on the material is stored in the material. Hence the term storage modulus ( $G'$ ), which is equivalent to shear modulus for elastic materials. [43]

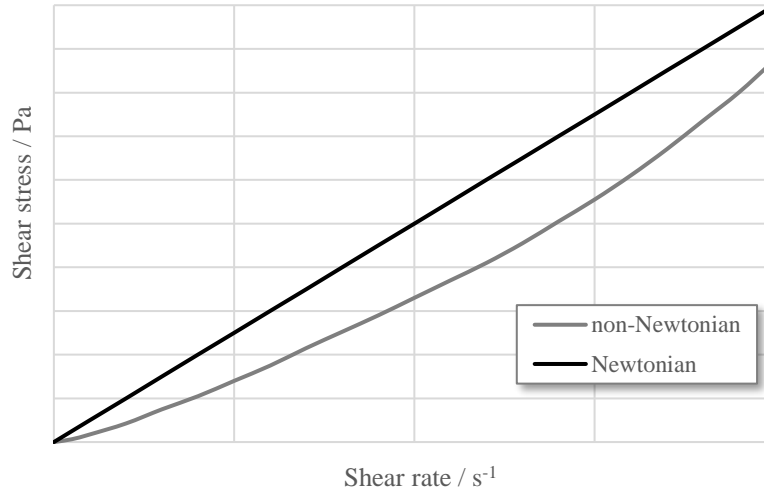


Figure 5: Example of two materials with a Newtonian and a non-Newtonian behaviour. The non-Newtonian behaviour is one example how it can behave.

As mentioned earlier, many materials are both elastic and viscous. These materials are so-called viscoelastic (and non-Newtonian) and during an applied stress the ratio between the stress and strain will change. Viscoelastic materials have both a loss and a storage modulus, which together make up the complex modulus for the material, seen in Equation (2):

$$G^* = G' + iG'' \quad (2)$$

Both of these moduli may change with time, temperature, rate of deformation etc, which means that a viscoelastic material can behave like both a viscous material and an elastic material, depending on the rate of deformation applied. [44]

## 2.6 Electrochemical testing

In order to evaluate the capacity of a material, electrochemical testing has to be performed. Electrochemical testing of battery cells can be performed by monitoring the voltage as a function of the charged passed. The obtained voltage information gives information about the materials and the chemical processes as they proceed during cycling. Galvanostatic cycling is an electrochemical method, where the current is held constant, measuring the changes in potential over time.

During cycling, the current of a battery is expressed as the C-rate. The C-rate is the fraction of a battery's capacity charged or discharged during one hour. It is expressed as  $C/t$ , where  $t$  is

time in hours for full charge/discharge. *E.g.* if the C-rate is 2C, the battery will charge or discharge completely in 0.5 hours, and if the C-rate is C/2, it will charge or discharge in 2 hours. High C-rates above C/2 are not recommended for LIBs as it shortens the lifetime. [45]

To achieve the maximum capacity of a battery cell, it is common to use the constant-current-constant-voltage (CCCV) method (galvanostatic cycling). In CCCV, a constant current is set during discharge until the voltage reaches a set cut-off voltage, then the cut-off voltage is held until a set cut-off current is reached. Thereafter an equivalent procedure is performed for the charging step. [46, 47]

An important parameter for secondary batteries is the Coulombic efficiency (C.E.), which is the output divided by the input. In batteries, output is the total specific capacity during discharge ( $C_{\text{dis}}$ ) and input is the total specific capacity during charge ( $C_{\text{cha}}$ ).

$$\text{C. E.} = \frac{C_{\text{dis}}}{C_{\text{cha}}}$$

The ideal case for secondary batteries is a *C.E.* of 100%, which means that the battery can be charged with the same amount of electric charge as it can deliver. It implies that the battery has an endless lifetime. Unfortunately, this is not possible in LIBs due to unwanted side reactions. [1]

## 3. Experimental

### 3.1 Materials

The materials used in the anode preparations were  $\mu\text{m}$ -sized silicon (Silgrain® e-Si 400, D50=3,1  $\mu\text{m}$ , ELKEM), nm-sized silicon (Alfa Aesar, crystalline, APS <50nm, 98%, laser synthesized from vapour phase, surface area 70–100  $\text{m}^2/\text{g}$ ), graphite powder (SLP30, particle size <30 $\mu\text{m}$ , Timcal Timrex), Carbon Black Super C65 (particle size 150 nm, Timcal C-Nergy), CMC-Na (Walocel CRT 2000 Pa, DS: 0.89, DOW), SBR (PSBR100, dispersed in water, 15%+-0.5% solid content. Targray) and as a solvent deionized water.

### 3.2 Lab-scale electrode preparations

The dry materials (silicon, graphite, CB and CMC-Na) were first premixed by lightly shaking the container before the liquids were added (SBR and water) and lightly shaken again. The slurries were thereafter ball-milled in a Retsch planetary ball mill for 90–120 minutes (until all solid components were dispersed). The slurries were coated on a 22  $\mu\text{m}$  thick copper foil (current collector) by a doctor-blade machine with a gap of 180  $\mu\text{m}$  and a coating speed of about 0.5 m/min, and then dried at ambient temperature for at least 24 h. 13 mm in diameter electrode discs were punched out and moved into an argon glovebox ( $\text{O}_2$ <10ppm and  $\text{H}_2\text{O}$ <3ppm) where they were dried in a vacuum oven at 80 °C for 12 h.

The surface finish of the electrodes was evaluated optically with a light optical microscopy and graded on a scale from 1 to 3 (3=best).

### 3.3 Pilot scale electrode preparations

The graphite and the solvent (water) were first premixed in a blender for 1 min at 500 rpm, before the silicon powder was added and mixed for 1 min at the same speed. Thereafter the CB was added and first mixed lightly with a spoon and then with the blender for 1.25 h at 4000 rpm. Then the binders were added (dissolved in water) and mixed for 45 min at 500 rpm, then a few more minutes at 700 rpm until all solids were dispersed. The slurry was coated on a pilot line at LiFeSiZE (company) on a copper foil with a thickness of 9  $\mu\text{m}$ . The slurry was coated with a gap of 180  $\mu\text{m}$  and a coating speed of 1 meter/min. The coating was rolled up and dried at ambient temperature for two weeks. 13 mm in diameter electrode discs were punched out and moved into an argon glovebox ( $\text{O}_2$ <10 ppm and  $\text{H}_2\text{O}$ <3 ppm) where they were dried in a vacuum oven at 80 °C for 12 h.

### 3.4 Mass loading

The mass loading for each electrode composition was obtained by weighing three electrodes, removing the coating (by washing in water and ethanol) and weighing them again. The mass

loading was then obtained by calculating an average value of the mass difference for each electrode. The mass loading was calculated this way because the substrate thickness (copper foil) varied between 19–23  $\mu\text{m}$ , which would affect the direct weight value of each electrode if they were weighed separately. The mass loading calculations were performed before the electrodes were dried in the vacuum oven, which means they may still have contained solvent traces. Four random samples were weighed after they were dried in a vacuum oven to evaluate the mass loading difference compared with before vacuum drying. The weight of each sample was well within the standard deviation for each electrode, which means the calculated mass loadings before vacuum drying are accurate.

### 3.5 Thickness

The thickness of the electrodes was obtained with an ABS Digimatic Indicator ID-C112B from Mitutoyo Corporation, by randomly measuring the thickness of the coating on the copper foil at seven different places and neglecting the highest and lowest values to minimize random thickness errors. The thickness was calculated from the remaining five values as an average value (copper foil thickness (22  $\mu\text{m}$ ) was first subtracted).

### 3.6 Adhesion testing

Two types of adhesion tests of the coatings on the current collector were performed on the electrode samples. In the first test, the electrodes were pulled over the edge of a table (pull test), and the electrodes were deformed in a 90° angle, shown in Figure 6A.

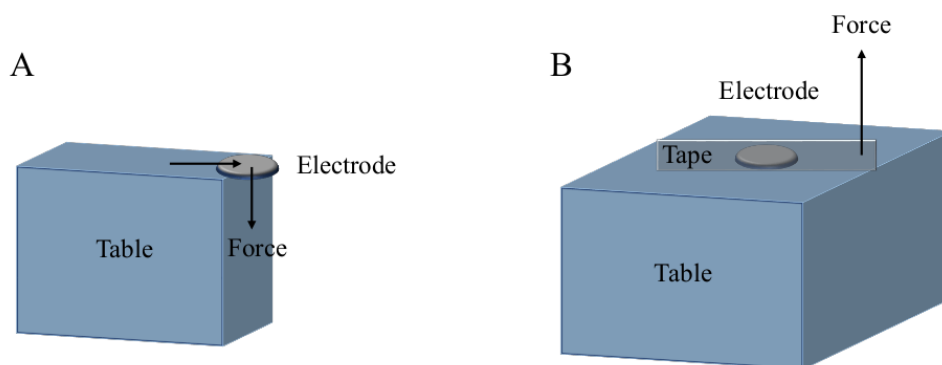


Figure 6: Schematic figure of the adhesion tests, where A is the pull test and B is the tape test.

In the second test, a piece of tape was attached on the surface of the electrode and stripped away in a 90° angle towards the surface of the electrode (tape test), shown in Figure 6B. Both tests were performed by hand, which implies that the deformation speed in the first test and the removal force of the tape will change between each test. To minimize the errors, all tests were performed at the same time and by the same person, believing the deformation speed and stripping force would be similar for all electrodes. The tape test is a common way to analyse the adhesion of the coating on the current collector, although it is typically performed with a machine to obtain an equal force for each measurement. [48, 49]

### 3.7 Rheology

The rheological measurements were carried out with an Advanced Rheometer 2000 (AR2000) from TA Instruments at 25 °C using a cone-and-plate geometry. A stainless steel cone with a diameter of 40 mm and cone angle of 2° was used for the measurements. During the measurements the sample area was covered with a hydrated cover to minimize the risk of dried-out samples during measurements. The density of the samples was assumed to be close to water (the solvent), as it contribute to most of the weight. A schematic setup over the measurement is shown in Figure 7.

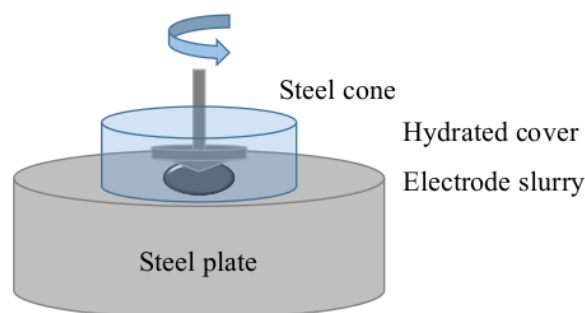


Figure 7: Schematic figure of the rheology measurement.

Two types of measurement were carried out on the samples: steady state flow and frequency sweep. The steady state flow measurement measures the flow in the material (the viscosity) and is performed with a constant spinning direction. During the steady state flow measurement, the controlled variable is the shear rate, *i.e.* the deformation speed of the material, which was set to start at  $0.01\text{ s}^{-1}$ , go up to  $500\text{ s}^{-1}$  exponentially and down again. 48 data points were recorded in this interval each way with a total of 96 data points. The steady state flow test gives the shear stress in the material at different shear rates. The frequency sweep measurement is an oscillation method, which means the spinning direction oscillates during the measurement. The frequency sweep measurement is used to measure the viscoelastic properties of a material. In this test, the controlled variables are the frequency (and the strain), which was set to go from 0.1 Hz up to 10 Hz. The instrument recorded 21 data points during this interval. Frequency sweep tests give information about the dynamic (complex) modulus in the material and its two parameters, the storage and loss modulus. The frequency sweep measurements were made on the samples to distinguish the differences between  $\mu\text{m-Si}$  and  $\text{nm-Si}$ . Before the steady state flow measurements, an initial pre-shear was performed on the samples for 1 min at a shear rate of  $1\text{ s}^{-1}$ , to simulate the initial action of the blade (of the casting machine) forcing the slurry to flow and break down its internal structure. [31]

### 3.8 Dynamic Light Scattering (DLS)

A Zetasizer Nano Range from Malvern Instruments was used to measure the particle size distribution of two different silicon powders, the silicon powder used in the electrodes of this thesis and of a small nanometre-sized silicon powder. The powders were dispersed in deionized water and put in disposable cuvettes during the measurements, which were carried out at a temperature of 25 °C. The reflective index of silicon and water was set to 4.000 and 1.330,

respectively during the measurement. The absorption of silicon was assumed to be zero. Three measurements were performed on each sample with a duration of 80 s for each measurement.

### 3.9 N<sub>2</sub>-physisorption

N<sub>2</sub>-physisorption measurements were performed on the two different silicon powders with an ASAP2020 physisorption equipment from micromeritics to distinguish the specific surface area of the powders. In order to perform the measurement of the samples, the sample holder (including the sample inside) has to be degassed and refilled with adsorbate gas (nitrogen gas). When the gas is replaced with nitrogen gas, the instrument measures how many nitrogen molecules adsorb on the surface of the measured sample. The measurement is carried out at the boiling temperature of the adsorbate gas, *i.e.* at 77 K (−196 °C), the boiling temperature of nitrogen.

### 3.10 Scanning electron microscopy (SEM) and Energy-dispersive spectroscopy (EDS)

A Zeiss 1550 with Aztec EDS was used to analyse the morphology and how homogenous the particle distribution in the electrodes were. The measurements were performed at different magnifications to achieve a good picture of the surface structure. To complement and give a complete picture of how homogenous the particle distribution of the active material was, EDS was used to map the surface of the electrodes.

### 3.11 Half-cell assembly

The battery half-cells were assembled in what is commonly called pouch cells. Pouch cells are bags made of aluminium foil, coated with a polyethylene layer to make it air- and waterproof. In the assembly of the pouch-cells, two electron-conducting nickel foil tabs were inserted into the bag, which was sealed at this side by heating and then moved into the glovebox.

In the glovebox, the pouch-cell assembly was finalised according to Figure 8.

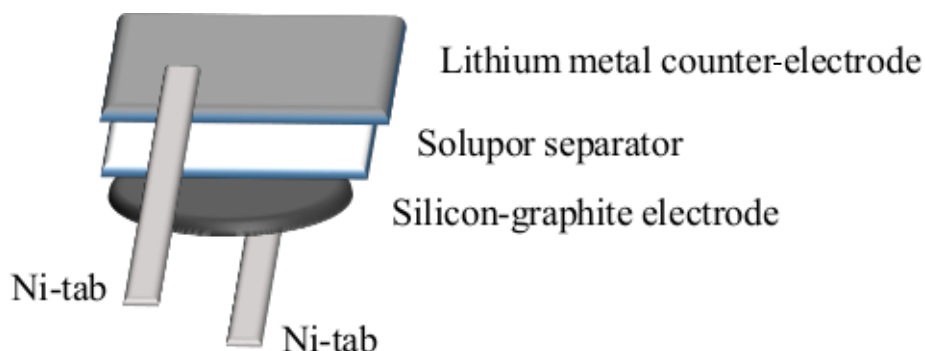


Figure 8: Schematic figure of the electrode setup in the pouch cell.

The silicon–graphite electrode was placed on one of the Ni-tabs in the pouch cell bag, on which a larger Solupor separator (polyethylene-based separator) was placed. The electrode and

separator were soaked in 50  $\mu$ l of the electrolyte LP57 (1 M  $\text{LiPF}_6$  in EC/EMC 3:7 wt/wt) + 10% FEC + 2% VC. On top of the separator, the counter electrode (lithium metal foil) and the second Ni-tab was placed. The lithium metal piece was large enough to cover the entire silicon electrode. The pouch cell was thereafter vacuum-sealed on the remaining three sides (down to 30 mbar).

### **3.12 Electrochemical testing**

In the electrochemical testing experiments, the galvanostatic CCCV method were used on the half-cells, which were cycled at the C-rates C/2 and C/10. Four different instruments were used for the electrochemical tests, three instruments (a Bio-Logic MPG2 and two Arbin BT-2043) were located at the Ångström laboratory and one was placed at the company LiFeSiZE (Arbin BT-2043). During the electrochemical tests, the lower cut-off potential was set to 0.05 V and the higher was set to 1.5 V. The cut-off current was set to C/50 for each electrode.

## 4. Results and discussion

In general, as an electrode material in LIBs, small nanometre-sized particles are favourable over larger particles due to shorter diffusion lengths for lithium-ion transport, higher surface area and better mechanical properties. The shorter diffusion lengths enhance the rate capability and power density of the battery, the higher surface area increases the contact area between the electrode and electrolyte resulting in a higher rate capability and the better mechanical properties increases the cycle life. The main drawback of smaller (nano) particles is the higher price compared with larger particles, which is an important parameter for commercial LIBs. [6, 50, 51] Therefore, a relatively cheap silicon powder in the micrometre scale is added as a minor component to the graphite electrodes used within this project. To concretise the price difference, the price for the nanometre silicon powder (<50 nm) in this project is between 11400–19500 SEK for 50 g, depending on the supplier, [52, 53] while the price for a silicon powder in the size range 0.2–0.3  $\mu\text{m}$  is 3100 SEK for 100 g [54] (no price information was available for the specific micrometre silicon powder used in this project).

### 4.1 Experimental setup

The anodes studied consist of the following components: the active materials silicon and graphite, the binders CMC-Na and SBR, the conductive additive CB and the solvent water. The electrode setup is shown in Figure 9.

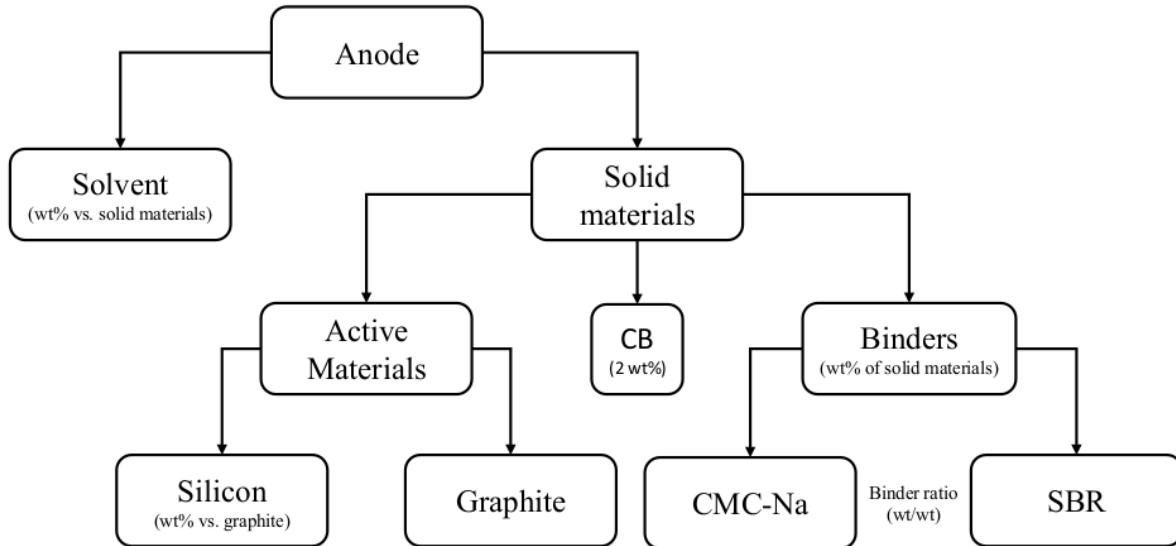


Figure 9: Setup of the components in the electrodes. The solvent, binders, silicon and binder ratio (CMC-Na vs. SBR) are the varied components in the electrodes.

To evaluate how these components affect the rheological properties of the electrode slurry and the performance of the anode, the amounts of each component in the anodes were varied (CB was kept at a set value of 2% of the total amount of solid material), as seen in Figure 9.

Each component amount was varied according to Table 1–4. The component marked in bold is the one that was varied, while the change of the counter-component was an effect of it.

Table 1: Solvent and solid material variations in the electrode slurries. Bold-marked (solvent) is the varied one.

Anode	
<b>Solvent</b> / wt%	Solid material / wt%
60	40
65	35
70	30

Table 2: Solid materials variations in the electrodes. Bold-marked (binder) is the varied component out of interest.

Solid material		
<b>Binder</b> / wt%	Active Material / wt%	CB / wt%
3	95	2
5	93	2
7	91	2

Table 3: Active material variations in the electrodes. Bold-marked (silicon) is the varied component out of interest.

Active material	
<b>Silicon</b> / wt%	Graphite / wt%
5	95
10	90
15	85

Table 4: Binder ratio variations in the electrodes.

Binder ratio	
CMC-Na / wt%	SBR / wt%
2	0
2	1
2	2
2	3

In total, there are 108 different possible electrode compositions within this matrix. To get a good picture of how each component affected the rheology and battery performance, without testing all different compositions, a software program called MODDE was used to obtain a setup of fewer samples to study. MODDE calculates and gives a diverse and representative set of compositions to study in a process containing two or more variables. It suggests an efficient number of experiments per variable, to give a good representative picture how of each variable is affecting the outcome. [55]

## 4.2 Electrode preparation and processing

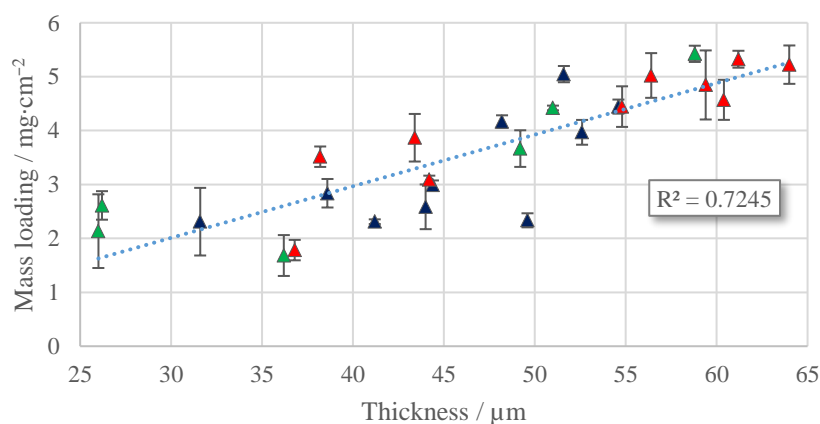


Figure 10: Correlation between the mass loading and thickness of the studied electrodes. The colours refer to the binder amount in the electrode according to: red = 7%, green = 5% and blue = 3%.

In Figure 10, the correlation between the mass loading and the coating thickness of the electrodes is shown. The results show a clear correlation between the mass loading and the coating thickness of the samples, where a high coating thickness gives a high mass loading. However, there are some deviations, especially for the electrodes with low mass loadings. The standard deviations for each sample varies a lot between the electrodes. Here there seems to be no clear trend between the deviation and mass loadings. The binder amount possibly has a small impact on the mass loading and thickness, where an increased amount correlates with increased mass loading and thickness.

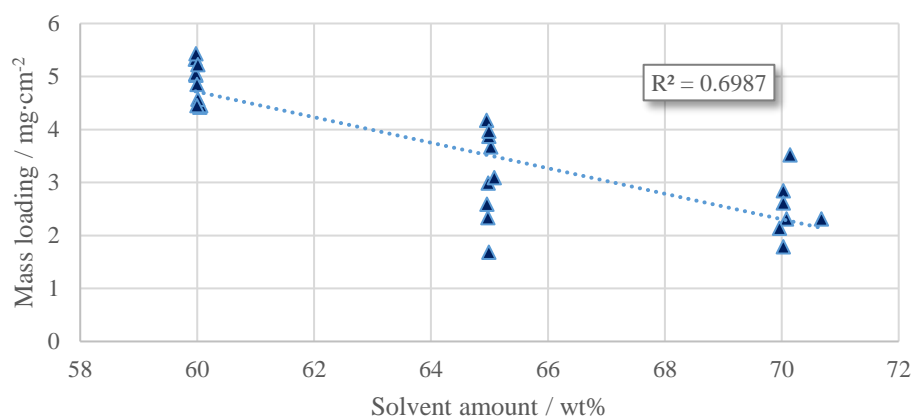


Figure 11: Correlation between the mass loading and solvent amount in the electrode slurries.

A parameter that strongly affects the mass loading of the electrode is the solvent amount in the electrode slurry, shown in Figure 11. The figure indicates that the mass loading decreasing with an increasing amount of solvent. This is true as long as the coating parameters are kept constant, which they have been between the coating processes. The mass loading becomes higher when the solvent amount is lower, because the slurry will be thicker and more concentrated. As the water-based coatings dried rather fast, the slurries did not have time to spread out on the surface, which implies that the coating becomes thicker and the mass loading higher.

As the binder seems to have some influence on the mass loading and thickness of the electrodes (seen in Figure 10), it is of interest to define if and to what degree each binder affects it. Figure 12 shows the correlation between the mass loading and the binders.

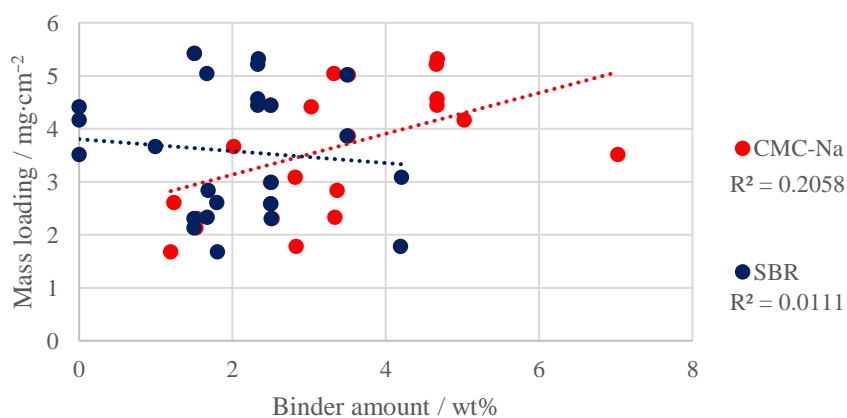


Figure 12: Correlation between amount of each binder (CMC-Na and SBR) in the electrode slurry and mass loading of the electrodes.

As it is seen in Figure 12, there is no clear correlation between the mass loading and the binders. However, to confirm this behaviour, the combined influence of CMC-Na (as it has a higher R-value than SBR) and the solvent on the mass loading of the electrodes is shown in Figure 13.

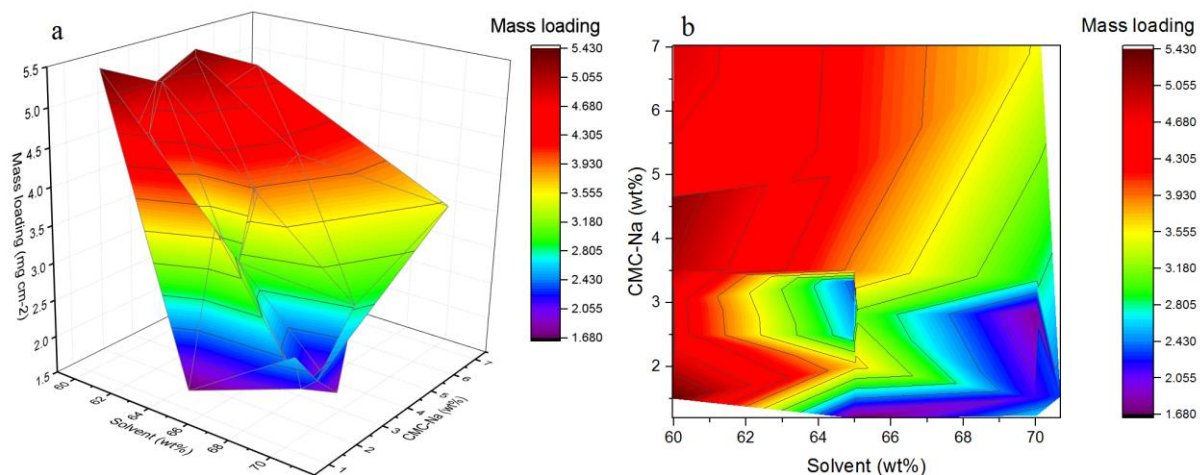


Figure 13: 3D (a) and 2D (b) representation of the influence from the amount of solvent and CMC-Na in the electrode slurry on the mass loading of the electrodes.

Figure 13 confirms the earlier results that there is a strong correlation between the solvent and the mass loading, but no strong correlation between CMC-Na and the mass loading. Nevertheless, an interesting behaviour is seen in Figure 13b when the CMC-Na amount is below ~3 wt%. Below this amount, the mass loading is uncertain with large variations. This implies that it is harder to control the mass loading of the electrodes when the CMC-Na amount is below 3 wt% in the electrode.

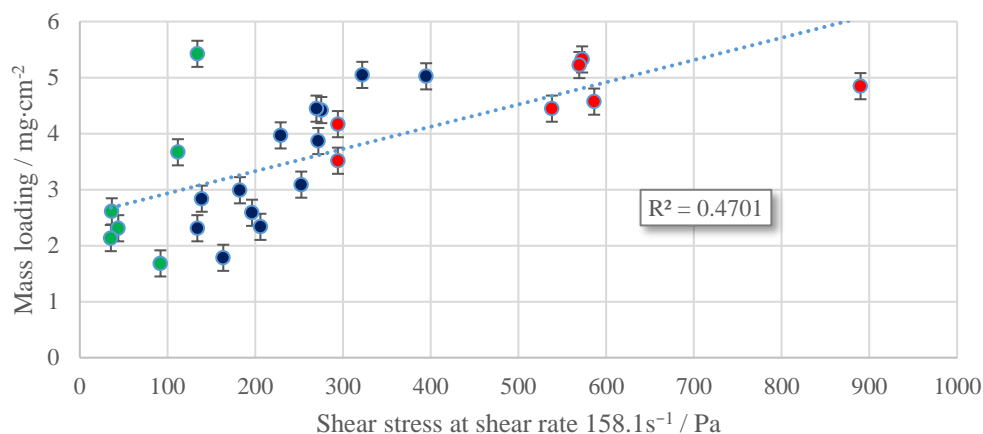


Figure 14: Correlation between the mass loading and shear stress at the shear rate 158.1 s<sup>-1</sup> of the electrode slurries. The colours are the CMC-Na amount in the slurry in following ranges: red=4–7% CMC-Na, blue=2.5–4% CMC-Na, green 0–2.5%.

By the look in Figure 14, it seems like the rheological properties of the electrode slurry and the shear stress have an impact on the mass loading of the electrodes, *i.e.*, the viscosity itself of the electrode slurries is affecting the mass loading. However, when the effect from the solvent is disregarded, by separating the electrode slurries with different solvent amounts from each other, the results in Figure 15 is obtained.

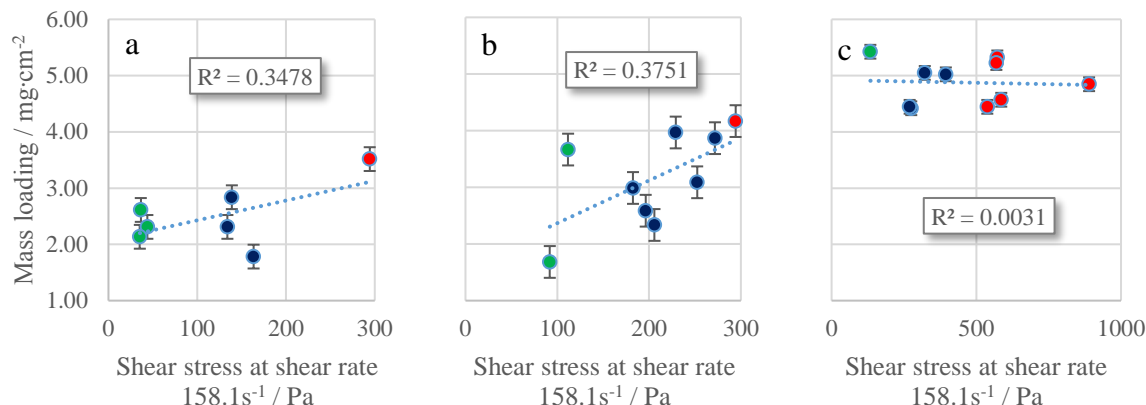


Figure 15: Correlation between the mass loading and shear stress at the shear rate  $158.1 \text{ s}^{-1}$  for each electrode slurry, where (a) is electrode slurries containing 70 wt% solvent, (b) 65 wt% solvent and (c) 60 wt% solvent. The colours are the CMC-Na amount in each slurry in following ranges: red=4–7% CMC-Na, blue=2.5–4% CMC-Na, green 0–2.5%.

When the solvent effect on the mass loading is isolated, it is possible to see in Figure 15 that the shear stress does not notably affect the mass loading of the electrodes, *i.e.*, it is the solvent amount in the electrode slurry that is affecting the mass loading directly by affecting the viscosity of the slurry. The shear stress is measured at the shear rate  $158.1 \text{ s}^{-1}$ , which is about the same shear rate as the electrode slurries experience during the coating process. This indicates that it is important to know the process parameters during the coating process to obtain the desired properties of the electrodes. Figure 14 and Figure 15 also reveal that the CMC-Na amount in the slurries has an influence on the shear stress (as it is increasing with increasing CMC-Na content).

To evaluate the influence of CMC-Na (and SBR) on the shear stress of the electrode slurries, the correlation between the shear stress and the binder amount is shown in Figure 16.

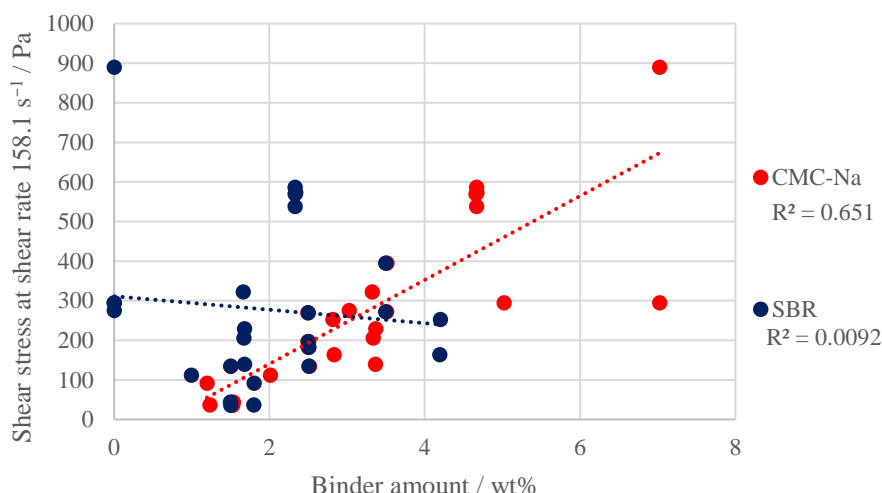


Figure 16: Correlation between the amount of each binder (CMC-Na and SBR) in the slurry and the shear stress at the shear rate  $158.1 \text{ s}^{-1}$ .

From the results in Figure 16, it is clear that there is a correlation between the CMC-Na amount and the shear stress, but not between the SBR and the shear stress. This could be explained by the strong interactions between CMC-Na and Si in the electrodes that bind particles together, which are increasing with an increased amount of CMC-Na. [17, 25, 26, 33] When these intermolecular carboxyl-bridges between the particles in the slurry increases, it results in a

higher degree of elasticity in the electrode slurry, which decreases its ability to deform and the shear stress becomes higher. [31] The reason why SBR is not affecting the shear stress of the electrode slurry is that it is a latex-based material (hydrophobic). In the slurry, SBR will be dispersed like small isolated particles not interacting with the solvent (water), and therefore not affecting the shear stress of the electrode slurries.

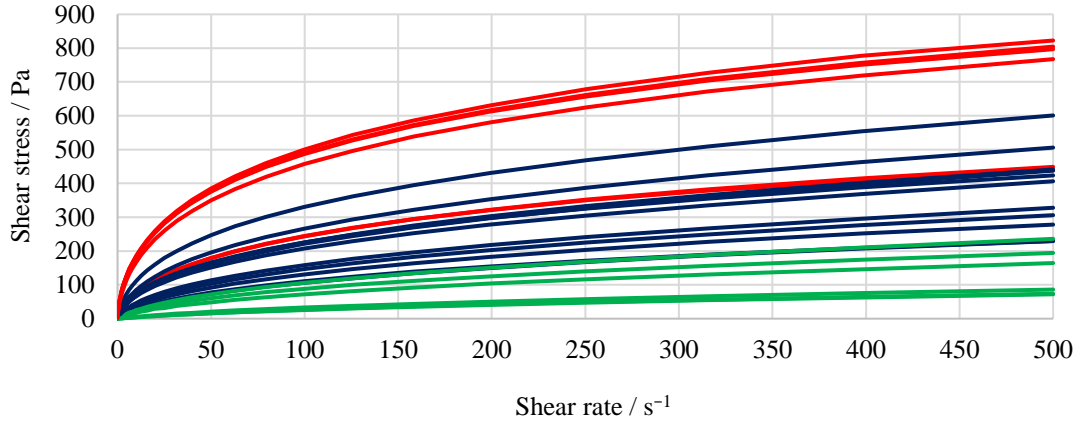


Figure 17: Shear stress as a function of the shear rate of the slurries. The colours are the CMC-Na amount in the slurry in the following ranges: red=4–7% CMC-Na, blue=2.5–4% CMC-Na, green 0–2.5%.

Figure 17 confirms the clear correlation between the shear stress and the CMC-Na amount in the electrode slurries and that it is a correlation over the whole shear rate interval 0–500 s<sup>-1</sup>.

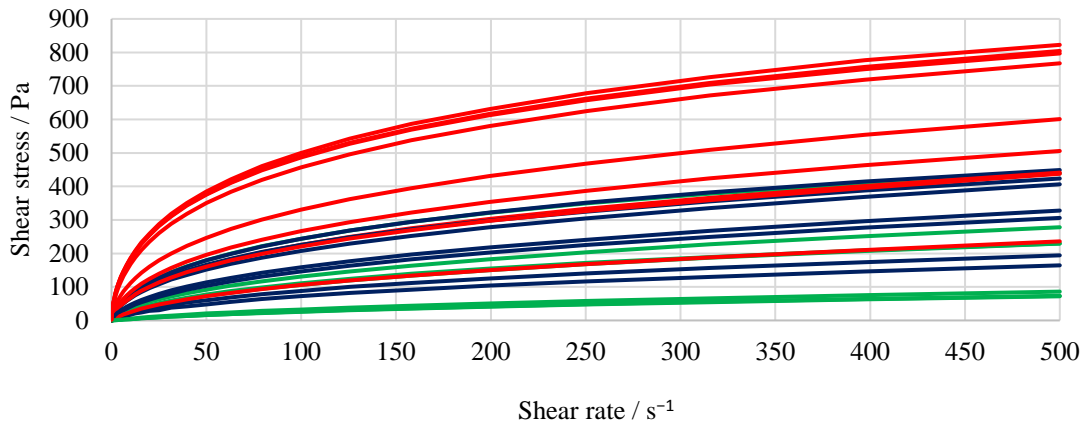


Figure 18: Shear stress as a function of the shear rate of the slurries. The colours are the solvent amount in the slurries in the following ranges: red=60% solvent, blue=65% solvent, green=70% solvent.

As the mass loading is strongly affected by the solvent amount and the shear stress is affecting the mass loading, it is of interest to evaluate the influence of the solvent on the shear stress. Figure 18 shows that there is a clear correlation also between the shear stress and the solvent amount, as the shear stress is increasing with a decreasing amount of solvent over the whole shear rate interval 0–500 s<sup>-1</sup>. The shear stress increases due to when the volume fraction of the particles in the slurry increases, it leads to a higher degree of interconnected particles throughout the system by weak attractive forces between the particles, which will lead to cluster formations (flocs). At lower solvent amounts, these flocs will interconnect to each other, creating a weak network structure in the electrode slurry, which is able to transmit a force and support shear stress. [56] Normally, a network structure implies that the slurry has a yield stress, but as the behaviour of suspended silicon can be approximated to the behaviour of hard-spheres,

it is not always the case. Hard-sphere colloidal suspensions do not experience interactions between the particles until the point of contact. [57] When the particle volume fraction in the suspension is low, the interactions between them are negligible and the rheology is Newtonian, but at high particle volume fractions, the suspension will develop a yield stress due to the formation of chains and networks of touching particles. [58]

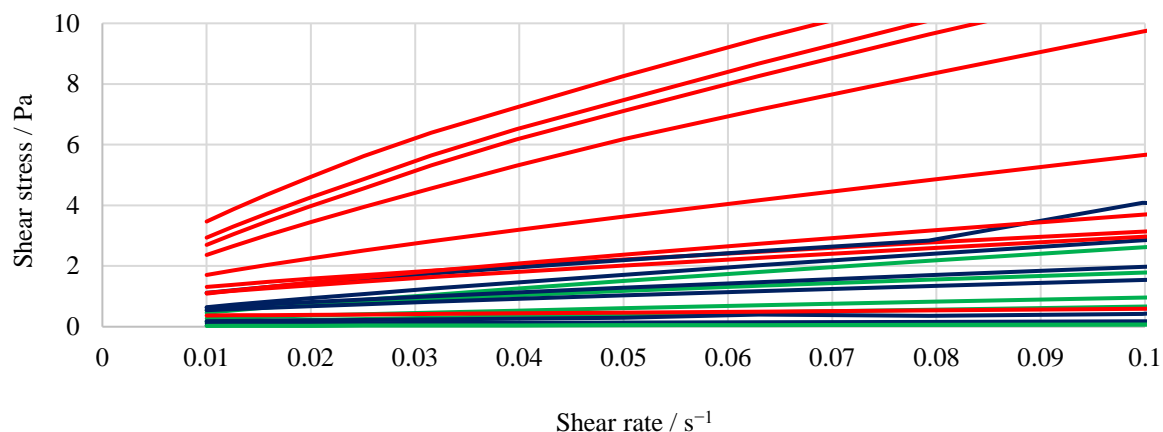


Figure 19: Shear stress as a function of the shear rate of the slurries at low shear stresses and shear rates. The colours are the solvent amount in the slurries in the following ranges: red=60% solvent, blue=65% solvent, green=70% solvent.

In Figure 19 the hard-sphere behaviour of the slurries is confirmed. At low particle volume fractions (high solvent amount), the slurries experience no yield stress but at high particle volume fractions (low solvent amount), a small yield stress might be developed.

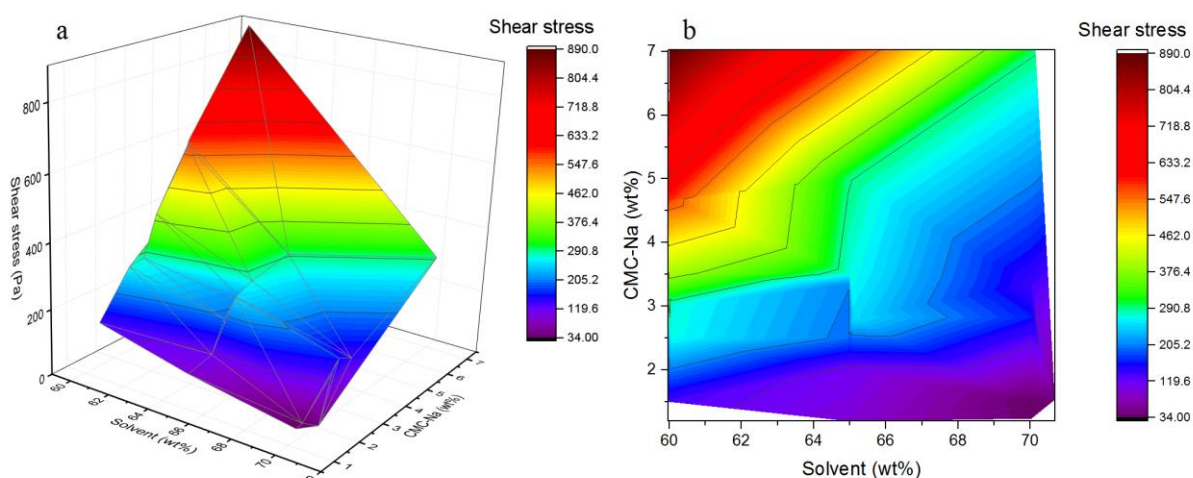


Figure 20: 3D (a) and 2D (b) representation of how the solvent amount in the electrode slurry and CMC-Na amount in the electrode affect the shear stress at the shear rate  $158.1 \text{ s}^{-1}$  of the electrodes.

Figure 20 confirms the results that both the particles and the CMC-Na have an effect on the shear stress, *i.e.*, both the CMC-Na and the solvent correlate with the shear stress. Visually it is clear in Figure 20 that the shear stress is increasing with an increasing CMC-Na amount and a decreasing solvent amount.

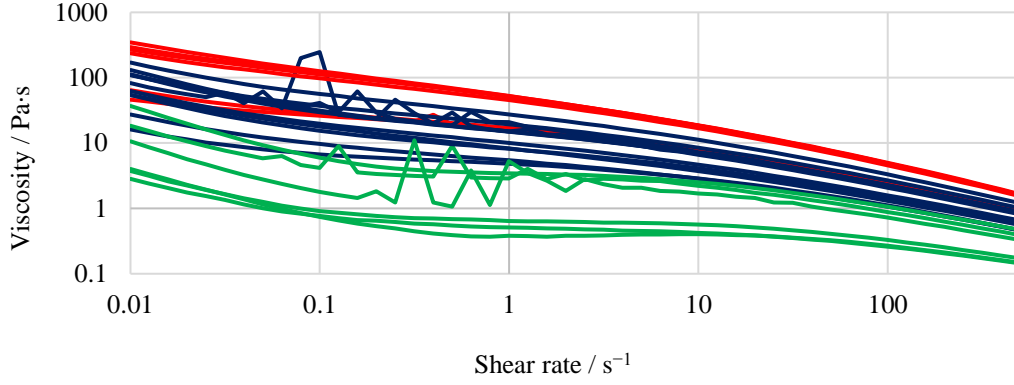


Figure 21: The apparent viscosity as a function of the shear rate for the studied electrode slurries. The colours are the binder amount in the slurry in following ranges: red=4–7% CMC-Na, blue=2.5–4% CMC-Na, green 0–2.5% CMC-Na.

As is seen in Figure 21, all slurries are showing a shear thinning behaviour (decreasing viscosity with increasing shear rate) [24, 31, 59] over the shear rate interval  $0.01 \text{ s}^{-1}$  to  $500 \text{ s}^{-1}$ . This implies that (any) agglomerates in the material break down and that the slurries are flowing over the whole shear rate interval. This behaviour favours a homogenous distribution of the particles without defects like strips on the electrode surface. [59–61] This behaviour also confirms that the slurries are behaving like hard-spheres. [57, 58] If the viscosity is increased with an increasing shear rate (shear thickening behaviour), it implies formation of agglomerates, which decreases the homogenous distribution of the particles on the electrode. [60, 61]

In summary, it is the CMC-Na amount and the solvent amount in the electrode slurry that is affecting the processing parameters in the preparation of the electrodes. These parameters are important to control to obtain desired mass loading, which will affect the cycling performance of the electrodes.

### 4.3 $\mu\text{m-Si}$ vs. $\text{nm-Si}$

An interesting behaviour of all electrode slurries is that they in contrast with slurries made from the more commonly used  $\text{nm-Si}$  powder [50, 51] show limited signs of viscoelastic properties; instead all electrodes show a viscous behaviour, as seen in Figure 17 and 18 (with no or only a very low yield stress). [57] To evaluate the behaviour of the  $\mu\text{m-Si}$  used here, its viscoelastic behaviour was analysed and compared with a  $\text{nm-sized}$  silicon material. An oscillation measurement was performed on both materials (with the same compositions, 10 wt% silicon (of the active material), 5 wt% binder, binder ratio 2:1 CMC-Na:SBR and 65 wt% solvent) with the results shown in Figure 22.

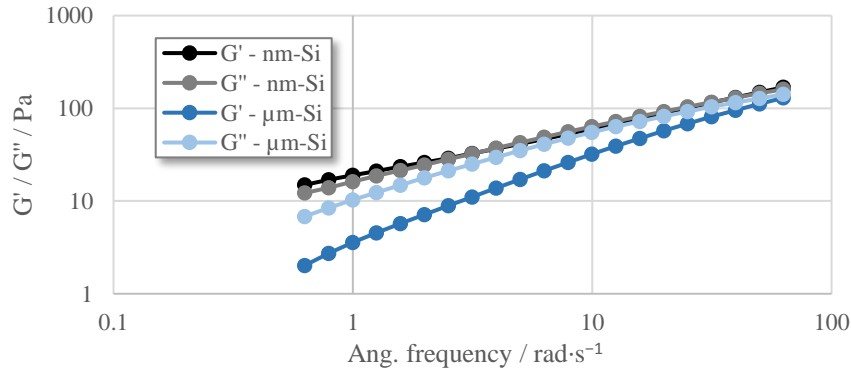


Figure 22: Oscillatory shear of a  $\text{nm-Si}$  and a  $\mu\text{m-Si}$  electrode composite (composition: 10% silicon, 5 wt% binder, binder ratio CMC-Na:SBR 2:1 (wt/wt) and 65 wt% solvent) with the storage ( $G'$ ) and the loss modulus ( $G''$ ).

From the results shown in Figure 22, it can be seen that the  $\mu\text{m-Si}$  shows a predominantly viscous behaviour as the loss modulus ( $G''$ ) is larger than the storage modulus ( $G'$ ) over the whole measured interval, while the nm-Si material shows a cross-over of  $G''$  and  $G'$ . The cross-over indicates that the material exhibits both predominantly elastic or viscous behaviour depending on the applied frequency (the applied shear stress) within the measured frequency range. [57]

When the slurries consist of solely silicon as the active material and the SBR binder is removed, the behaviour of the respective silicon material is clear, as seen in Figure 23.

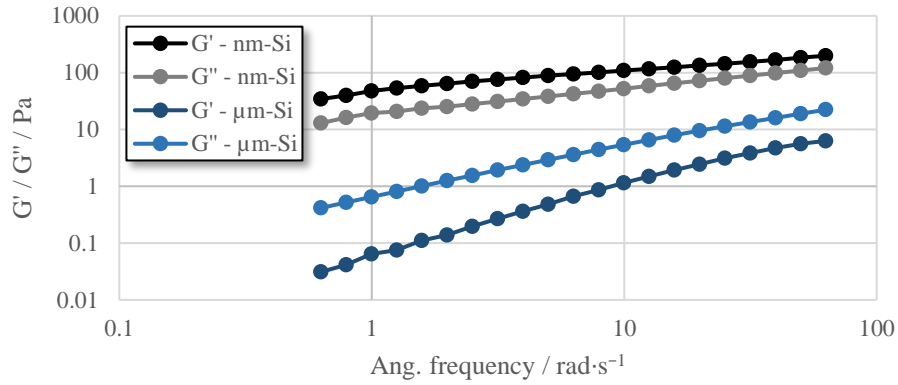


Figure 23: Oscillation measurement (FS) of the nm-Si and  $\mu\text{m-Si}$  powder with the slurry composition of the solid materials 80:12:8 – Si:CB:CMC-Na and a solvent amount of 86.5 wt%.

The electrode slurries in Figure 23 consist of the following composition of the solid materials: 80:12:8 – (Si:CB:CMC-Na) and the solvent amount is about 86.5 wt% for each slurry. When the slurries consist of solely silicon as the active material, the viscous behaviour at high frequencies in the nm-Si composite electrode disappears and it shows predominantly elastic behaviour over the whole frequency interval. This is an indication that the viscous behaviour arises from the graphite when nm-Si is used.

To evaluate the impact of CMC-Na on the viscoelastic behaviour of nm-Si, the CMC-Na was removed from the nm-Si slurry in Figure 22 and replaced with water. The results are shown in Figure 24.

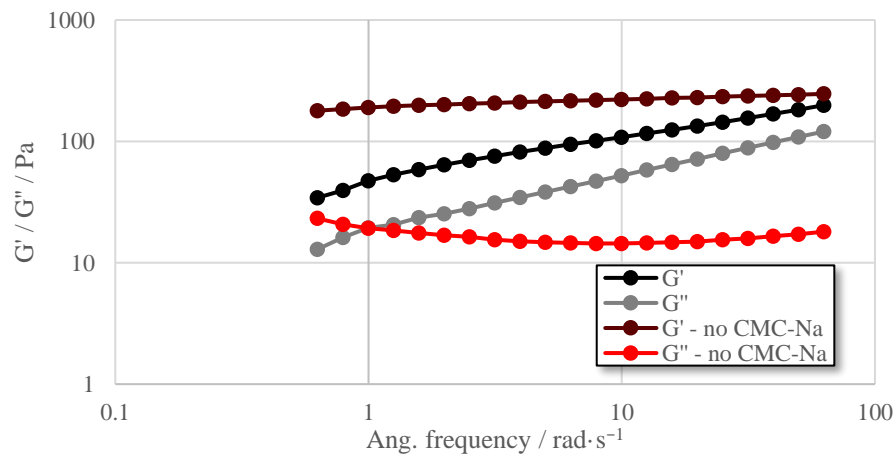


Figure 24: The storage modulus ( $G'$ ) and the loss modulus ( $G''$ ) of nm-Si electrode slurries (80:12:8 composition, with CMC-Na replaced with water for one sample) with and without CMC-Na.

When CMC-Na is removed from the electrode slurry, the nm-Si slurry still shows a predominantly elastic behaviour, indicating that it is the silicon itself that induces the viscoelastic behaviour.

To be sure the silicon powders actually are the sizes the suppliers declare, DLS measurements were performed on each powder. DLS is an optical method used for measuring the size distribution of particles. DLS measures the Brownian motion of suspended particles in a liquid; the rate depends of the size of the particles. These movements are measured with a laser beam in the DLS technique. [62]

In order for the DLS measurement to work properly the analysed particles have to be well-dispersed in the solvent and it should be almost see-through. This was not the case for any of the samples. Both were turbid, and it was possible to see bigger particles in the cuvette. Both samples were diluted many times, with not much of improvement. The measurement was performed anyway as the instrument itself gives a prognosis of the quality of the analysis when it is finished. The instrument indicated good quality, so the results were used. In Figure 25, a graphical size distribution of  $\mu\text{m-Si}$  and nm-Si from three individual measurements of each silicon powder is shown.

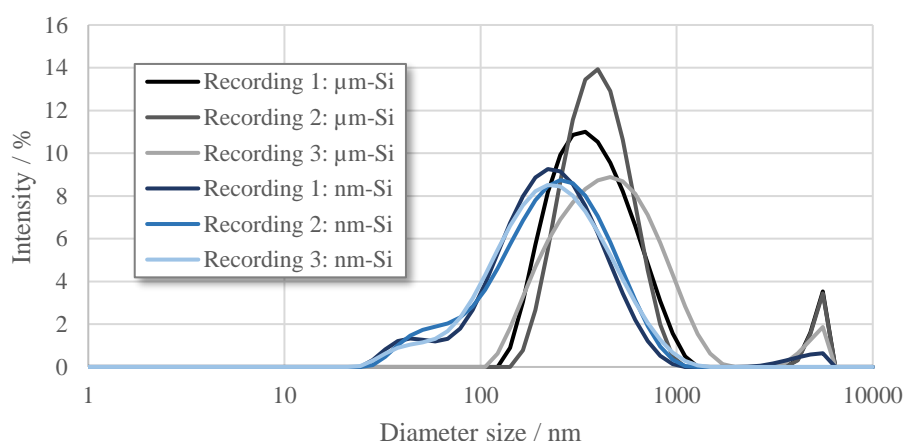


Figure 25: Size distribution of the  $\mu\text{m-Si}$  and nm-Si powder obtained from the DLS measurements.

$\mu\text{m-Si}$  has a relatively clear size distribution with nice Gaussian distribution of the particles and an average size of 400–500 nm (mean value 436.3 nm). Interestingly, the nm-Si powder have a wide-spread size distribution up to 1000 nm, when according to the supplier it is supposed to be <50 nm. A small peak average at 44.66 nm is visible, but it only accounts for 6.1% of the whole sample. This is a common phenomenon for DLS when measuring small nanometre particles [63–65]. The main peak from the three measurements that arises between 260–270 nm (average 267.4 nm) can be a contribution from aggregates (as mentioned above), dust particles or simply undesired larger silicon particles [63]. This is a problem with DLS, as the signal can be dominated by larger particles which scatter the light more. [65] The peaks for a size in the high range around 5000 nm most probably arise from aggregates of the particles in the dispersions. [63]

As the DLS measurement did not present clear results about the size difference between the two silicon powders, a  $\text{N}_2$ -physisorption measurement was performed on each silicon powder.  $\text{N}_2$ -physisorption is a method to measure the specific surface area and the pore size distribution of a sample. The method is explained by the Brunauer-Emmett-Teller Theory (BET), which

calculates the specific surface area and pore size distribution of the sample. The BET-theory includes the following criteria: The adsorbate can physically adsorb on adsorbent in infinite layers, the molecules can only interact with adjacent layers and Langmuir's theory is applied on each layer. The most common adsorbate gas is nitrogen gas ( $N_2$ ) and the experiments are carried out at its boiling temperature of 77 K. [66]

From the measurement and with the BET-theory, the specific surface area for each silicon powder were calculated to:

- nm-Si: 45.22  $m^2/g$
- $\mu m$ -Si: 4.10  $m^2/g$

These results indicate that the specific surface area of each silicon powder is accounting for the difference in their rheological behaviour. To verify if this is true, a dilution series was formed, where the nm-Si slurry in Figure 23 was diluted until its surface area per solvent volume/weight was the same as the  $\mu m$ -Si in the same figures. The shear stress/viscosity was measured for each slurry in the dilution series. A solution with only CMC-Na was also made, to confirm its influence on the slurries.

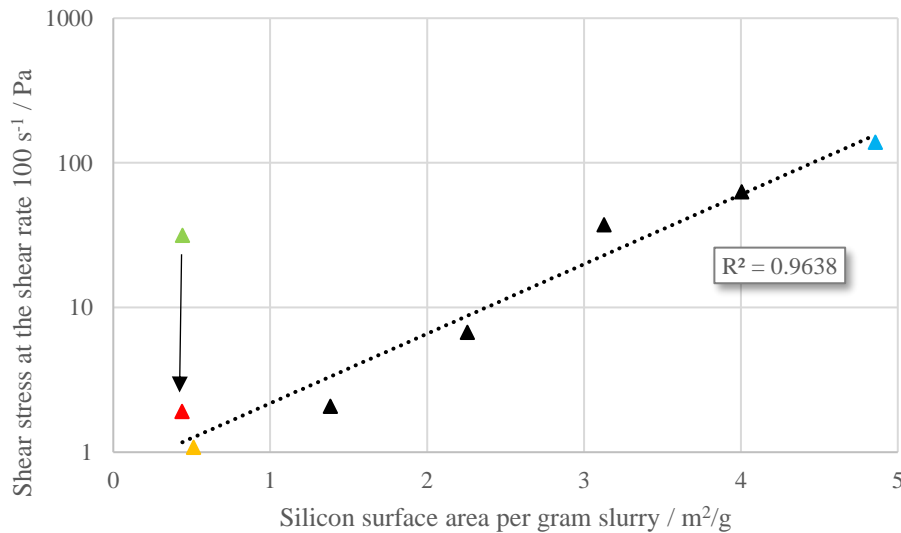


Figure 26: Results from the dilution series of nm-Si. The black, blue and golden triangles are the slurries from the dilution series of the nm-Si, the red triangle is the  $\mu m$ -Si slurry with the same amount of CMC-Na per gram slurry as the nm-Si, and the green triangle is the  $\mu m$ -Si slurry a higher amount of CMC-Na per gram slurry than the nm-Si.

Figure 26 shows the results from the dilution series of nm-Si including two  $\mu m$ -Si slurries. The green ( $\mu m$ -Si) and blue (nm-Si) triangles are the two original slurries in Figure 23, the red triangle is the  $\mu m$ -Si slurry with the same ratio CMC-Na:gram slurry as the nm-Si slurries in the dilution series and the golden triangle is the final nm-Si slurry. As is seen in Figure 26 the  $R^2$ -value is close to 1 (not including the green  $\mu m$ -Si triangle), which demonstrates that the correlation between the surface area per gram slurry is good. However, the shear stress is not the same for the diluted nm-Si slurry (golden triangle) as for the original  $\mu m$ -Si slurry. Therefore the CMC-Na amount in the  $\mu m$ -Si slurry was decreased until the CMC-Na:gram slurry was the same as for the nm-Si. It resulted in the red triangle in Figure 26, which coincides with the trend line of the nm-Si dilution series. To confirm the contribution of CMC-Na, a solution containing only the binder was made. Its shear stress was close to the green  $\mu m$ -Si slurry ( $11.7s^{-1}$ ), which confirms its influence on the shear stress.

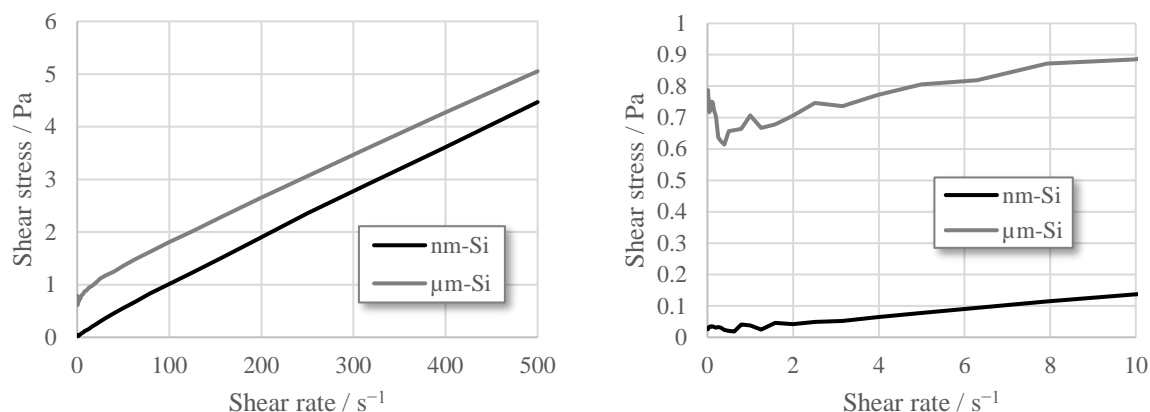


Figure 27: Shear stress as a function of the shear rate for the most diluted nm-Si composite electrode with the solid material composition 80:12:8 Si:CB:CMC-Na and the  $\mu\text{m-Si}$  with the same amount CMC-Na and surface area per gram solvent as the nm-Si electrode.

Figure 27 confirms that very similar rheological behaviour is obtained for the nm-Si and the  $\mu\text{m-Si}$  composite electrode when they have the same amount of CMC-Na and surface area per gram slurry. A difference is that the nm-Si has close to Newtonian behaviour (linear) while it is possible to see a small yield stress for  $\mu\text{m-Si}$ .

In conclusion, the differences in rheological behaviour between the two silicon powder arises due to that the particles have different surface area. This differences in behaviour will affect the processing parameters, which directly affect the cycling performance of the electrodes.

## 4.4 Morphology

To analyse the morphology and confirm the homogenous distribution of the components in the electrodes, SEM was used to analyse some of the electrodes. SEM is an electron microscopy technique that produces a magnified image of an object with an electron beam. The electron beam in SEM is known as the electron probe and it defines the resolution of the instrument. SEM produces a picture of the sample by detecting either of two types of electron emissions from the sample; secondary and backscattered electron. Detected secondary electrons produce an image of the surface structure and the backscattered electrons produce an image of the variations in the chemical composition of the sample. [67] Energy-dispersive spectroscopy (EDS) is a built-in function in the SEM instrument, which uses emitted X-rays to map the chemical composition of the analysed material. [68]

Eight different samples with different compositions were chosen (the amounts of spots on the holder in the instrument) for the analysis. Table 5 shows the samples imaged in SEM.

Table 5: Content in the electrodes analysed in SEM.

Electrode	Silicon / wt%	Binder / wt%	CMC-Na:SBR	Solvent / wt%	Mass loading / g
Sample 1	10	3	2:0	60	4.42
Sample 2	15	3	2:2	60	5.42
Sample 3	10	7	2:2	60	5.02
Sample 4	5	5	2:2	60	4.45
Sample 5	15	7	2:1	60	4.57
Sample 6	5	7	2:1	60	5.22
Si	100	5	2:1	65	2.34
Graphite	0	5	2:1	65	3.97

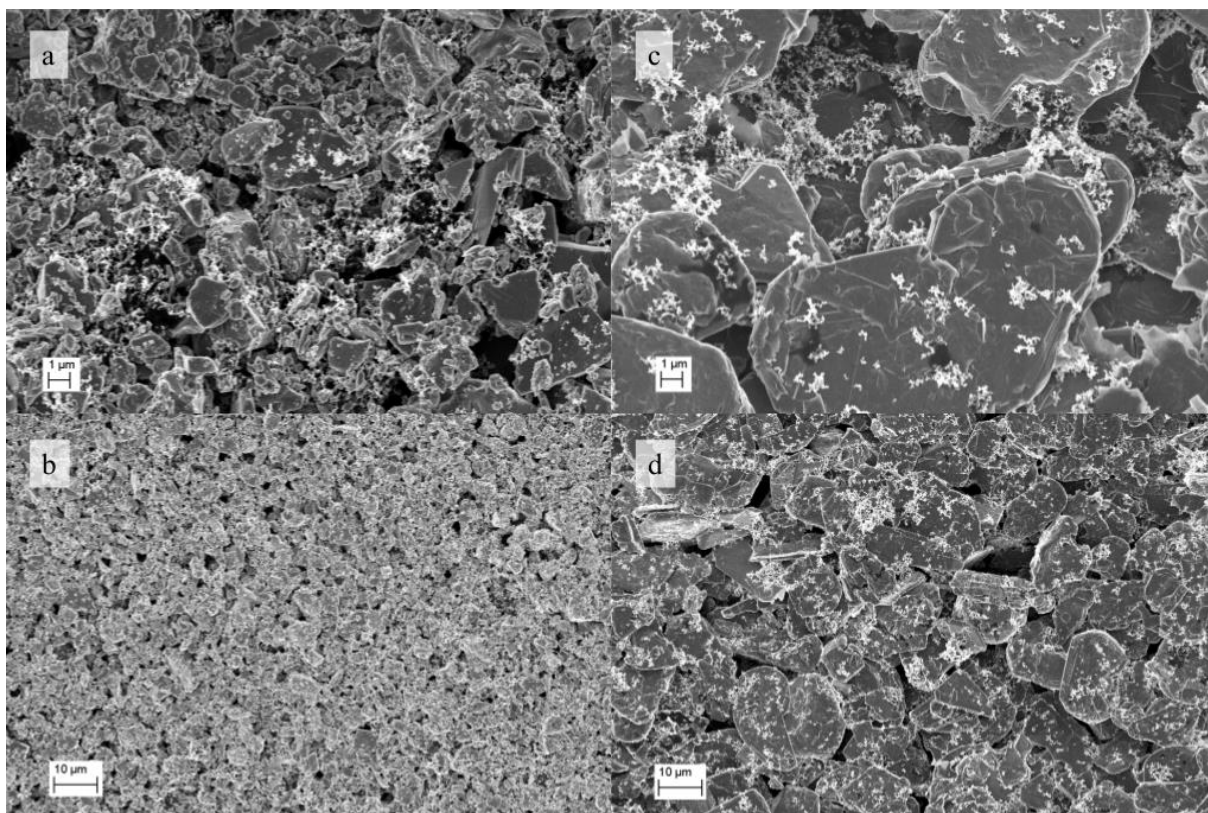


Figure 28: SEM images at different magnifications of a pure silicon electrode (a–b) and a pure graphite electrode (c–d).

Figure 28 shows the surface morphology of a pure silicon electrode (a–b) and a pure graphite electrode (c–d) at two different magnifications. The SEM images confirm the results from the DLS measurements of  $\mu\text{m-Si}$  that the particle sizes are in the range 0.4–0.5  $\mu\text{m}$  with some larger particles up to 5  $\mu\text{m}$  wide. It also confirms the graphite particle size <30  $\mu\text{m}$ .

Both electrodes show a homogenous distribution of CB (the small with stuff) all over the surface, which is in accordance with the literature [24, 26, 30] when CMC-Na is used as the binder in the system. It is hard to see the distribution of the binder, but at some places it can be seen as a spider web-like pattern in the micrographs (*e.g.* in the bottom right corner of Figure 28c). The binder is also visible as darker spots on the surface of the graphite sheets in Figure 28c. The binder becomes darker on the surface in SEM due to its poor conductivity, which results in charged surfaces by electrons from the electron probe.

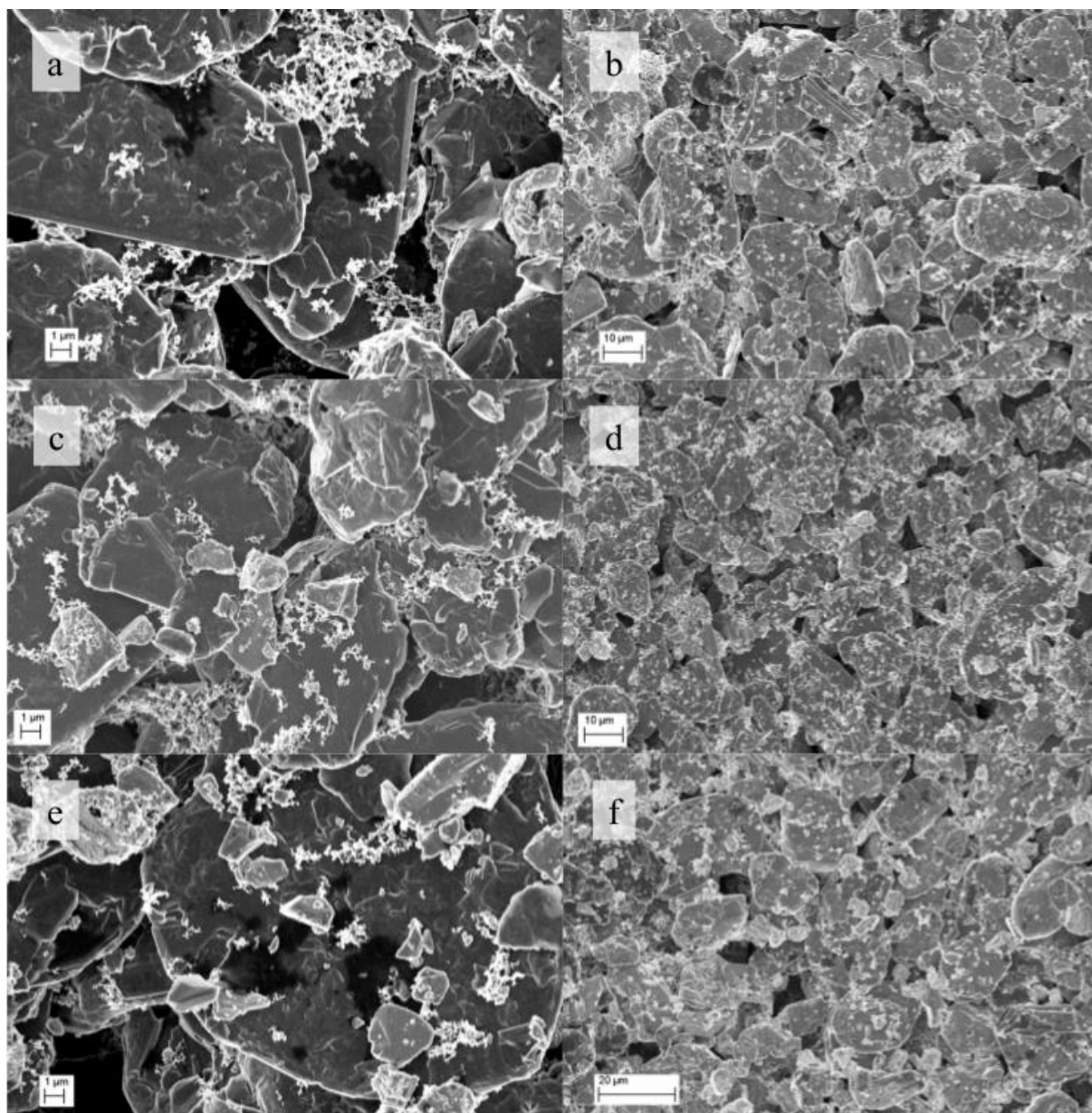


Figure 29: SEM images at different magnifications of three composite electrodes. The two top images (a–b) have a 5% silicon content of the total active material. The middle images (c–d) have a silicon content of 10% and the bottom images have a silicon content of 15%.

Figure 29 reveals the morphology and the particle distribution in three composites containing 5 wt%, 10 wt% and 15 wt% silicon (percentage is of the total amount active material, remainder is graphite). In the images, the smaller brighter particles are silicon and the larger darker particles are graphite (the difference is visible in Figure 28). As seen, all three composite electrodes have a very homogenous distribution of the silicon and graphite particles. This is important as it improves the electrochemical and mechanical performance of the electrode. [69, 70] When the particle distribution is homogenous, the silicon expansion will not stress the surrounding particles as much, as the local expansion of the particle is smaller compared with if the expansion of silicon particles agglomerated in clusters. It is also possible to see that the CB particles are homogeneously distributed over the surface for all three electrodes, just like for the pure electrodes of silicon and graphite.

An EDS imaging was performed on sample 3 with 10 wt% silicon to confirm the homogenous distribution of the silicon and graphite particles in the electrodes from the SEM measurement. Figure 30 shows the results from this EDS imaging, where the red parts in the image are graphite particles and the green are silicon particles. The image reaffirms the results from SEM that the active material is homogenously distributed in the electrode.

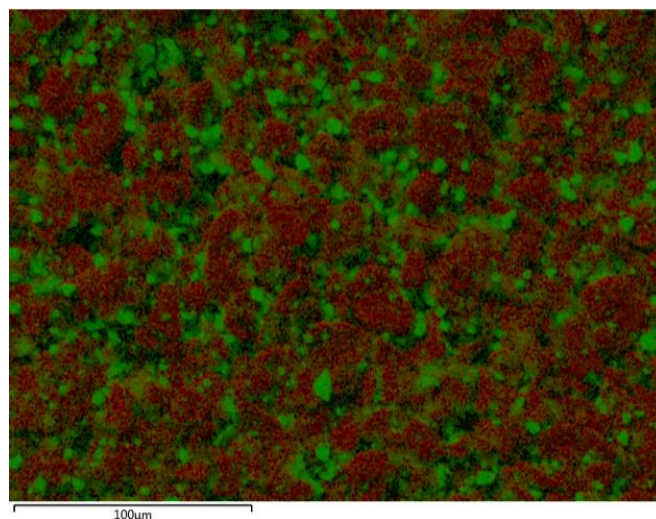


Figure 30: EDS imaging of a sample with 10% silicon active material. The red parts are carbon (graphite atom) and the green parts are silicon.

The results from the adhesion pull tests were hard to evaluate. The results did not differ much between the electrodes and almost all electrode coatings were still well-attached to the current collectors. The tape test gave more information about the adhesion. For some of the electrodes, the coatings were still well-attached to the current collector, while others almost completely fell off. Table 6 shows the adhesion test results from the tape test graded on a scale from 1 to 3 (3=best adhesion).

Table 6: Adhesion results of the electrode coatings on the current collector on a scale 1–3 with 3 as the best adhesion.

				Adhesion strength							
3				2				1			
Silicon / %	Binder / wt%	Binder ratio	Solvent / wt%	Silicon / %	Binder / wt%	Binder ratio	Solvent / wt%	Silicon / %	Binder / wt%	Binder ratio	Solvent / wt%
5	3	2:2	70	15	7	2:0	70	10	3	2:0	60
5	3	2:3	70	5	5	2:0	65	10	5	2:2	70
5	7	2:2	65	10	5	2:1	70	15	7	2:3	70
10	3	2:3	65	15	5	2:2	65	15	3	2:1	65
10	7	2:3	65	10	3	2:2	70	5	7	2:1	60
15	3	2:2	60	15	7	2:0	60	15	5	2:1	60
5	5	2:2	60					15	7	2:1	60
0	5	2:1	65					10	5	2:2	65
								5	7	2:1	60
								15	7	2:1	60

The results from the tape tests show a small influence of the silicon on the adhesion of the coating to the current collector. The results indicate that the lower amount of silicon in the

coating, the better the adhesion to the current collector is. This is in accordance with the literature [71], which also indicates that the roughness of the current collector should be considered for the adhesion during processing, which improves the electrochemical performance when larger amounts of materials that undergo large volume changes (like silicon) are used, especially when a low binder amount is used.

## 4.5 Electrochemical testing

From the cycling profiles of the electrode composites with the voltage as a function of the capacity, it is possible to see the reduction and oxidation reactions of silicon occurring during lithiation and delithiation (mentioned in Section 2). The capacity and voltage profile of one of the studied electrode composites is shown in Figure 31. During lithiation it is possible to see the onset potential of the reduction reaction (phase transition) of crystalline silicon to the amorphous phase  $\text{Li}_x\text{Si}$  at 0.30 V (not visible in the pure graphite in Figure 4), which is within the onset potential for silicon of 0.3–0.4 V vs  $\text{Li}/\text{Li}^+$  according to the literature. [5, 17, 22, 28, 29]

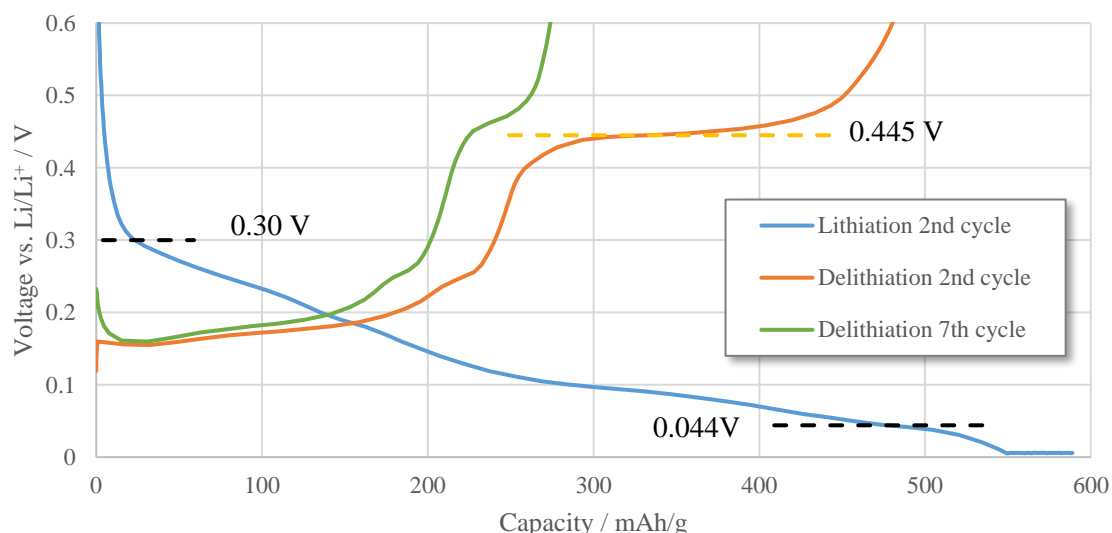


Figure 31: Capacity and voltage profile for a silicon and graphite composite electrode during the second cycle (and seventh for delithiation). Marked potentials are not visible for a pure graphite electrode (Figure 4) and arise due to reduction and oxidation reactions of the silicon material.

Furthermore, it is possible to see the severely lifetime-decreasing reduction reaction (phase transition) of the amorphous  $\text{Li}_x\text{Si}$  to one of the crystalline phases  $\text{Li}_{22}\text{Si}_5$  or  $\text{Li}_{15}\text{Si}_4$  at 0.044 V. During delithiation this crystalline phase dissipates, by an oxidation reaction, back to the amorphous phase  $\text{Li}_x\text{Si}$  at 0.445 V, which is in accordance with the literature. [7, 16, 22, 23, 29] During further cycling this oxidation reaction disappears (see Figure 31), which is an indication that the silicon alloy stays amorphous. [16]

As LIBs in general and silicon-based anodes in particular have a big capacity loss during the first cycles, it is common to perform one or two CCCV conditioning cycles (pre-lithiate the anode) of the studied electrode at a low C-rate ( $C/10$  and below) to a low cut-off voltage (down to 0.01 V) to complete the SEI formation layer on the surface of the electrodes before the electrochemical testing begins. [72, 73] These conditioning cycles were not performed in the

electrochemical tests of this thesis, which implies that the electrodes will have a big capacity drop during the first cycles. By not performing the conditioning cycles, the cycling performance and cycling retention will be impaired of the electrodes. [74, 75]

The theoretical specific capacities of the electrode composites were calculated to 563.2 mAh/g for composites containing 5% silicon, 754.6 mAh/g for 10% silicon composites and 945.9 mAh/g for 15% silicon composites (see Appendix A). All C-rates in the electrochemical tests are based on these capacities. Important to know, is that these capacities are based on the theoretical specific capacity of the silicon phase  $\text{Li}_{22}\text{Si}_5$ , which is 4198.8 mAh/g. But as this phase will only appear at elevated temperatures above 400 °C during cycling [76] and that the electrochemical tests were performed at ambient temperature, the most probable silicon phase appearing should be  $\text{Li}_{15}\text{Si}_4$ , with a theoretical specific capacity of 3579 mAh/g. [7, 17, 74] This implies that the theoretical capacities of the electrodes should be 532.3 mAh/g for 5% silicon composites, 692.6 mAh/g for 10% silicon composites and 853.0 mAh/g for 15% silicon composites. In the following discussion, it should also be noted that by the capacity, it is the discharge capacity that is considered.

All electrodes were cycled for 200 cycles, to be able to evaluate their long-term performance. To have a reference to compare the cycled electrode composites with, a pure graphite electrode with the composition 5 wt% binder, binder ratio CMC-Na:SBR 2:1, 65 wt% solvent and a mass loading of 3.97 mg/cm<sup>2</sup> were cycled (same graphite as in the composites) with the results shown in Figure 32.

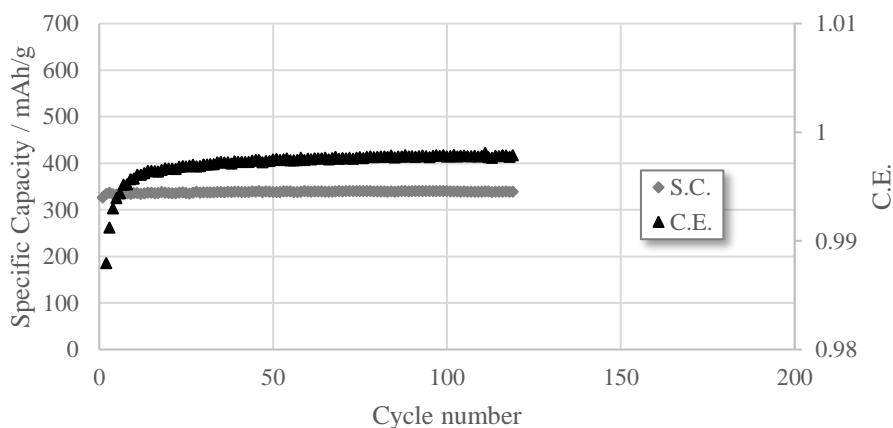


Figure 32: Specific capacity (S.C.) and C.E. of a pure graphite electrode at C/10. The cycling of the electrode was still running when the data was collected after 119 cycles (95 days).

The pure graphite electrode was cycled at C/10 and due to the end of this project; the data was collected already after 119 cycles (95 days) even though the electrode cycling was still running. In Figure 32 the discharge capacity and the C.E. of a pure graphite electrode is shown. As can be seen, the pure graphite electrode shows excellent cycling performance with a stable capacity of 338 mAh/g after 119 cycles. The C.E. of the pure graphite electrode is 91% for the first cycle, which is common for graphite electrodes, [77] but increases rapidly with increasing cycles to close to 100% still after 119 cycles.

To reduce the number of electrodes to perform the electrochemical tests on, the adhesion pull tests were performed, unfortunately not giving much information as mentioned earlier. Nevertheless, light optical microscopy gave the results seen in Figure 33 about the surface finish of the electrodes (surface finish meaning how nice and smooth the surface is).

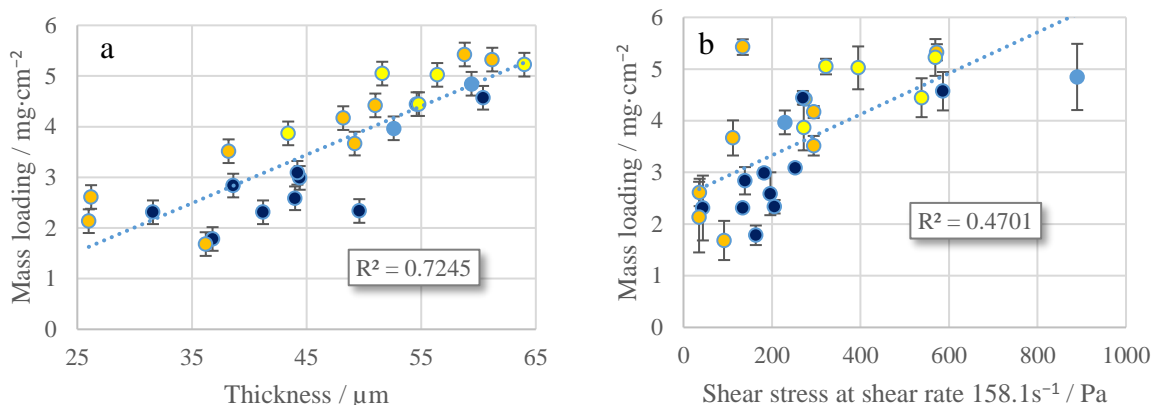


Figure 33: Mass loading as a function of the thickness (a) and shear stress (b) respectively. Colours indicate the surface finish according to: gold=great, yellow=good, dark blue=bad (light blue=not studied).

According to these results, a nice surface finish seems to be achieved with a high mass loading/thickness and a high shear stress in the electrode slurry. This could be explained by the fact that the chances are higher that the surface becomes uniform when the mass loading is higher. Therefore, the electrodes with the highest mass loading/thickness and shear stress were tested electrochemically.

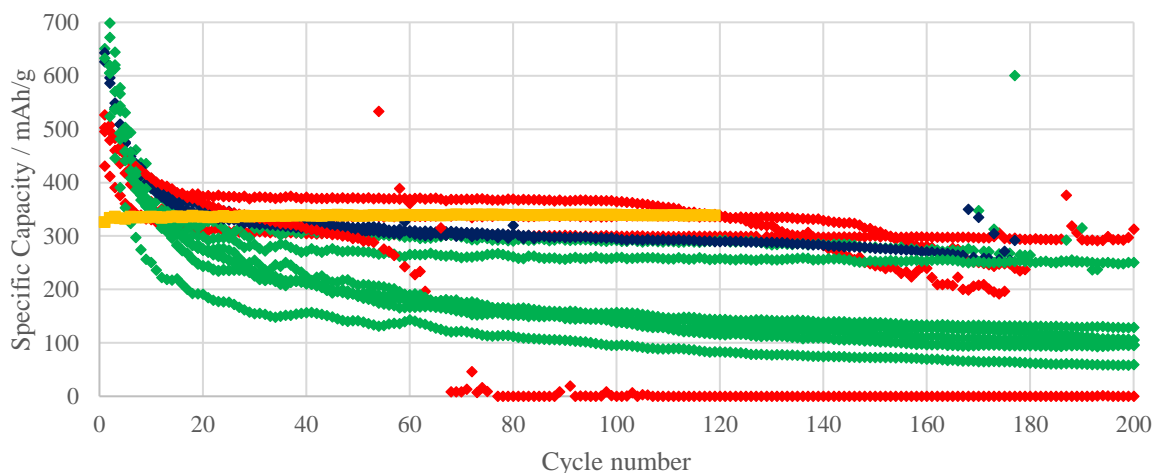


Figure 34: Specific discharge capacity for the electrodes cycled at C/10. The different colours indicate the silicon amount in the electrodes: yellow=pure graphite, red=5 wt% silicon, blue=10 wt% silicon, green=15 wt% silicon.

Figure 34 shows the results from the cycling tests of the electrode composites and the pure graphite electrode. The electrodes were cycled at C/10 for 200 cycles. As can be seen, the capacity loss is huge during the first cycles for all composites and especially the ones containing the largest amount of silicon. This is in accordance with the literature and due to the SEI formation on the surface of the active material and the cracks and pulverisation of the silicon material arising from the mechanical stresses contributed by the extreme volume changes during cycling, which itself exposes new surface area where further SEI formation can occur. [2, 5–7, 18–20, 23–25] This SEI formation and silicon pulverisation also continues for many more cycles on the active material surface because no conditioning cycles were performed and further impairs the battery performance. [74, 75]

Remarkable is that all silicon composites have a poor capacity performance compared with the pure graphite electrode, even though the calculated theoretical capacity is higher. All electrode composites have a higher capacity during the first cycles, but it decreases rapidly below the capacity for the pure graphite electrode. This could be an indication that all silicon material in the electrode composites has become completely inactive for further lithiation due to the SEI formation and pulverisation, and only graphite becomes lithiated. This explains why some electrodes obtain a stable capacity after 20-40 cycles, when only graphite is the material becoming lithiated, as these composites contain less graphite per total weight of the active material.

There is only one electrode composite with a stable capacity higher than the pure graphite electrode. It has a stable capacity of  $\sim 370$  mAh/g over about 100 cycles before it drops below 200 mAh/g after about 160 cycles and finally stops after 180 cycles.

At this point, the tape test of the coating adhesion had been performed with the results shown in Figure 35.

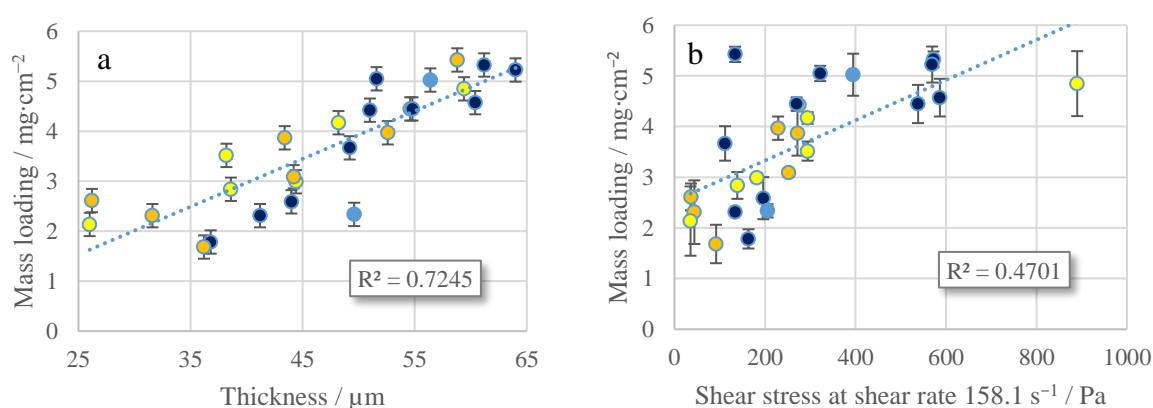


Figure 35: Mass loading as a function of the thickness (a) and shear stress (b) respectively. Colours indicate the coating adhesion to the current collector according to gold=great, yellow=good, dark blue=poor (light blue= tape test not performed).

As can be seen in Figure 35, the electrodes with the best adhesion does not necessarily have the highest mass loading and shear stress during processing. The explanation for this might be that the mechanical properties for thin-film coatings decrease with the coating thickness until the bulk properties are reached, which impairs with the adhesion. [78] When the mass loading and thickness is high, the preparation conditions are more important to consider [79] as well as the molecular length of the binder. [26] When the drying conditions are slow, it creates a binder gradient in the electrode which decreases the adhesion (as well as the electrochemical performance) [79] and an increased molecular length of the binder increases the intermolecular bridging in the electrode, which increases the adhesion. [26]

It is well-known that the battery performance and cycle life is decreased with increasing mass loading [26, 30, 79] due to the increasing volume expansions of the electrode, which increases the mechanical stresses at the interface of the current collector. As the adhesion is better for the electrodes with a lower mass loading and as the electrodes cycled at C/10 performed very poorly, the electrodes with the best adhesion in the tape test where also cycled. These were cycled at C/2 (with no conditioning cycles) for 200 cycles.

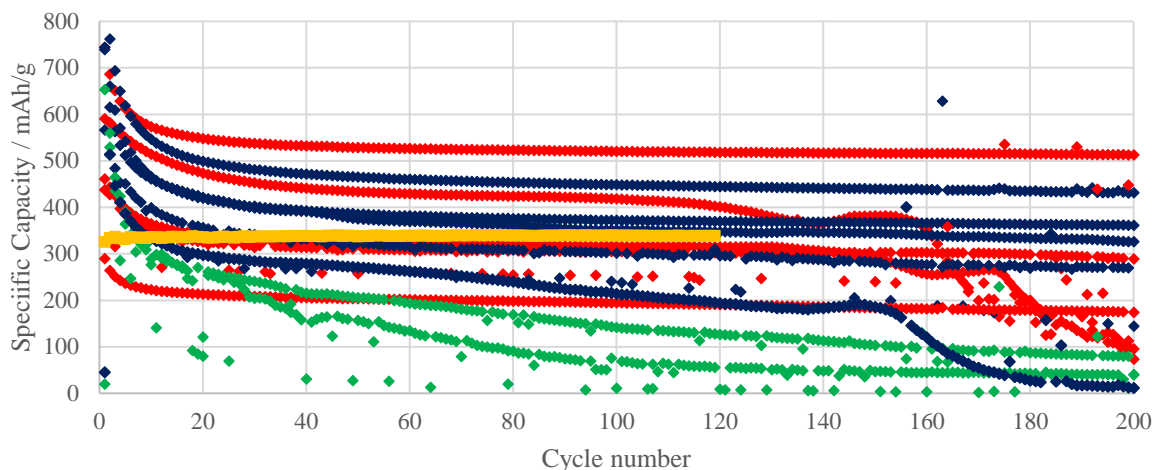


Figure 36: Specific discharge capacity for the electrodes cycled at C/2. The different colours indicate the silicon amount in the electrodes: yellow=pure graphite, red=5 wt% silicon, blue=10 wt% silicon, green=15 wt% silicon.

In Figure 36, the specific capacity as a function of the cycle number is shown for the cycling of the new set of electrodes and the pure graphite (same as in Figure 34). The behaviour is the same as for electrodes cycled at C/10, where the electrodes with the highest amount of silicon (15 wt%) have the lowest capacity after the initial capacity drop. Interestingly, many of these electrodes show a fairly high and stable capacity over 200 cycles after the capacity drop in the first ~20 cycles due to SEI formation and silicon pulverisation. It can also be seen that electrodes with both 5 wt% and 10 wt% silicon show good capacity performance (high and stable) over 200 cycles. The two best-performing electrodes have a capacity of 512 mAh/g (5 wt% silicon) and 431 mAh/g (10 wt% silicon) after 200 cycles, which is big improvement compared with the capacity of the pure graphite electrode (338 mAh/g).

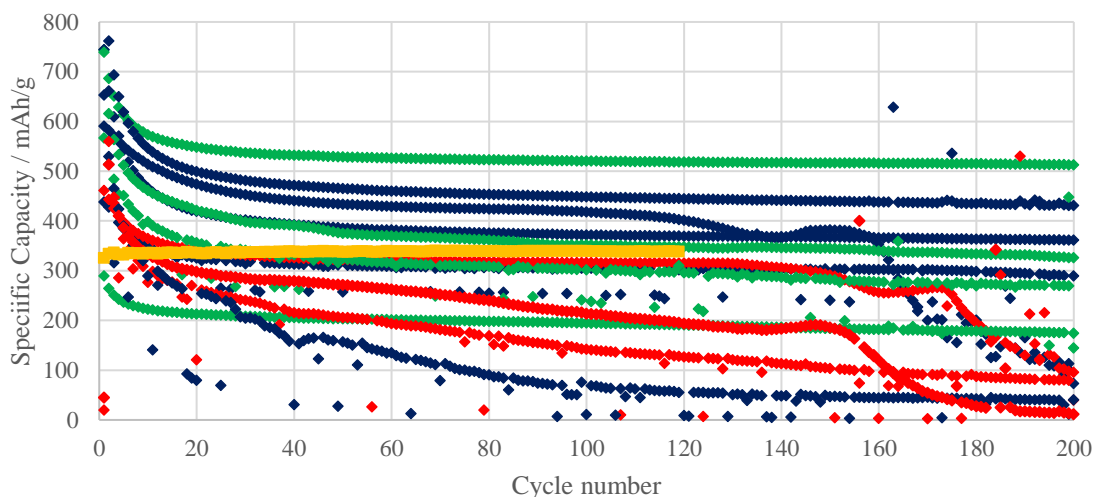


Figure 37: Specific discharge capacity for the electrodes cycled at C/2. The different colours indicate the solvent amount in the electrodes: yellow=pure graphite (65 wt%), red=60 wt% solvent, blue=65 wt% solvent, green=70 wt% solvent.

As seen in Figure 37, the solvent amount has some influence on the capacity of the electrodes. It seems like a solvent amount of 60 wt% (equivalent to a high mass loading) in the electrode slurry impairs with the cycling performance of the electrode. No difference between the electrodes from slurries containing 65 wt% or 70 wt% can be seen.

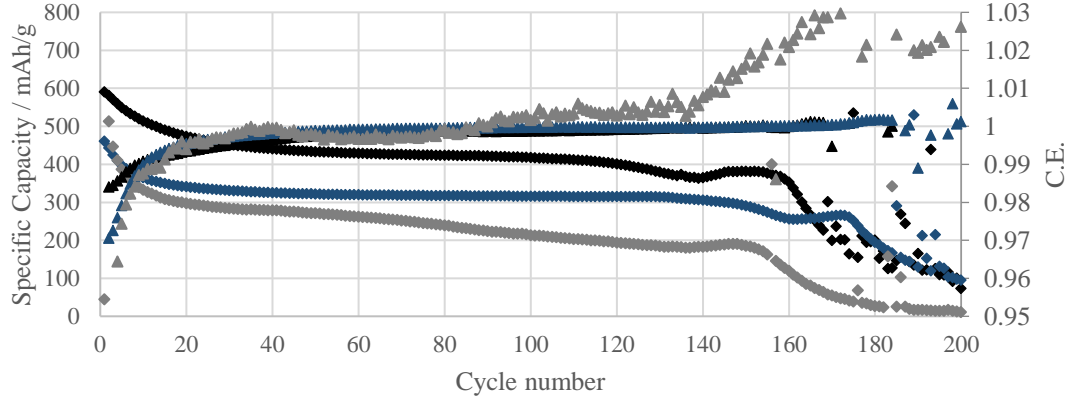


Figure 38: Specific capacity (left axis) and C.E. (right axis) as a function of the cycle number for three composite electrodes (shown with three different colours) with a rapid capacity drop. Triangles are the C.E. and diamonds are the specific capacity.

A behaviour seen for three of the electrodes cycled at C/2 is a rapid capacity drop after about 150 cycles (shown in Figure 38). Interestingly, the capacity first increases for a few cycles, before it drops rapidly to a stop. At the same time as the capacity drops, the coulombic efficiency increases to above 100%. This indicates that the electrodes delithiate more than they lithiate, *i.e.*, more lithium ions leave the studied electrodes than entering them. This phenomenon might arise due to the high C-rate and slow lithium ion diffusion in crystalline Li-Si-alloy (which is observed at low potentials), which could trap lithium ions in the silicon structure, which are released when the capacity decreases. [5, 14] The capacity drop of the electrode can occur due to several reasons. It can occur due to a complete degradation of the electrolyte on the electrode surface or that the added additives FEC and VC, which are added to prolong the cycle life of silicon and graphite electrodes, are consumed. [16, 19, 20] However, a more probable reason is that the binder amount in the electrode is too low, as a common denominator is the low or non-existent SBR binder in those electrodes. SBR is added to enhance the mechanical properties and the flexibility in the electrode to suppress risks of cracks, at the same time as it enhances the adhesion to the current collector. [24, 34] If the binder amount is too low, not covering all the surface area of the electrode, it may lead to particle isolation and poor electrical wiring, which promotes a rapid capacity drop as seen in Figure 38. [30]

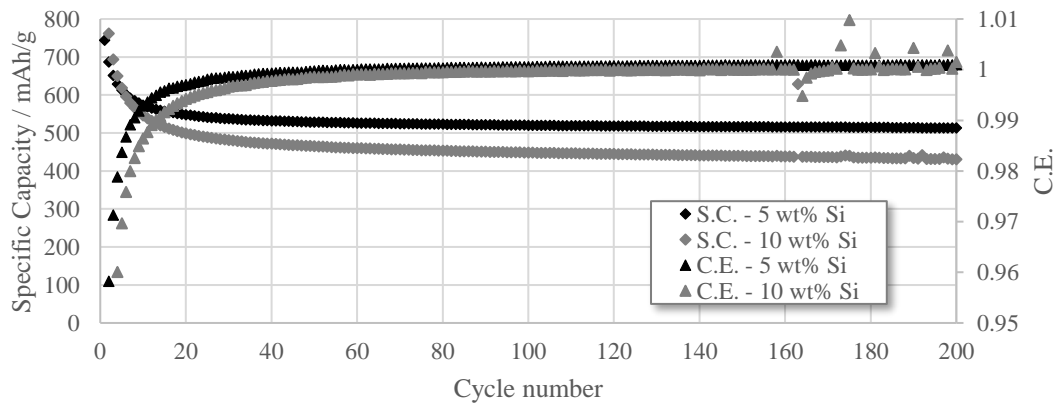


Figure 39: Specific capacity (left axis) and C.E. as a function of the cycle number for the two electrodes with the highest and most stable capacity, cycled at C/2.

In Figure 39, the specific capacity and the C.E. for the two electrodes with the highest and most stable capacity over 200 cycles are shown. The electrode with the highest capacity has the

following electrode composition: 5 wt% silicon, 3 wt% binder, binder ratio CMC-Na:SBR 1:1 (wt/wt) with 70 wt% solvent. The second electrode has the following composition: 10 wt% silicon, 3 wt% binder, binder ratio CMC-Na:SBR 2:3 (wt/wt) with 65 wt% solvent. For the first cycle, the electrodes have a C.E. of 89% and 87% and a capacity loss of 84.1 mAh/g and 120.9 mAh/g respectively. This is in accordance with the literature, which suggest that the capacity loss during the first cycle is supposed to be between 0.0178–0.0278 mAh/cm<sup>2</sup> for all silicon systems. [80] For the best-performing electrode with a composition of 5 wt% silicon and 95 wt% graphite as the active material, the capacity loss is supposed to be between 70.8–92.3 mAh/g (see Appendix A), a range that includes the lost capacity (84.1 mAh/g).

Both electrodes have a large capacity loss over the initial ~20 cycles, arising due to the continued SEI formation and silicon pulverisation during cycling. From the initial cycle to the 20th, the C.E. is 66% and 50% respectively for each electrode (capacity loss 279.8 mAh/g and 495.1 mAh/g). However, thereafter the electrode with 5 wt% silicon only has a capacity decrease from 549 mAh/g to 512 mAh/g between the 20<sup>th</sup> and 200<sup>th</sup> cycle, while the electrode with 10 wt% silicon has a capacity decrease from 499 mAh/g to 431 mAh/g. This is a capacity decrease with only about 7% and 14% respectively.

An interesting feature for both these electrodes is that they only contain 3 wt% binder, but still performed well in the electrochemical tests. It seems like it is sufficient with only 3 wt% of the binders to obtain a homogenous particle distribution with a stable battery performance, as long as the SBR binder is at least in the ratio 1:1 (wt/wt) with CMC-Na. SBR is necessary as it supresses the risk of crack formation as well as it improves the coating adhesion to the current collector. [24, 34]

Worth noting with these two electrodes is that both have an initial capacity higher than their calculated theoretical capacity. This contribution might arise due to two reasons, the initial SEI formation (which can increase the capacity to above the theoretical because of side-reactions) and the way the mass loading was calculated, as it is an average value for the whole batch of the electrode composition. Nevertheless, the electrodes demonstrated a high and stable capacity and therefore the electrode with the highest capacity was evaluated further. From now on, this electrode composition will be referred to as RA017.

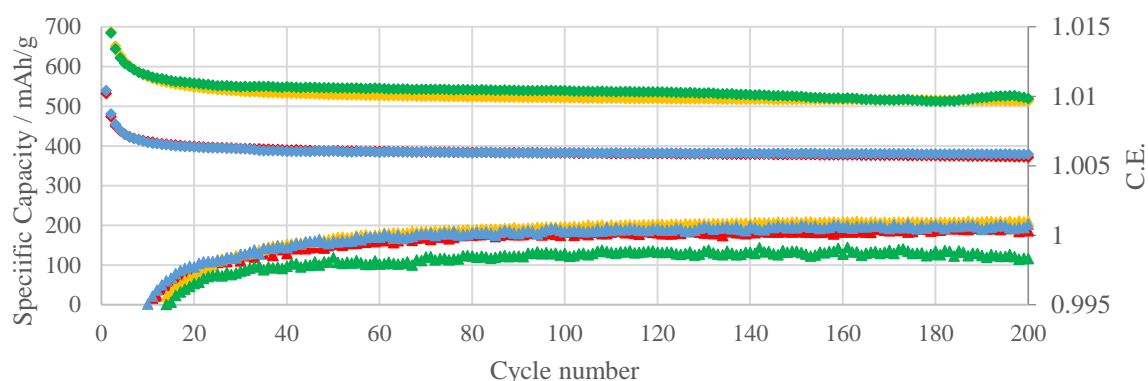


Figure 40: Repeated cycling tests of four RA017 electrodes, cycled at C/2. The figure shows the specific capacity (left axis) and C.E. (right axis) as a function of the cycle number. RA017 have the composition: 5 wt% Si, 3 wt% binder, binder ratio CMC-Na:SBR 1:1 (wt/wt) with 70 wt% solvent.

As can be seen in Figure 40, all RA017 electrodes show a stable capacity over 200 cycles with a C.E. close to 100% (after an initial C.E. between 84–87% for the first cycle). By comparing

the shape of the curves, it seems like the green RA017 is in the beginning of the capacity drop seen for the electrodes in Figure 38 (small increase after 180 cycles and a decrease closer to 200 cycles). The capacity for the green and yellow RA017 electrodes is however greater than the theoretical capacity (532.3 mAh/g) for reasons unclear, and the discussion will therefore focus on the red and blue RA017 electrodes. The red and blue RA017 electrodes have a specific capacity of 371 mAh/g and 378 mAh/g respectively after 200 cycles, with an initial capacity of 531 mAh/g and 538 mAh/g in the first cycle. These capacities are in accordance with the calculated theoretical capacity of the electrodes (532.3 mAh/g for electrodes containing 5 wt% Si). It is not a big improvement compared with the pure graphite electrode (338 mAh/g), but it should be remembered that it only has been cycled for 119 cycles. At 119 cycles, the RA017 electrodes had the capacities 380 mAh/g and 382 mAh/g, which is an improvement of 12.4% and 13.0%. Indeed, the capacity is improved with the added silicon, and it is cycled with stable capacity for 200 cycles.

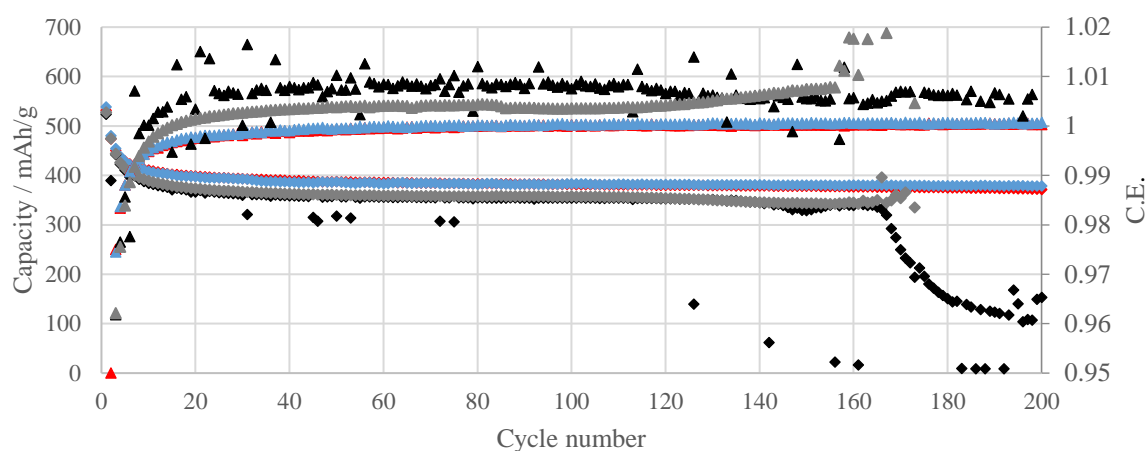


Figure 41: Cycling tests of two RA017 electrodes (blue, red) and two electrodes produced on a pilot line (referred to as PILOT, black and grey), cycled at C/2. The figure shows the specific capacity (diamonds, left axis) and C.E. (triangles, right axis) as a function of the cycle number. RA017 have the composition: 5 wt% Si, 3 wt% binder, binder ratio CMC-Na:SBR 1:1 (wt/wt) with 70 wt% solvent and PILOT have the composition: 5 wt% Si, 3 wt% binder, binder ratio CMC-Na:SBR 1:1 (wt/wt) with 65 wt% solvent.

As the aim of this project is to be able to produce the electrodes on a commercial scale, the RA017 electrode composition, which has an increased capacity compared with pure graphite and a stable cycling performance, was scaled up. The scaled-up electrode was produced on LiFeSiZE's pilot line. The composition of the solid materials in the up-scaled electrode was kept the same, but the solvent amount was decreased to 65 wt% due to the new process. The slurry processing was also changed to fit the up-scaled format (described in the experimental section). The cycling results for the PILOT electrodes are shown in Figure 41, where they are compared with RA017. The PILOT electrodes show a stable cycling performance during the first 140 cycles, before they exhibit a similar capacity drop as the electrodes in Figure 38. However, they do not have the same capacity as the RA017 electrodes. Both of the electrodes have similar specific capacity to RA017 in the initial cycle (527 mAh/g and 523 mAh/g, respectively), but it drops to only 342 mAh/g and 338 mAh/g after 200 cycles, which is about the same as for the pure graphite, *i.e.*, not an improvement of the capacity at all. This shows the importance of the process parameters in the production the electrode (slurry preparation and the coating process).

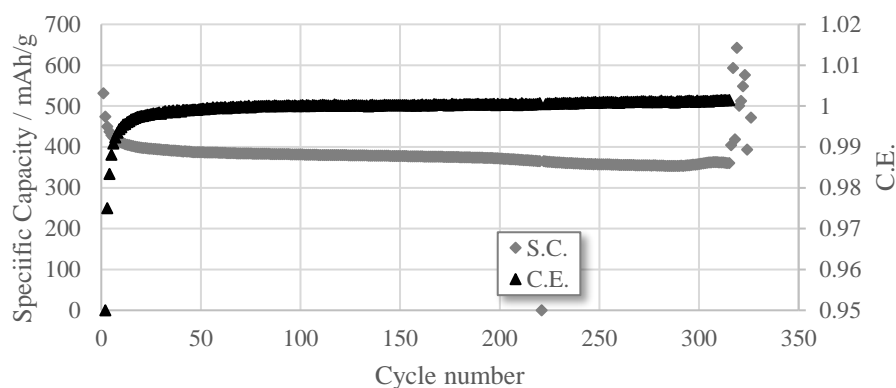


Figure 42: Specific capacity (left axis) and C.E (right axis) as a function of the cycle number of a RA017 electrode, cycled until it failed.

Figure 42 shows the cycle performance of one of the RA017 electrodes. The electrode was cycled until it failed, *i.e.*, it shows the lifetime of the cell. The electrode shows both a good C.E. close to 100% for 315 cycles and a stable cycling performance for the same amount of cycles. At 315 cycles, the electrode still shows a capacity of 360 mAh/g, which is an improvement of the capacity compared with pure graphite. The improvement as compared to the reference is only 6.5%, but it should again be noted that the graphite was only cycled for 119 cycles. After 315 cycles, the capacity of the electrode drops rapidly to a failure, in a similar way as the PILOT-electrodes mentioned above exhibits. However, it should be noted that these tests have been performed in half-cells, where lithium metal is the counter electrode. Therefore, the failure can be due to the well-known issues with electrical cycling of lithium metal. [81, 82]

## 5. Conclusion

One purpose of this project was to improve the capacity of LIBs for commercial use by replacing a small amount of the graphite material in the anode with silicon, which has about ten times higher capacity per weight than graphite. To perform this, the components in the electrodes have been varied to determine what properties give the highest and most stable cycling performance. The second purpose was to evaluate the rheological properties of the electrode slurries and to study how the process parameters affects the electrode performance. The third purpose was to study the differences between a nm-Si and  $\mu\text{m}$ -Si powder and to evaluate the influence of the different particle size.

The results from the rheological measurements of the electrodes indicates that the parameters affecting the mass loading of the electrodes and the shear stress of the electrodes slurries are the CMC-Na amount and the solvent amount in the slurries. When the CMC-Na amount is increased, and the solvent amount decreased, the mass loading and the shear stress increases.

In the comparison study of the two silicon powders, there was a clear difference between the powders in terms of slurry rheology. The nm-Si slurry behaved like a viscoelastic material, while the  $\mu\text{m}$ -Si showed a more purely viscous behaviour. When the properties of each material were evaluated, it was revealed that it is the surface area of the particles per volume unit in the slurry that contributed to the difference.

In the electrochemical testing of the electrodes, it was clear that electrodes containing 15 wt% (of the active material) silicon have the worst cycling performance. When the silicon amount is higher than 10 wt%, the capacity drops rapidly with increasing cycles to a worse performance than pure graphite. It was also discovered that a solvent amount less than 65 wt% in the electrode slurry impairs the capacity performance. Adhesion tests shows that a good coating adhesion to the current collector improves the cycling performance, and that the adhesion is better for electrodes with low mass loading. The results also indicate that as low as 3 wt% binder is sufficient for good cycling performance of the electrodes and that both CMC-Na and SBR are necessary for good cycling performance.

The best-performing electrode consists of 5 wt% silicon, 3 wt% binder, binder ratio CMC-Na:SBR 1:1 (wt/wt) with 70 wt% solvent in the slurry and it has a stable specific capacity of 380 mAh/g at 119 cycles. This is an improvement of 12.4% compared with pure graphite, which shows a specific capacity of 338 mAh/g at 119 cycles.

# Acknowledgements

I would like to thank my supervisor Jonas for tutoring and helping me with everything throughout the project. I would also like to say thanks to Henrik, Guiomar, Andoria and Andy for the helping me with the lab work. A special thanks to Josh for letting me use the coating equipment at LiFeSiZE. Many thanks to all the people at the chemistry department for supporting me and interesting discussions.

## References

- [1] Park JK. Principles and Applications of Lithium Secondary Batteries. Weinheim: Wiley-VCH Verlag & Co. KGaA; 2012.
- [2] Julien C, Mauger A, Vijh A, Zaghib K. Lithium Batteries. Science and Technology. New York & London: Springer International Publishing Switzerland; 2016.
- [3] Nitta N, Wu F, Lee JT, Yushin G. Li-ion battery materials: present and future. *Materials Today*. 2015;18: 252–264.
- [4] Lee J, Oh C, Kim N, Hwang JY, Sun YK. Rational design of silicon-based composites for high-energy storage devices. *J Mater Chem*. 2016; 7: 5366–5384.
- [5] Liang B, Liu Y, Xu Y. Silicon-based materials as high capacity anodes for next generation lithium ion batteries. *J Power Sources*. 2014; 21: 469–490.
- [6] Casimir A, Zhang H, Ogoke O, Amine J.C, Lu J, Wu G. Silicon-based anodes for lithium-ion batteries: Effectiveness of materials synthesis and electrode preparation. *Nano Energy*. 2016; 21: 360–375.
- [7] Beattie SD, Larcher D, Morcrette M, et al. Si Electrodes for Li-Ion Batteries—A New Way to Look at an Old Problem. *J Electrochem Soc* 2008; 155: A158.
- [8] Nivaldo JT. *Principles of Chemistry. A molecular Approach*. New Jersey: Pearson Education, Inc.; 2010.
- [9] Qian J, Henderson WA, Xu W, et al. High rate and stable cycling of lithium metal anode. *Nat Commun*; 6. Epub ahead of print December 2015. DOI: 10.1038/ncomms7362.
- [10] Zhang W-J. Lithium insertion/extraction mechanism in alloy anodes for lithium-ion batteries. *J Power Sources* 2011; 196: 877–885.
- [11] Freire M, Kosova NV, Jordy C, et al. A new active Li–Mn–O compound for high energy density Li-ion batteries. *Nat Mater* 2016; 15: 173–177.
- [12] Myung S-T, Hitoshi Y, Sun Y-K. Electrochemical behavior and passivation of current collectors in lithium-ion batteries. *J Mater Chem* 2011; 21: 9891.
- [13] Oltean G. *From Current Collectors to Electrodes: Aluminium Rod Structures for Three-dimensional Li-ion Micro-battery Applications*. Acta Universitatis Upsaliensis, 2014.
- [14] Rehnlund D, Lindgren F, Böhme S, et al. Lithium trapping in alloy forming electrodes and current collectors for lithium based batteries. *Energy Environ Sci* 2017; 10: 1350–1357.
- [15] Terranova ML, Orlanducci S, Tamburri E, et al. Si/C hybrid nanostructures for Li-ion anodes: An overview. *J Power Sources* 2014; 246: 167–177.

- [16] Klett M, Gilbert JA, Pupek KZ, Trask SE, Abraham DP. Layered Oxide, Graphite and Silicon-Graphite Electrodes for Lithium-Ion Cells: Effect of Electrolyte Composition and Cycling Windows. *J Electrochem Soc.* 2017;164: A6095–A6102.
- [17] Gómez-Cámer JL, Bünzli C, Hantel MM, et al. On the correlation between electrode expansion and cycling stability of graphite/Si electrodes for Li-ion batteries. *Carbon* 2016; 105: 42–51.
- [18] Peled E, Menkin S. Review-SEI: Past, Present and Future. *J Electrochem Soc.* 2017;164: A1703–A1719.
- [19] Petibon R, Chevrier VL, Aiken CP, et al. Studies of the Capacity Fade Mechanisms of  $\text{LiCoO}_2$ /Si-Alloy: Graphite Cells. *J Electrochem Soc* 2016; 163: A1146–A1156.
- [20] Jung R, Metzger M, Haering D, et al. Consumption of Fluoroethylene Carbonate (FEC) on Si-C Composite Electrodes for Li-Ion Batteries. *J Electrochem Soc* 2016; 163: A1705–A1716.
- [21] Komaba S, Itabashi T, Watanabe M, Groult H, Kumagai N. Electrochemistry of Graphite in Li and Na Salt Codissolving Electrolyte for Rechargeable Batteries. *J Electrochem Soc.* 2007;154: A322–A330.
- [22] Nitta N, Yushin G. High-Capacity Anode Materials for Lithium-ion Batteries: Choice of Elements and Structure for Active particles. *Particle & Particle System Characterization.* 2014;31: 317–336.
- [23] Hovington P, Dontigny M, Guerfi A, et al. In situ Scanning electron microscope study and microstructural evolution of nano silicon anode for high energy Li-ion batteries. *J Power Sources* 2014; 248: 457–464.
- [24] Nguyen BPN, Chazelle S, Cerbelaud M, et al. Manufacturing of industry-relevant silicon negative composite electrodes for lithium ion-cells. *J Power Sources* 2014; 262: 112–122.
- [25] Hernandez CR, Etienne A, Douillard T, et al. A Facile and Very Effective Method to Enhance the Mechanical Strength and the Cyclability of Si-Based Electrodes for Li-Ion Batteries. *Adv Energy Mater* 2017; 1701787.
- [26] Mazouzi D, Karkar Z, Reale Hernandez C, et al. Critical roles of binders and formulation at multiscales of silicon-based composite electrodes. *J Power Sources* 2015; 280: 533–549.
- [27] Obrovac MN, Christensen L. Structural Changes in Silicon Anodes during Lithium Insertion/Extraction. *Electrochem Solid-State Lett* 2004; 7: A93.
- [28] Kim H, Yun Y, Lee Y-C, et al. Synthesis of silicon–carbon black composite as anode material for lithium ion battery. *Jpn J Appl Phys* 2018; 57: 0102B2.
- [29] Chevrier VL, Liu L, Le DB, et al. Evaluating Si-Based Materials for Li-Ion Batteries in Commercially Relevant Negative Electrodes. *J Electrochem Soc* 2014; 161: A783–A791.

- [30] Jeschull F, Lindgren F, Lacey MJ, et al. Influence of inactive electrode components on degradation phenomena in nano-Si electrodes for Li-ion batteries. *J Power Sources* 2016; 325: 513–524.
- [31] Karkar Z, Guyomard D, Roué L, et al. A comparative study of polyacrylic acid (PAA) and carboxymethyl cellulose (CMC) binders for Si-based electrodes. *Electrochimica Acta* 2017; 258: 453–466.
- [32] Kil KC, Paik U. Lithium salt of carboxymethyl cellulose as an aqueous binder for thick graphite electrode in lithium ion batteries. *Macromol Res* 2015; 23: 719–725.
- [33] Lestriez B, Bahri S, Sandu I, et al. On the binding mechanism of CMC in Si negative electrodes for Li-ion batteries. *Electrochem Commun* 2007; 9: 2801–2806.
- [34] Chong J, Xun S, Zheng H, et al. A comparative study of polyacrylic acid and poly(vinylidene difluoride) binders for spherical natural graphite/LiFePO<sub>4</sub> electrodes and cells. *J Power Sources* 2011; 196: 7707–7714.
- [35] Teng X, Xu H, Liu Q, et al. The influence of conductive additives on the performance of a SiO/C composite anode in lithium-ion batteries. *New Carbon Mater* 2017; 32: 572–580.
- [36] Takei Y, Takeno K, Morimoto H, et al. Effects of nonaqueous electrolyte solutions mixed with carbonate-modified siloxane on charge–discharge performance of negative electrodes for secondary lithium batteries. *J Power Sources* 2013; 228: 32–38.
- [37] Takeuchi T, Noguchi S, Morimoto H, et al. Carbonate-modified siloxanes as solvents of electrolyte solutions for rechargeable lithium cells. *J Power Sources* 2010; 195: 580–587.
- [38] Profatilova IA, Langer T, Badillo JP, et al. Thermally Induced Reactions between Lithiated Nano-Silicon Electrode and Electrolyte for Lithium-Ion Batteries. *J Electrochem Soc* 2012; 159: A657.
- [39] Nakai H, Kubota T, Kita A, et al. Investigation of the Solid Electrolyte Interphase Formed by Fluoroethylene Carbonate on Si Electrodes. *J Electrochem Soc* 2011; 158: A798.
- [40] Ullidemolins M, Le Cras F, Pecquenard B, et al. Investigation on the part played by the solid electrolyte interphase on the electrochemical performances of the silicon electrode for lithium-ion batteries. *J Power Sources* 2012; 206: 245–252.
- [41] Lindgren F, Xu C, Niedzicki L, et al. SEI Formation and Interfacial Stability of a Si Electrode in a LiTfDI-Salt Based Electrolyte with FEC and VC Additives for Li-Ion Batteries. *ACS Appl Mater Interfaces* 2016; 8: 15758–15766.
- [42] Technology Networks. A basic introduction to Rheology. [Internet] [Retrieved 2017-11-02] <https://cdn.technologynetworks.com/TN/Resources/PDF/WP160620BasicIntroRheology.pdf>.
- [43] Janmey PA, Schliwa M. Rheology. *Curr Biol* 2008; 18: R639–R641.

- [44] Jeschull F. Polymers at the Electrode-Electrolyte Interface. Negative Electrode Binds for Lithium-Ion Batteries. *Acta Universitatis Upsaliensis*, 2017.
- [45] *Jelley N. A Dictionary of Energy Science. Oxford. Oxford University Press; 2017.*
- [46] Yang J, Xia B, Huang W, et al. Online state-of-health estimation for lithium-ion batteries using constant-voltage charging current analysis. *Appl Energy* 2018; 212: 1589–1600.
- [47] Wu X, Shi W, Du J. Multi-Objective Optimal Charging Method for Lithium-Ion Batteries. *Energies* 2017; 10: 1271.
- [48] Son B, Ryou M-H, Choi J, et al. Measurement and Analysis of Adhesion Property of Lithium-Ion Battery Electrodes with SAICAS. *ACS Appl Mater Interfaces* 2014; 6: 526–531.
- [49] Kierzek K. Influence of Binder Adhesion Ability on the Performance of Silicon/Carbon Composite as Li-Ion Battery Anode. *J Mater Eng Perform* 2016; 25: 2326–2330.
- [50] Manthiram A, Vadivel Murugan A, Sarkar A, et al. Nanostructured electrode materials for electrochemical energy storage and conversion. *Energy Environ Sci* 2008; 1: 621.
- [51] Breitung B, Schneider A, Chakravadhanula VSK, et al. Artificial Composite Anode Comprising High-Capacity Silicon and Carbonaceous Nanostructures for Long Cycle Life Lithium-Ion Batteries. *Batteries & Supercaps*; 2018: 1–7.
- [52] Nanometre Silicon Powder. Fisher Scientific. Thermo Fisher Scientific. [Internet] [Retrieved 2018-03-20] <https://www.fishersci.co.uk/gb/en/home.html>.
- [53] Nanometer silicon powder. VWR. [Internet] [Retrieved 2018-03-20] <https://se.vwr.com/store/>.
- [54] Micrometre silicon powder. Sigma Aldrich. [Internet] [Retrieved 2018-03-20] <https://www.sigmaaldrich.com/catalog/product/sigma/s5505?lang=en&region=SE>.
- [55] Sartorius Stedim Biotech. DOE in MODDE. [Internet] [Retrieved 2018-02-11] <https://umetrics.com/content/methods>.
- [56] Ligneel E, Lestriez B, Hudhomme A, et al. Effects of the Solvent Concentration (Solid Loading) on the Processing and Properties of the Composite Electrode. *J Electrochem Soc* 2007; 154: A235.
- [57] Lewis JA. Colloidal Processing of Ceramics. *J Am Ceram Soc* 2004; 83: 2341–2359.
- [58] Mueller S, Llewellyn EW, Mader HM. The rheology of suspensions of solid particles. *Proc R Soc Math Phys Eng Sci* 2010; 466: 1201–1228.
- [59] Versaci D, Nasi R, Zubair U, et al. New eco-friendly low-cost binders for Li-ion anodes. *J Solid State Electrochem* 2017; 21: 3429–3435.
- [60] Schulz SC, Schlutter J, Bauhofer W. Influence of Initial High Shearing on Electrical and Rheological Properties and Formation of Percolating Agglomerates for MWCNT/Epoxy Suspensions. *Macromol Mater Eng* 2010; 295: 613–617.

- [61] Yokozeki T, Carolin Schulz S, Buschhorn ST, et al. Investigation of shear thinning behavior and microstructures of MWCNT/epoxy and CNF/epoxy suspensions under steady shear conditions. *Eur Polym J* 2012; 48: 1042–1049.
- [62] Malvern Instruments. [Internet] [Retrieved 2018-01-03]  
[https://warwick.ac.uk/fac/cross\\_fac/sciencecity/programmes/internal/themes/am2/bookin g/particlesize/intro\\_to\\_dls.pdf](https://warwick.ac.uk/fac/cross_fac/sciencecity/programmes/internal/themes/am2/bookin g/particlesize/intro_to_dls.pdf).
- [63] Khlebtsov BN, Khlebtsov NG. On the measurement of gold nanoparticle sizes by the dynamic light scattering method. *Colloid J* 2011; 73: 118–127.
- [64] Keene AM, Tyner KM. Analytical characterization of gold nanoparticle primary particles, aggregates, agglomerates, and agglomerated aggregates. *J Nanoparticle Res* 2011; 13: 3465–3481.
- [65] Jiang W, Hibbert DB, Moran G, et al. Characterisation of gold agglomerates: size distribution, shape and optical properties. *RSC Adv* 2013; 3: 7367.
- [66] Rouquerol F, Rouquerol J, Sing KSW, Llewellyn PL, Maurin G. *Adsorption by Powders and Porous Solids: Principles, Methodology and Applications*. 2nd Ed. Oxford: Elsevier; 2014.
- [67] Egerton RF. *Physical Principles of Electron Microscopy: An Introduction to TEM, SEM and AEM*. New York: Springer Science+Business Media, Inc; 2005.
- [68] Ayache J, Beaunier L, Boumendil J, et al. *Sample Preparation Handbook for Transmission Electron Microscopy*. New York, NY: Springer New York. Epub ahead of print 2010. DOI: 10.1007/978-1-4419-5975-1.
- [69] Ko M, Chae S, Ma J, et al. Scalable synthesis of silicon-nanolayer-embedded graphite for high-energy lithium-ion batteries. *Nat Energy* 2016; 1: 16113.
- [70] Hou G, Cheng B, Cao Y, et al. Scalable production of 3D plum-pudding-like Si/C spheres: Towards practical application in Li-ion batteries. *Nano Energy* 2016; 24: 111–120.
- [71] Jeon H, Cho I, Jo H, et al. Highly rough copper current collector: improving adhesion property between a silicon electrode and current collector for flexible lithium-ion batteries. *RSC Adv* 2017; 7: 35681–35686.
- [72] Nordh T, Jeschull F, Younesi R, et al. Different Shades of  $\text{Li}_4\text{Ti}_5\text{O}_{12}$  Composites: The Impact of the Binder on Interface Layer Formation. *ChemElectroChem* 2017; 4: 2683–2692.
- [73] Jeschull F, Brandell D, Wohlfahrt-Mehrens M, et al. Water-Soluble Binders for Lithium-Ion Battery Graphite Electrodes: Slurry Rheology, Coating Adhesion, and Electrochemical Performance. *Energy Technol* 2017; 5: 2108–2118.
- [74] Domi Y, Usui H, Iwanari D, et al. Effect of Mechanical Pre-Lithiation on Electrochemical Performance of Silicon Negative Electrode for Lithium-Ion Batteries. *J Electrochem Soc* 2017; 164: A1651–A1654.

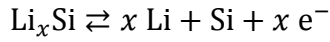
- [75] Holtstiege F, Bärmann P, Nölle R, et al. Pre-Lithiation Strategies for Rechargeable Energy Storage Technologies: Concepts, Promises and Challenges. *Batteries* 2018; 4: 4.
- [76] Chevrier VL, Zwanziger JW, Dahn JR. First principles study of Li–Si crystalline phases: Charge transfer, electronic structure, and lattice vibrations. *J Alloys Compd* 2010; 496: 25–36.
- [77] Patil A, Patil V, Wook Shin D, et al. Issue and challenges facing rechargeable thin film lithium batteries. *Mater Res Bull* 2008; 43: 1913–1942.
- [78] Bouchet J, Roche A., Hamelin P. Internal stresses, Young’s modulus and practical adhesion of organic coatings applied onto 5754 aluminium alloy. *Thin Solid Films* 1999; 355–356: 270–276.
- [79] Haselrieder W, Westphal B, Bockholt H, et al. Measuring the coating adhesion strength of electrodes for lithium-ion batteries. *Int J Adhes Adhes* 2015; 60: 1–8.
- [80] Nadimpalli SPV, Sethuraman VA, Dalavi S, et al. Quantifying capacity loss due to solid-electrolyte-interphase layer formation on silicon negative electrodes in lithium-ion batteries. *J Power Sources* 2012; 215: 145–151.
- [81] Krause A, Dörfler S, Piwko M, et al. High Area Capacity Lithium-Sulfur Full-cell Battery with Prelithiated Silicon Nanowire-Carbon Anodes for Long Cycling Stability. *Sci Rep*; 6. Epub ahead of print September 2016. DOI: 10.1038/srep27982.
- [82] Zhang SS. Problem, Status, and Possible Solutions for Lithium Metal Anode of Rechargeable Batteries. *ACS Appl Energy Mater* 2018; 1: 910–920.

# Appendix A: Calculations

Calculations of the theoretical specific capacity of the electrode composites:

$$Q_{\text{theoretical}} = \frac{nF}{M_w}$$

Silicon anode reaction during discharge/charge:

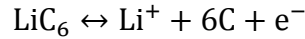


Silicon has a capacity to bind in average 4.4 lithium atoms per silicon in its microstructure. Assuming lithium alloy silicon fully, the following stoichiometry for the anode is achieved:  $\text{Li}_{4.4}\text{Si}/\text{Li}_{22}\text{Si}_5$ . [6]

Calculation of the theoretical capacity for pure silicon anodes:

$$\begin{aligned} M_{w,\text{Si}} &= 28.0855 \text{ g/mol} \\ n &= 4.4 \text{ (Li} = 4.4\text{)} \\ F &= 96485.33289 \text{ C/mol} \\ Q_{\text{theoretical,Si}} &= \frac{4.4 \times 96485.33289 \text{ C/mol}}{28.0855 \text{ g/mol}} = 15115.82 \text{ C/g} \\ 1 \text{ C} &= 3600 \text{ Ah} \\ Q_{\text{theoretical,Si}} &= \frac{15115.82 \text{ C/g}}{3600 \text{ Ah}} = 4198.8 \text{ mAh/g} \end{aligned}$$

Graphite anode reaction during discharge/charge:



Calculation of the theoretical capacity for pure graphite anodes:

$$\begin{aligned} M_{w,\text{graphite}} &= 6 \times 12.0107 \text{ g/mol} = 72.0642 \text{ g/mol} \\ n &= 1 \text{ (Li} = 1\text{)} \\ Q_{\text{theoretical,graphite}} &= \frac{1 \times 96485.33289 \text{ C/mol}}{72.0642 \text{ g/mol} \times 3600 \text{ Ah}} = 371.9 \text{ mAh/g} \end{aligned}$$

If the active material in the electrode is a mix consisting of between 5–15 wt% silicon and the rest graphite, the following theoretical capacity is calculated for electrodes:

5 wt% silicon:

$$\text{Anode capacity: } 0.05 \times 4198.8 \text{ mAh/g} + 0.95 \times 371.9 \text{ mAh/g} = 563.2 \text{ mAh/g}$$

10 wt% silicon:

$$\text{Anode capacity: } 0.10 \times 4198.8 \text{ mAh/g} + 0.90 \times 371.9 \text{ mAh/g} = 754.6 \text{ mAh/g}$$

15 wt% silicon:

$$\text{Anode capacity: } 0.15 \times 4198.8 \text{ mAh/g} + 0.85 \times 371.9 \text{ mAh/g} = 945.9 \text{ mAh/g}$$

Calculation capacity loss for  $\mu\text{m-Si}$  electrode composite during first cycle:

Literature: 0.0178–0.0278 mAh/cm<sup>2</sup> [81]

Surface area  $\mu\text{m-Si}$ : 4.1 m<sup>2</sup>/g = 4.1·10<sup>4</sup> cm<sup>2</sup>/g

Capacity loss pure silicon:

$$4.1 \cdot 10^4 \text{ cm}^2/\text{g} \times 0.0178 \text{ mAh}/\text{cm}^2 = 729.8 \text{ mAh}/\text{g}$$

$$4.1 \cdot 10^4 \text{ cm}^2/\text{g} \times 0.0278 \text{ mAh}/\text{cm}^2 = 1139.8 \text{ mAh}/\text{g}$$

Capacity loss with 5 wt% silicon material:

$$729.8 \text{ mAh}/\text{g} \times 0.05 = 36.49 \text{ mAh}/\text{g} \approx 36.5 \text{ mAh}/\text{g}$$

$$1139.8 \text{ mAh}/\text{g} \times 0.05 = 56.99 \text{ mAh}/\text{g} \approx 57.0 \text{ mAh}/\text{g}$$

Capacity loss (first cycle) pure graphite: 10% [77]

$$372 \text{ mAh}/\text{g} \times 0.1 = 37.2 \text{ mAh}/\text{g}$$

Capacity loss with 95 wt% graphite material:

$$37.2 \text{ mAh}/\text{g} \times 0.95 = 35.34 \text{ mAh}/\text{g} \approx 35.3 \text{ mAh}/\text{g}$$

Capacity loss electrode composite (active material = 5 wt% silicon, 95 wt% graphite):

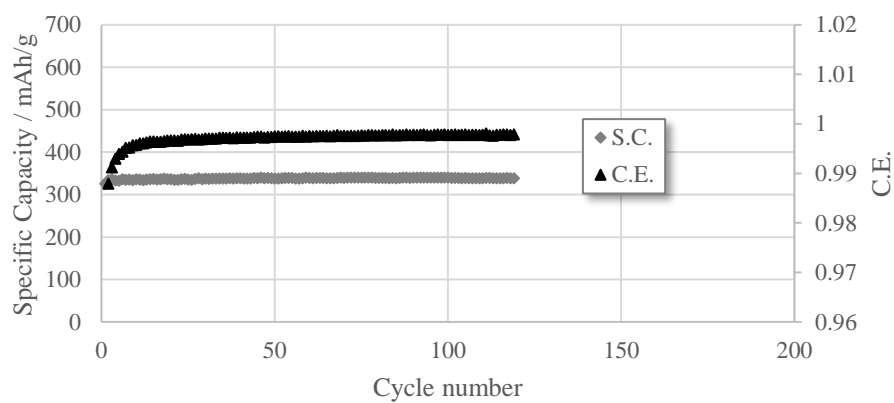
$$35.5 \text{ mAh}/\text{g} + 35.3 \text{ mAh}/\text{g} = 70.8 \text{ mAh}/\text{g}$$

$$57.0 \text{ mAh}/\text{g} + 35.3 \text{ mAh}/\text{g} = 92.3 \text{ mAh}/\text{g}$$

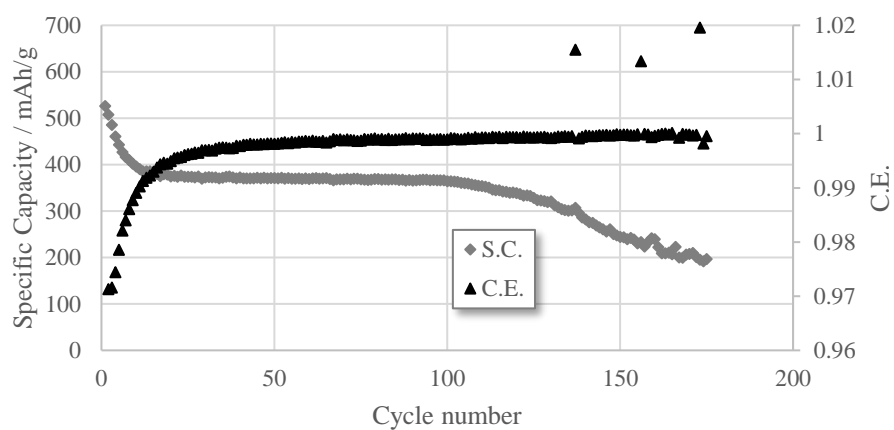
## Appendix B: Cycling data

C/10:

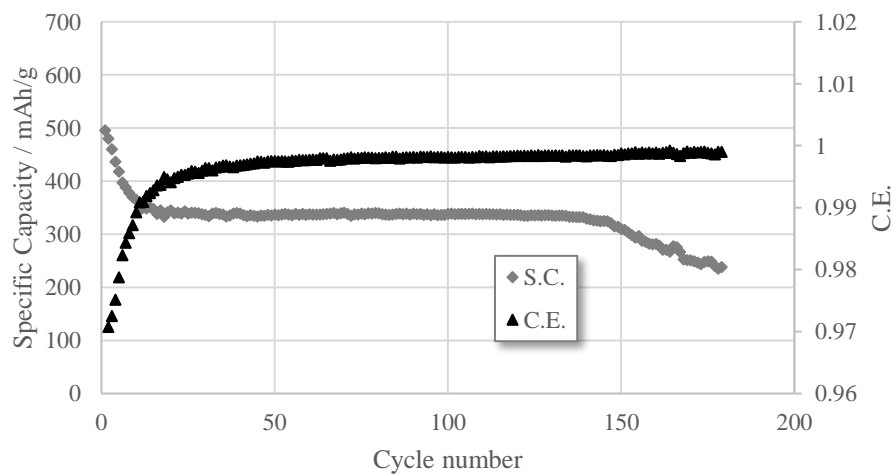
RA041 - Graphite - 5%-2:1 - 93%AM - 35% solv

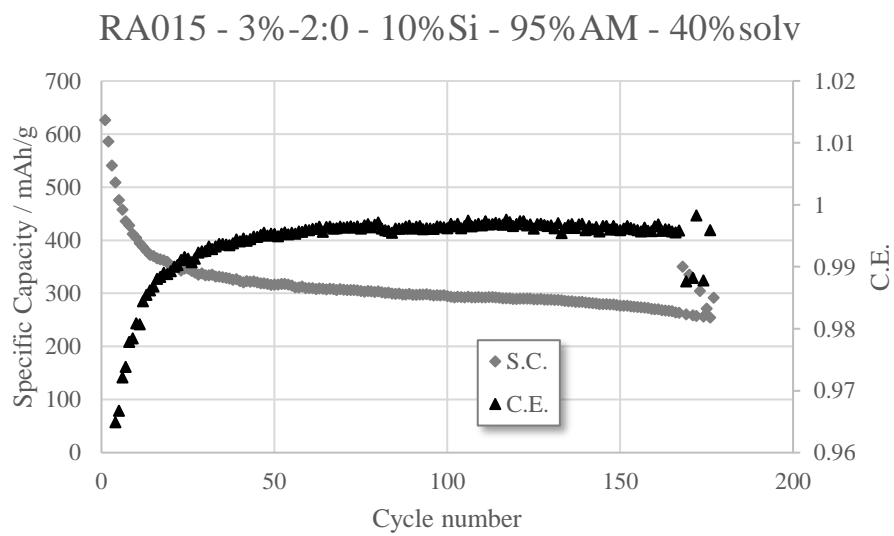
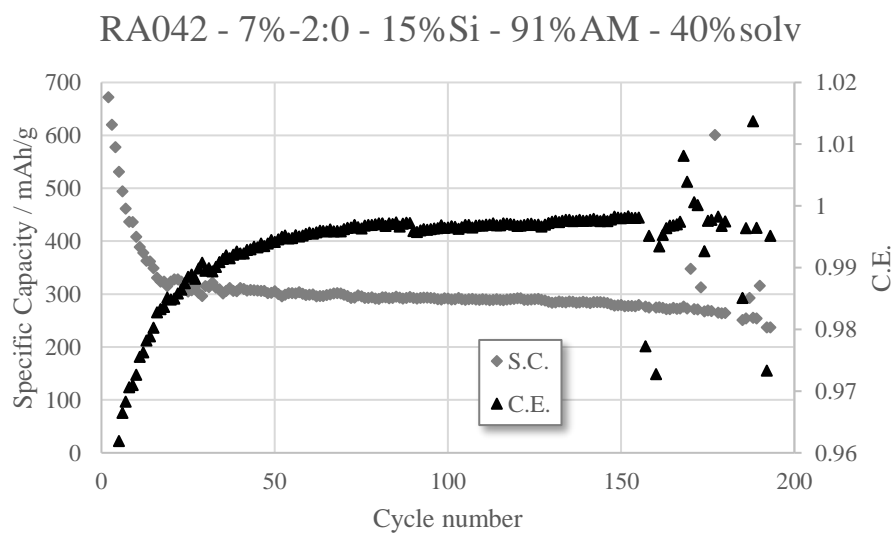
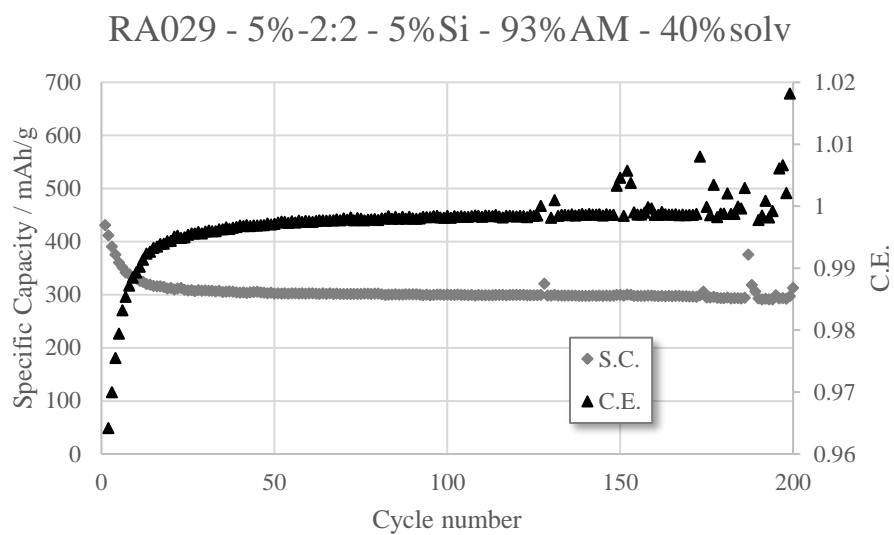


RA035 - 7%-2:1 - 5%Si - 91%AM - 40% solv

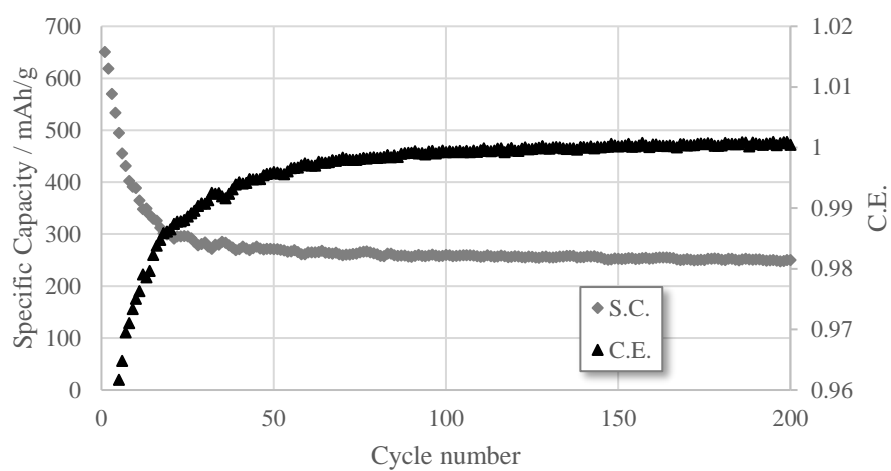


RA026 - 7%-2:1 - 5%Si - 91%AM - 40% solv

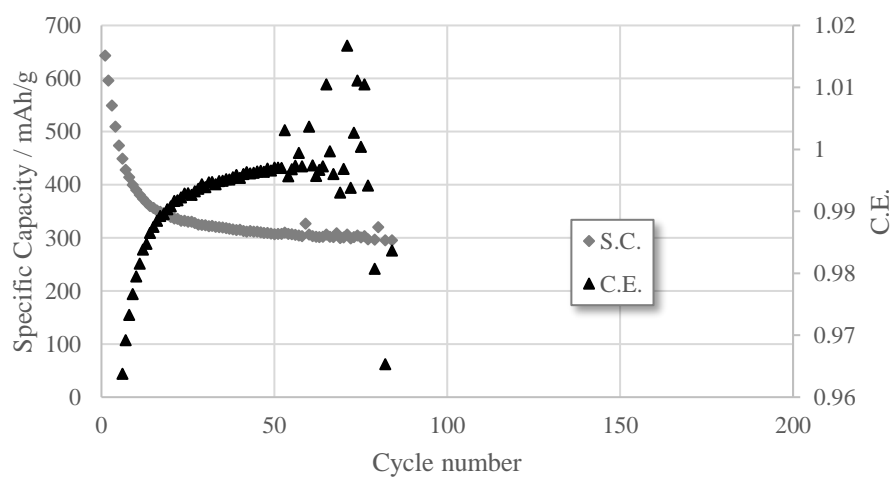




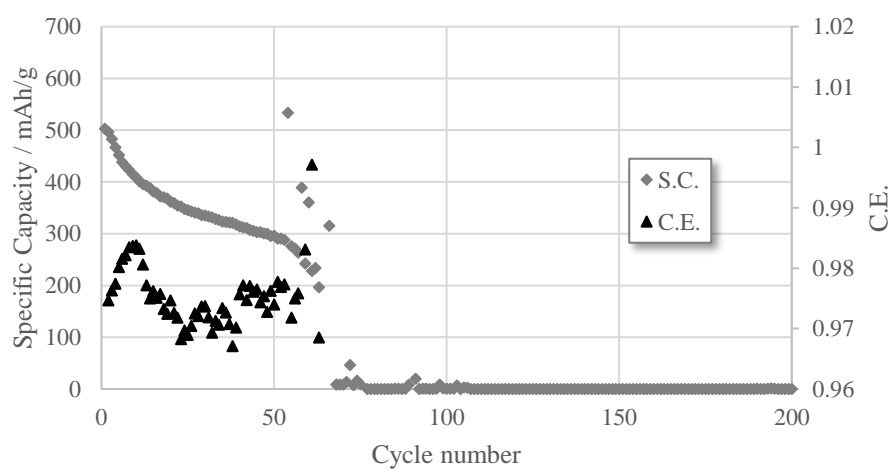
RA013 - 7%-2:0 - 15%Si - 91%AM - 30%solv



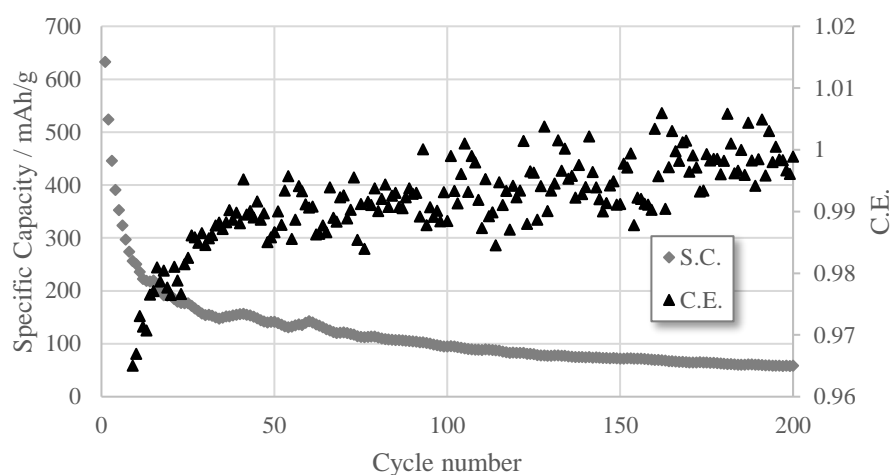
RA028 - 7%-2:2 - 10%Si - 91%AM - 40%solv



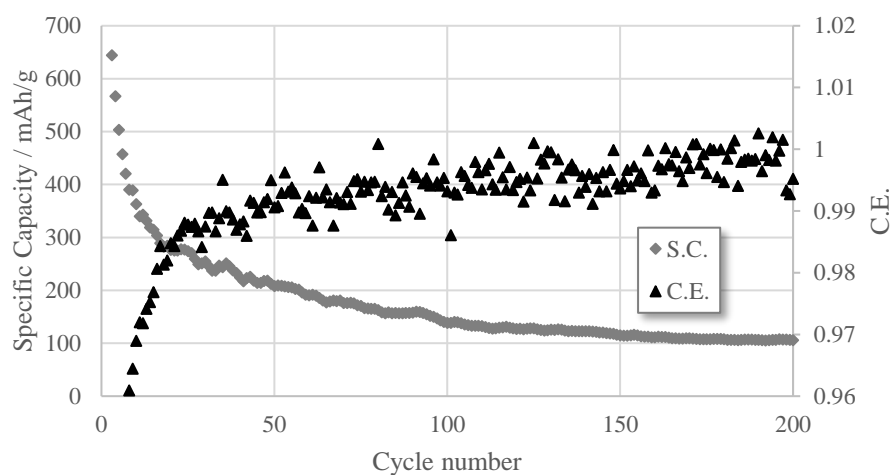
RA014 - 5%-2:0 - 5%Si - 93%AM - 35%solv



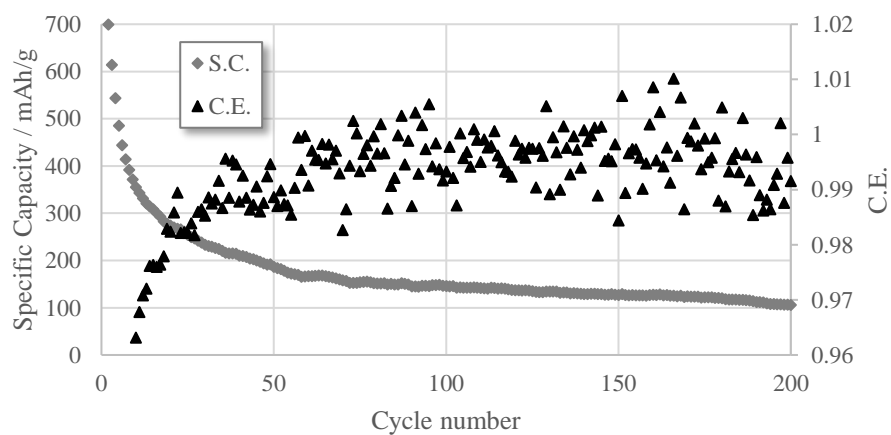
RA031 - 7%-2:1 - 15%Si - 91%AM - 40%solv



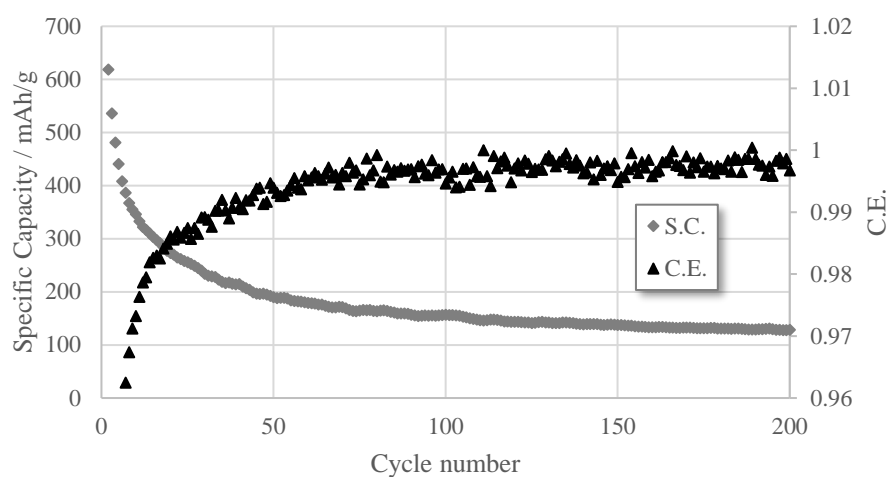
RA036 - 7%-2:1 - 15%Si - 91%AM - 40%solv



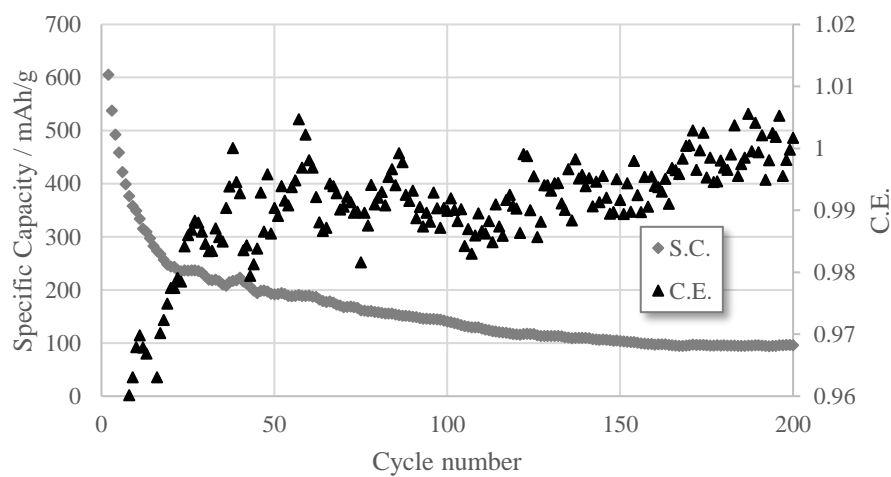
RA036-MPG - 7%-2:1 - 15%Si - 91%AM -  
40%solv



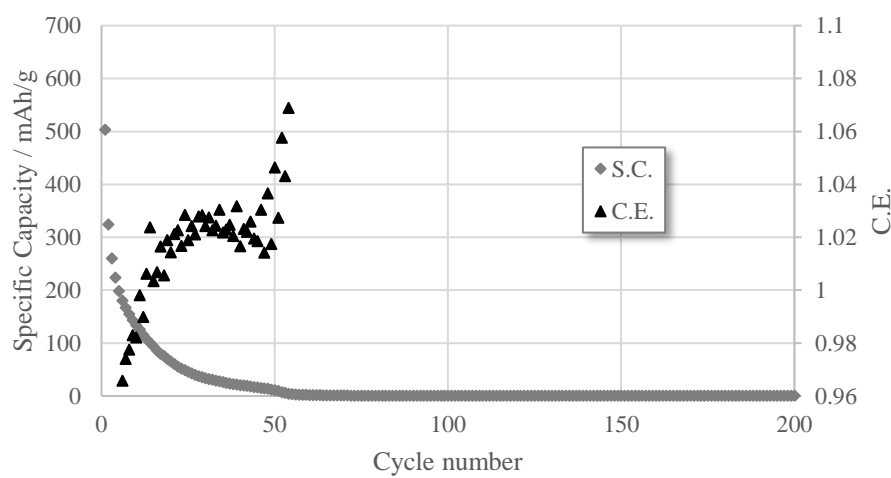
RA027 - 3%-2:2 - 15%Si - 95%AM - 40%solv



RA030 - 5%-2:1 - 15%Si - 93%AM - 40%solv

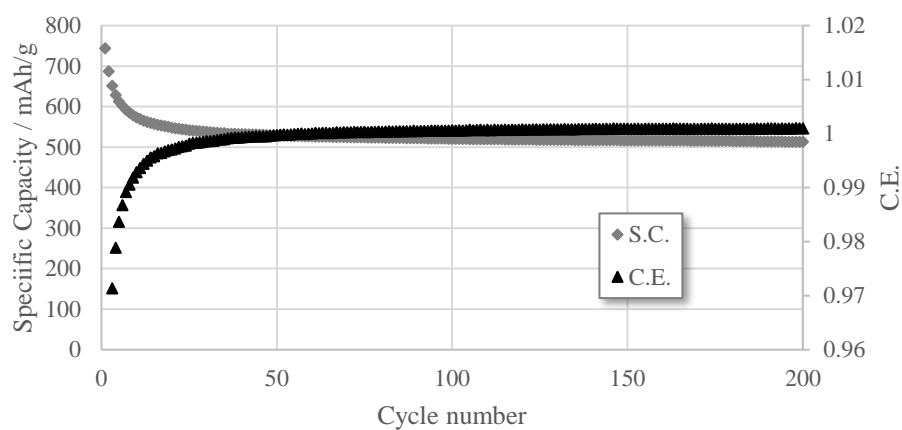


RA034 - Si - 5%-2:1 - 93%AM - 35%solv

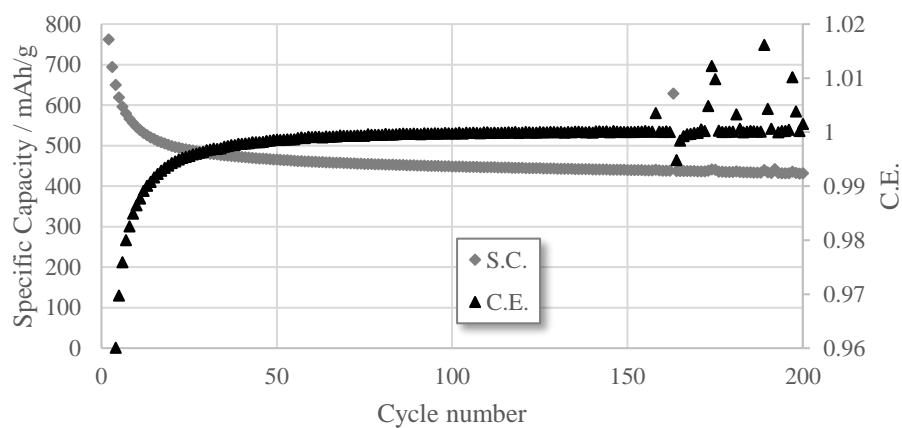


**C/2:**

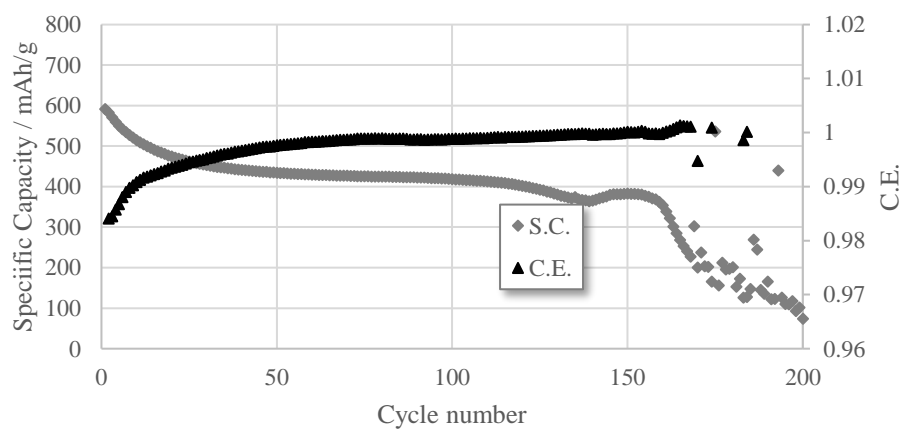
RA017 - MPG - 3%-2:2 - 5%Si - 95,0% AM -  
30% solv



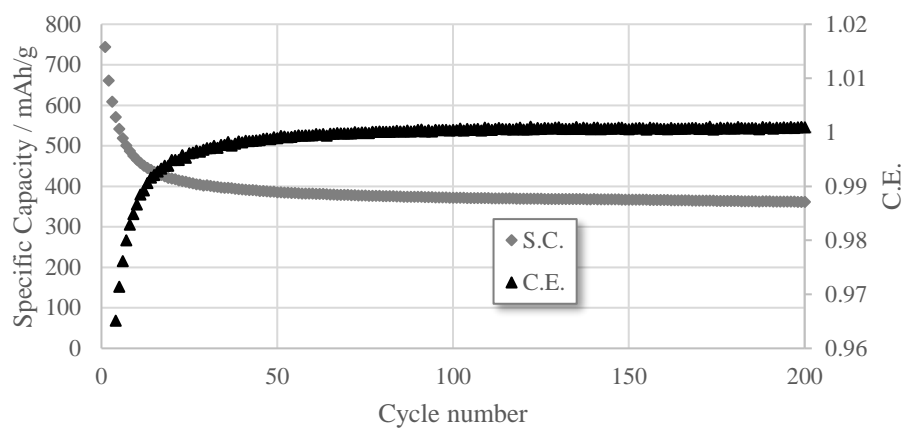
RA024-New Arbin - 3%-2:3 - 10%Si - 95,0% AM  
- 35% solv



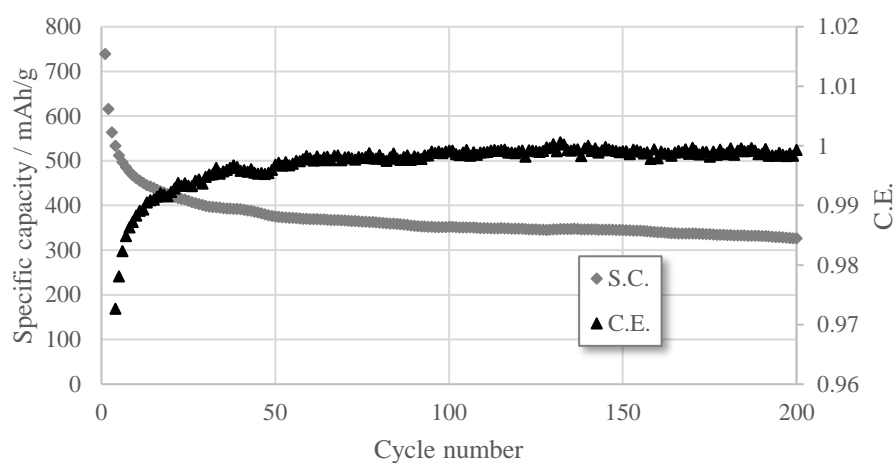
RA014 - MPG - 5%-2:0 - 5%Si - 93,0% AM -  
35% solv



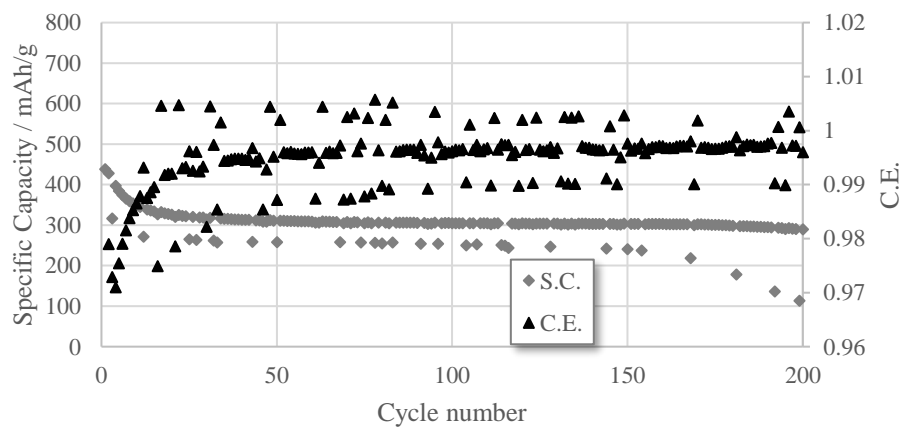
RA025-New Arbin - 7%-2:3 - 10%Si - 91,0%AM  
- 35% solv

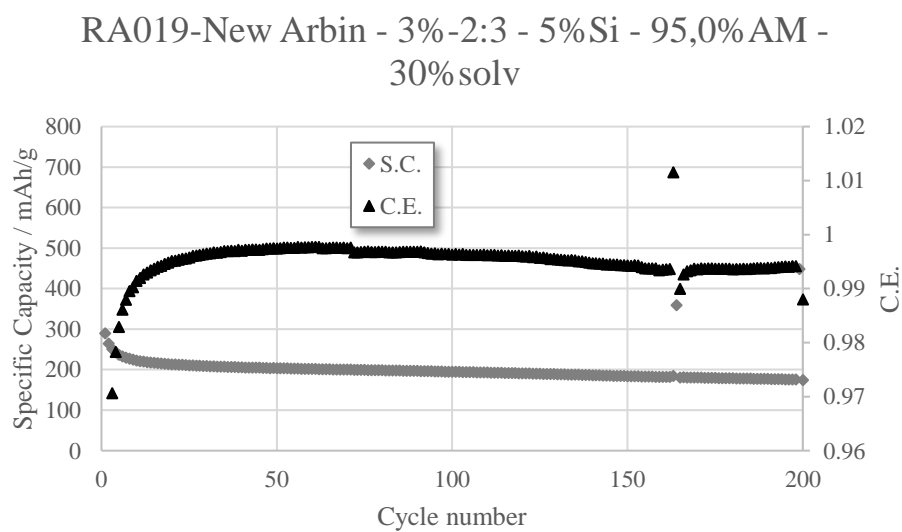
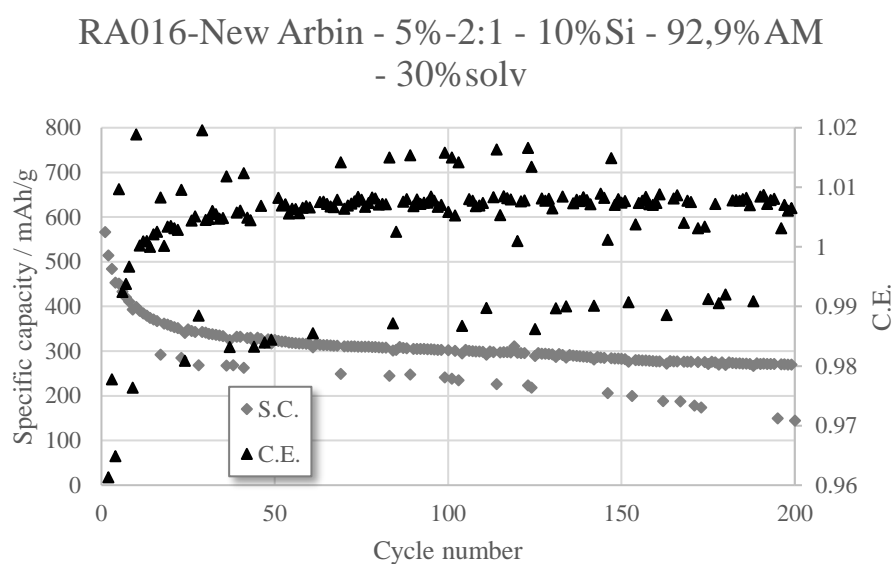
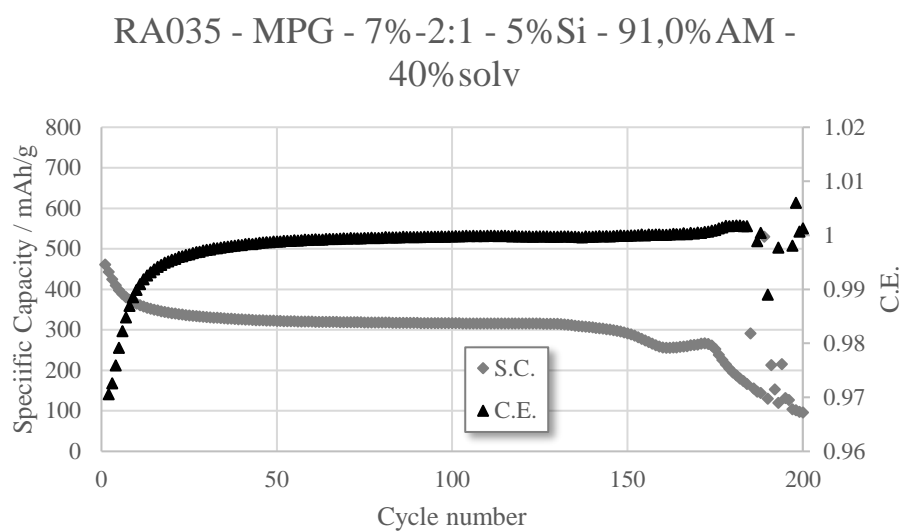


RA033-New Arbin - 3%-2:2 - 10%Si - 95,0%AM  
- 30% solv

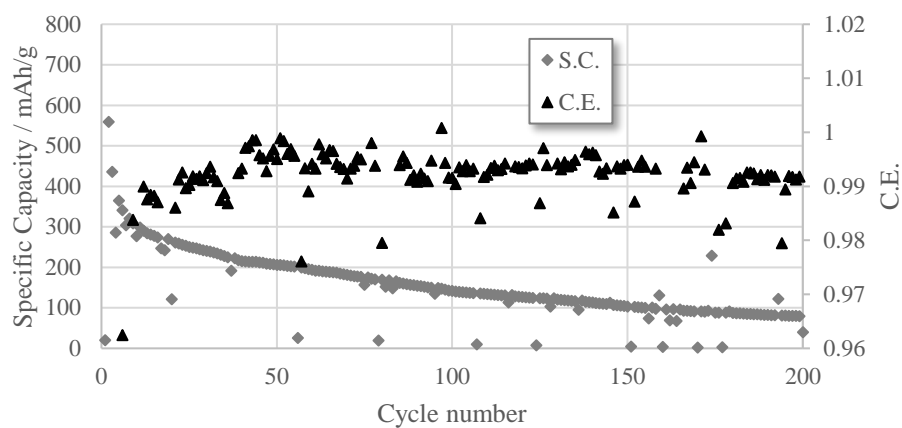


RA023 - Old Arbin - 7%-2:2 - 5%Si - 91,0%AM -  
35% solv

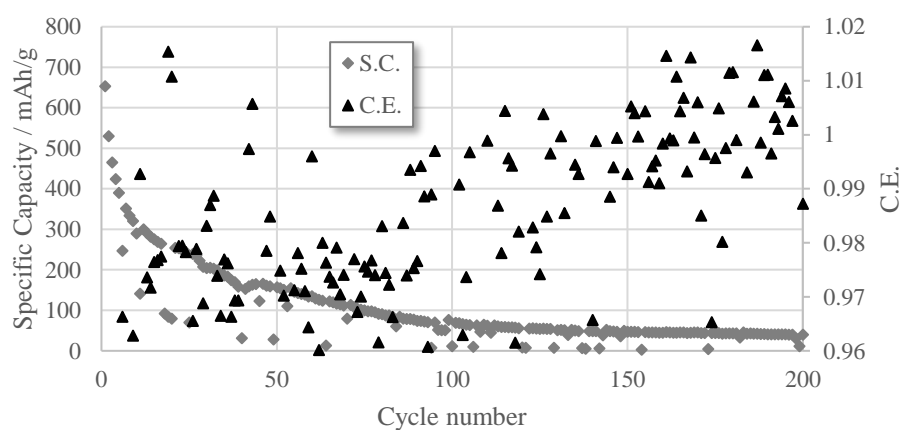




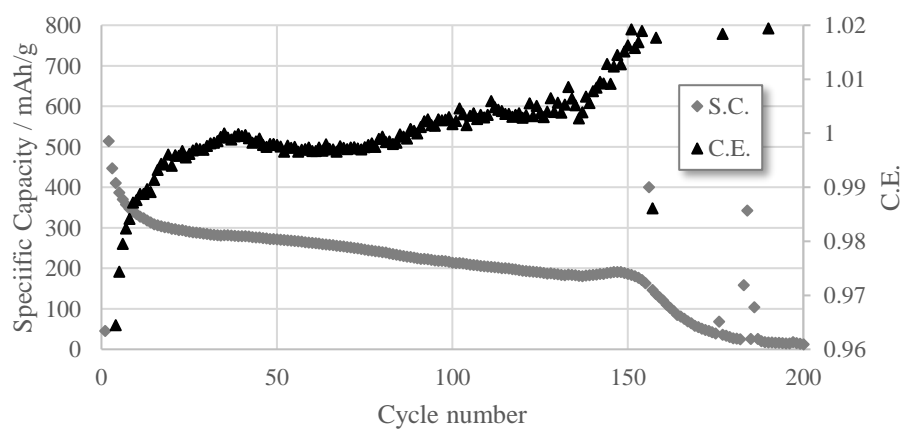
RA027-New Arbin - 3%-2:2 - 15%Si - 95,0%AM  
- 40% solv



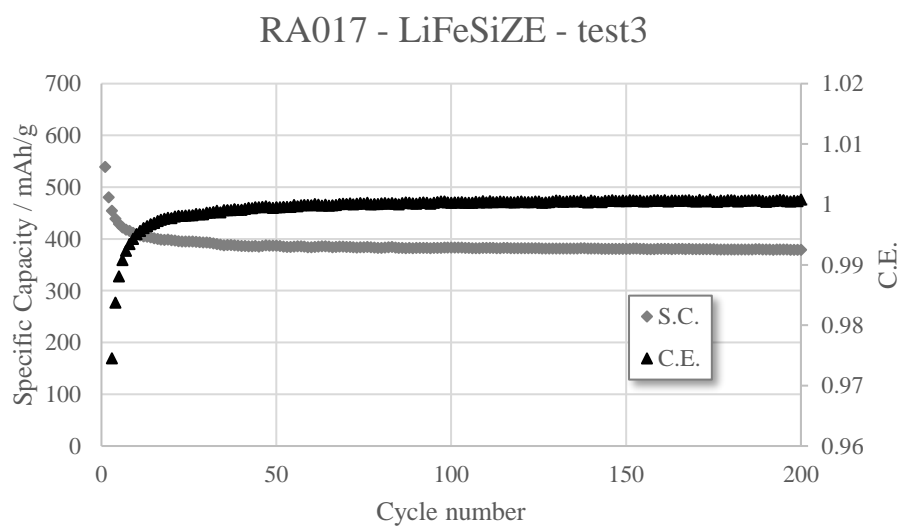
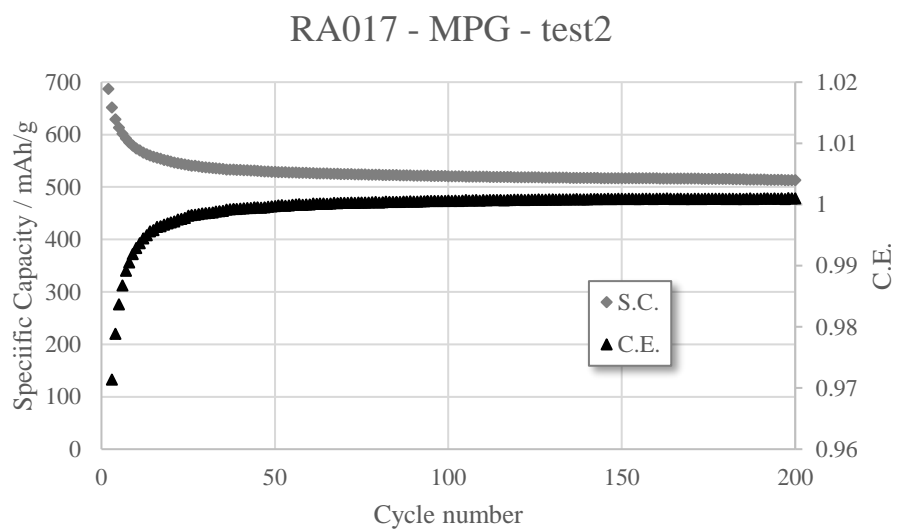
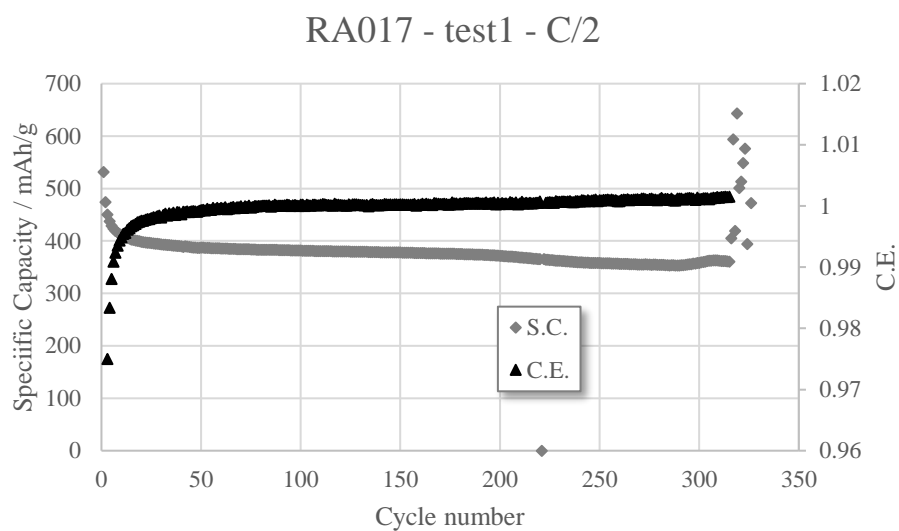
RA022 - Old Arbin - 5%-2:2 - 15%Si - 93,0%AM  
- 35% solv



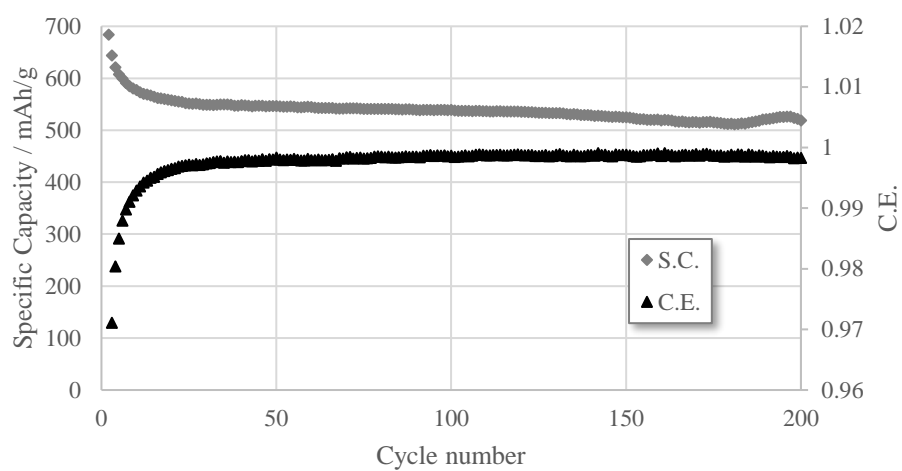
RA044 - MPG - 5%-2:1 - 10%Si - 93,0%AM -  
45% solv



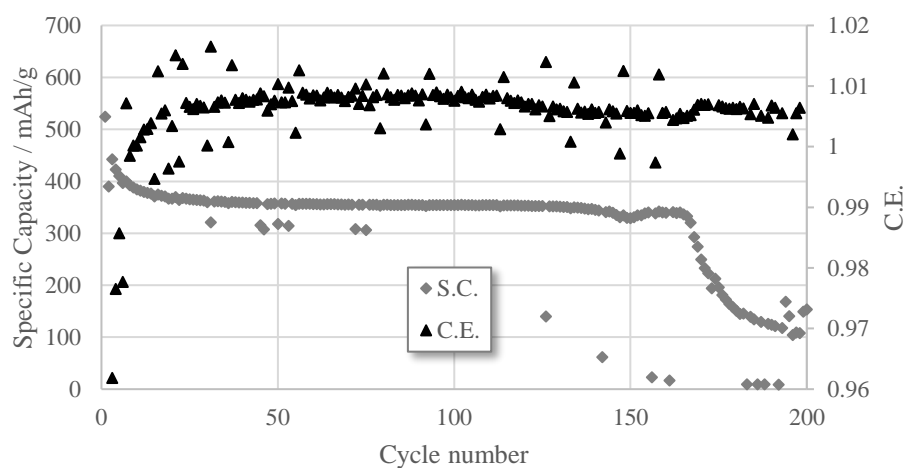
## RA017 C/2:



RA017 - LiFeSiZE - test4



RA017 - LiFeSiZE coating 1



RA017 - LiFeSiZE coating 2

